Instrument Science Report WFPC2 2009-04

Wavelength Stability of the WFPC2 Narrow Band and Linear Ramp Filters

J. Biretta and P. L. Lim
May 11, 2009

ABSTRACT

As part of the WFPC2 close-out calibrations, we test for long-term changes in the wavelength calibration of the narrow band and linear ramp filters. Relative wavelength measurements are made by crossing each narrow band filter with one of the linear ramp filters and taking a VISFLAT, and then noting the position of the resulting bright spot in the field of view. We test the stability of the central wavelengths by using this procedure on data from 1995 and 2008, and then compare the results. Twelve pairings of narrow band + ramp filter were tested in this way, and most were found to be highly stable. Ten showed a central wavelength change less than 1.1± 0.6 Å. The largest change was for FR868N+F953N of 3.8 Å, and the second largest change was for FR680N+FQCH4N-C of 1.8 Å. In general, the wavelength changes are a small fraction of the filter bandwidths (7% or less) and should not impact the vast majority of science observations. The four narrow band filters most often used for science – F502N, F656N, F658N, and F673N – were noted to be especially stable.

1. Introduction

WFPC2 contains 13 narrow band (NB) filters with typical bandwidths ~30 Å. Together these comprise ~15% of the WFPC2 science program, and have provided some of the most spectacular images taken by HST (Eagle Nebula, etc.). WFPC2 also contains a set of linear ramp filters (LRFs) whose wavelength varies with position in the field of view.

Operated by the Association of Universities for Research in Astronomy, Inc., for the National Aeronautics and Space Administration

These have bandwidths typically 1.3% of the central wavelength, and comprise about 2% of the science program. The band-passes of both types of filter are primarily defined by multi-layer interference filters.

The long-term stability of such filters is a potential issue which we address herein. Porous layers in the filters can out-gas water and other materials, changing the refractive indices and filter properties. Also, microscopic irregularities in the filter layers can anneal slowly over time, changing their thicknesses and again leading to evolution in the filter properties. Changes in the central wavelength of order 1 to 2 Å per year have been seen in such filters, depending on details of the manufacturing process (e.g., Potter & Simons 1993; Trauger, private communications). Given the 15+ year duration of the WFPC2 mission and the narrow bandpass of the filters, such changes could potentially become important.

In an effort to address these concerns, we have investigated the wavelength stability of the WFPC2 narrow band and linear ramp filters. While we do not have access to a spectrometer on-orbit, we can nonetheless obtain indications of the stability by obtaining flat-field exposures where each narrow band filter is crossed with the linear ramp filters. Crossing these filters will produce a bright spot in the field of view corresponding to the central wavelength of the narrow band filter (c.f., Biretta et al. 1996).

By comparing similar measurements taken at different epochs in the WFPC2 mission, we can test for changes in the filter wavelengths. Of course, this is a relative measurement, and we cannot rule out that the narrow band and ramp filters might change in exactly the same way, but such a scenario seems unlikely given differences in their detailed properties and manufacturing. It is also possible to make an absolute calibration of the LRF filters using external targets, though that work is left for future reports.

2. Observations

We selected WFPC2 VISFLAT observations with LRFs crossed with NB filters from Proposals 6140 (hereafter *Epoch 1*) and 11038 (hereafter *Epoch 2*). They are listed in Table 1 and Table 2, respectively. These images were selected because they had matching filter settings in both epochs for meaningful comparisons.

3. Data Reduction

We retrieved the images from the HST archive using standard pipeline calibrations. As the pipeline does not perform flat-fielding on cross-filter VISFLATs, we flat-fielded them using the nearest-matching wavelength (and most recent) NB flat-field reference

Table 1: Exposures used from Proposal 6140 (*Epoch 1*).

Image Name	Ramp Filter	NB Filter	Observation Date (YYYY-MM-DD)	Exposure Time (s)
u2mm0101t	FR418N	F375N	1995-02-25	2000
u2mm0301t	FR418N	F437N	1995-02-25	600
u2mm0302t	FR418N	F469N	1995-02-25	300
u2mm0401t	FR533N	F487N	1995-02-22	300
u2mm0402t	FR533N	F502N	1995-02-22	180
u2mm0501t	FR533N18	F502N	1995-03-01	180
u2mm0403t	FR533N	F588N	1995-02-22	20
u2mm0502t	FR533N18	F588N	1995-03-01	20
u2mm0601t	FR533N33	F588N	1995-03-01	20
u2mm0602t	FR680N	F631N	1995-03-01	20
u2mm0603t	FR680N	F656N	1995-03-01	20
u2mm0604t	FR680N	F658N	1995-03-01	20
u2mm0605t	FR680N	F673N	1995-03-01	12
u2mm0705t	FR680N18	F673N	1995-03-03	12
u2mm0901p	FR680N33	F673N	1995-03-07	12
u2mm0701t	FR680N	FQCH4N-C	1995-03-03	20
u2mm0903p	FR868N	F953N	1995-03-07	40

Table 2: Exposures used from Proposal 11038 (*Epoch 2*).

Image Name	Ramp Filter	NB Filter	Observation Date (YYYY-MM-DD)	Exposure Time (s)
u9w10801m	FR418N	F375N	2008-01-24	1800
u9w10802m	FR418N	F375N	2008-01-24	1800
u9w10803m	FR418N	F437N	2008-01-24	500
u9w10804m	FR418N	F469N	2008-01-24	260
u9w10905m	FR533N	F487N	2008-01-23	260
u9w10907m	FR533N	F502N	2008-01-23	180
u9w11002m	FR533N18	F502N	2008-01-25	160
u9w11001m	FR533N	F588N	2008-01-25	20
u9w11003m	FR533N18	F588N	2008-01-25	20
u9w11004m	FR533N33	F588N	2008-01-25	20
u9w11005m	FR680N	F631N	2008-01-25	20
u9w11006m	FR680N	F656N	2008-01-25	20
u9w11007m	FR680N	F658N	2008-01-25	20
u9w11008m	FR680N	F673N	2008-01-25	12
u9w1100am	FR680N18	F673N	2008-01-25	12
u9w1100bm	FR680N33	F673N	2008-01-25	12
u9w11009m	FR680N	FQCH4N-C	2008-01-25	20
u9w1100fm	FR868N	F953N	2008-01-25	40

files, as published in Table 10 of WFPC2 ISR 02-02 (Koekemoer, Biretta, & Mack 2002). Then we did an iterative 10×10-pixel median filtering and smoothing on the images, replacing each pixel by the median of a 10×10-pixel box surrounding it. During this process discrepant pixels, as well as pixels adjacent to them, were replaced by the local median value. The intention here was to reject cosmic rays, uncorrected hot pixels,

and other pixels that were too high or low. Any systematic error introduced by the median filter would not affect the relative comparison between 2 epochs.

The bright spot might span multiple chips on WFPC2, so we mosaicked the 4 chips together for each exposure using IRAF task "*wmosaic"* prior to measuring the spot position. We deemed it unnecessary to correct for the 34th-row effect, pixel area effects, and CTE loss, as these would be minimal in flat field observations. Since we required only the spot position, not the flux, and since the spots on WF4 never straddled other CCDs, we did not correct for the WF4 anomaly in *Epoch 2* data. An example of the final mosaic used for spot position measurement is shown in Figure 1. Hereafter, X and Y are the wavelength and spatial directions of the mosaicked image, respectively.

Figure 1: Left image is the mosaic emphasizing chip boundaries (brightness range *z1* = -0.23, *z2* = 2.06). Right image is the same mosaic adjusted to show the spot location (*z1* = 0, *z*2 = 20). The *z1* and *z2* values are the brightness scales used in IRAF task "*display*." Top left quadrant is PC1, followed by WF2, WF3, and WF4 in the counter-clockwise direction.

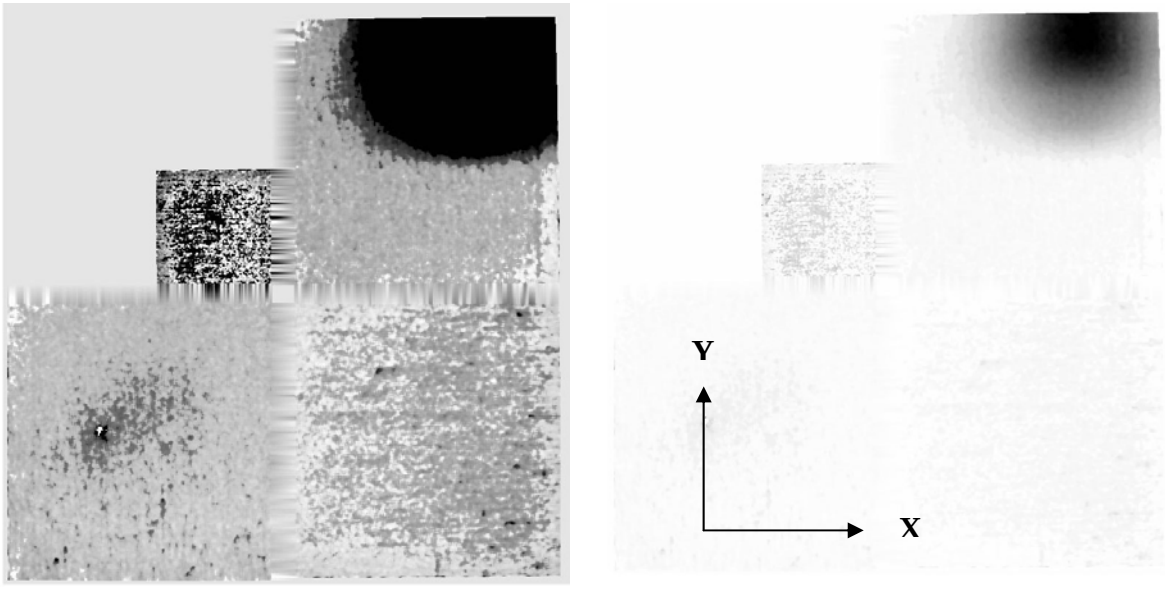

Each initial spot position was determined by visual inspection on the mosaicked image. The spot was also checked for saturation by looking at maximum pixel value from the IRAF task "*imstat*" performed on a 400×400-pixel box around the spot. Saturation was defined as any pixel in the box with more than 3,500 DN. For our VISFLAT data, no saturation was found. Any saturated image would have been excluded from analysis.

4. Analysis

For consistency's sake, we measured the spots from both *Epoch 1* and *Epoch 2* with our own algorithm as described below. We did not use the spot positions published in WFPC2 ISR 96-05 (Biretta et al. 1996).

4.1. Gaussian Fitting on Spot Position

To determine the final spot positions, we used a non-linear least-squares Gaussian fit on a region around the initial spot position on the mosaicked image, fitting for X and Y separately. When fitting in the X (wavelength) position, we used a ±150 pixel region about the intensity peak in X-direction, and collapsed (averaged) ±100 pixels of the image in the Y (spatial) direction. A corresponding procedure was used when fitting the Y position. We avoided the edges (25 pixels on left/bottom and 70 pixels on right/top) of the mosaic and the empty area in the PC1 quadrant; thus the number of pixels considered was sometimes less than the default values mentioned. We also avoided any other regions with obvious artifacts (errors at chip boundaries, etc.).

We took the Gaussian peak in the X direction as the measured X position, and similarly for the Y direction. Fitted X and Y positions are given in Table 3. This method was sufficient for X (wavelength direction) but not all Y positions because the Gaussian fit was less accurate if the spot lay very near the edge of the field of view or fell between two chips on the mosaic. Where Gaussian fitting failed in the Y direction, we used alternate methods described in Section 4.2. Plots of the resulting fits are shown in Appendix A.

4.2. Measuring Spot Position Shifts between Epochs

We measured shifts in spot positions for exposures with the same filter settings taken at different epochs. For good Gaussian fits, we simply took the differences in fitted X and Y coordinates, as shown in Equation 1, where ΔX and ΔY are shifts in X and Y respectively.

$$\Delta X = X_{Epoch\,2} - X_{Epoch1} \qquad (1\text{ a})$$

$$\Delta Y = Y_{Epoch\,2} - Y_{Epoch1} \qquad (1\text{ b})$$

Five filter combinations had unreliable Gaussian fits for Y (the spatial direction; see Table 3); hence, we computed the optimal ΔY by maximizing the correlation function of the 2 images. Unlike our 1-D Gaussian fitting, this correlation was done with 2-D image arrays. We empirically determined the image subsection used to cross-correlate for meaningful results. These subsections were normalized by their respective maximum pixel values prior to comparison.

Table 3: Gaussian-fitted spot positions for our exposures.

Image Names	Ramp Filter	NB Filter	NB Filter λ (Å)	Spot Position in Mosaic (pixel) X	Spot Position in Mosaic (pixel) Y [i]	Notes
u2mm0101t	FR418N	F375N	3732.0	1274.5	(1493.5)	Inaccurate Y-peak due to edge proximity
u9w10801m				1287.9	(1479.5)	
u9w10802m				1287.1	(1479.4)	
u2mm0301t	FR418N	F437N	4369.0	465.0	576.4	
u9w10803m				458.5	576.2	
u2mm0302t	FR418N	F469N	4694.0	1357.4	(104.3)	Inaccurate Y-peak due to edge proximity
u9w10804m				1362.8	(93.2)	
u2mm0401t	FR533N	F487N	4865.0	843.8	88.7	
u9w10905m				847.9	87.5	
u2mm0402t	FR533N	F502N	5012.0	65.9	101.2	Non-Gaussian Y-profile but fits were consistent for both epochs
u9w10907m				65.7	101.7	
u2mm0501t	FR533N18	F502N	5012.0	45.5	169.3	
u9w11002m				46.5	160.2	
u2mm0403t	FR533N	F588N	5894.0	953.6	1494.1	
u9w11001m				960.7	1478.7	
u2mm0502t	FR533N18	F588N	5894.0	1295.6	(765.7)	Inaccurate Y-peak due to WF3-WF4 border
u9w11003m				1291.3	(756.9)	
u2mm0601t	FR533N33	F588N	5894.0	1402.7	(76.2)	Inaccurate Y-peak due to edge proximity
u9w11004m				1396.5	(82.7)	
u2mm0602t	FR680N	F631N	6306.0	1060.6	103.4	
u9w11005m				1060.9	101.6	
u2mm0603t	FR680N	F656N	6564.0	917.5	589.0	
u9w11006m				921.9	573.5	
u2mm0604t	FR680N	F658N	6591.0	830.7	589.0	
u9w11007m				833.7	571.7	
u2mm0605t	FR680N	F673N	6732.0	349.5	582.4	
u9w11008m				353.8	570.5	
u2mm0705t	FR680N18	F673N	6732.0	132.1	628.5	Spot #1
u9w1100am				133.6	627.5	
u2mm0705t	FR680N18	F673N	6732.0	415.8	61.1	Spot #2
u9w1100am				417.0	59.7	
u2mm0901p	FR680N33	F673N	6732.0	222.7	257.8	
u9w1100bm				222.5	256.9	
u2mm0701t	FR680N	FQCH4N-C	7279.0	1384.9	(1600.0)	Gaussian diverged due to off-edge Y-peak
u9w11009m				1389.7	(1600.0)	
u2mm0903p	FR868N	F953N	9545.0	931.9	126.9	
u9w1100fm				922.6	125.4	

[i] Values in parentheses were not used to measure changes in spot position and wavelength. See Section 4.2.

For filter combination FR533N18+ F588N (*u2mm0502t* and *u9w11003m*), the spots fell on the border between chips WF3 and WF4 in the Y-direction, rendering their Y-peaks unusable for fitting of any kind. We cross-correlated 2 subsections of the images on either side of their peaks in the Y-direction and used the average value as the final ΔY.

For filter combination FR418N+F469N (*u2mm0302t* and *u9w10804m*), the peaks in the Y-directions were flattened, their right slopes were "bumpy" and left slopes were cut off

by the mosaic edge. Thus neither Gaussian fitting nor cross-correlation produced good results. We resorted to superposing the spot profiles and visually determining ΔY.

Final ΔX and ΔY values are tabulated in Table 4. In the "Method for ΔY" column, "Gaussian" means Gaussian fitting as described in Section 4.1 and Equation 1, "X-Corr" means cross-correlation, and "By Eye" means visual measurement. Plots of the latter two are also in Appendix A.

Table 4: Spot position shifts between *Epoch 1* and *Epoch 2*.

Epoch 1 Image	*Epoch 2* Image	Ramp Filter	NB Filter	ΔX (pix)	ΔY (pix)	Method for ΔY	Notes
u2mm0101t	u9w10801m	FR418N	F375N	13.4	-18.0	X-Corr	
u2mm0101t	u9w10802m	FR418N	F375N	12.6	-20.0	X-Corr	
u2mm0301t	u9w10803m	FR418N	F437N	-6.5	-0.2	Gaussian	
u2mm0302t	u9w10804m	FR418N	F469N	5.3	-20.0	By Eye	See Section 4.2
u2mm0401t	u9w10905m	FR533N	F487N	4.1	-1.2	Gaussian	
u2mm0402t	u9w10907m	FR533N	F502N	-0.2	0.5	Gaussian	
u2mm0501t	u9w11002m	FR533N18	F502N	1.0	-9.1	Gaussian	
u2mm0403t	u9w11001m	FR533N	F588N	7.1	-15.4	Gaussian	
u2mm0502t	u9w11003m	FR533N18	F588N	-4.3	0.0	X-Corr	See Section 4.2
u2mm0601t	u9w11004m	FR533N33	F588N	-6.1	-1.0	X-Corr	
u2mm0602t	u9w11005m	FR680N	F631N	0.3	-1.8	Gaussian	
u2mm0603t	u9w11006m	FR680N	F656N	4.3	-15.5	Gaussian	
u2mm0604t	u9w11007m	FR680N	F658N	3.0	-17.3	Gaussian	
u2mm0605t	u9w11008m	FR680N	F673N	4.3	-12.0	Gaussian	
u2mm0705t	u9w1100am	FR680N18	F673N	1.5	-1.0	Gaussian	Spot #1
u2mm0705t	u9w1100am	FR680N18	F673N	1.2	-1.4	Gaussian	Spot #2
u2mm0901p	u9w1100bm	FR680N33	F673N	-0.2	-0.9	Gaussian	
u2mm0701t	u9w11009m	FR680N	FQCH4N-C	4.8	-16.0	X-Corr	
u2mm0903p	u9w1100fm	FR868N	F953N	-9.2	-1.5	Gaussian	

4.3. Uncertainty Estimation for Spot Positions

The uncertainties were difficult to estimate in a formal fashion. The spot profiles are only approximately Gaussian; hence, the fit residuals and coefficient sigma values do not accurately portray the uncertainties. We also have only one image for each particular filter setting and epoch (except for FR418N+F375N for *Epoch 2)*, and thus cannot measure the scatter among different data sets.

Instead, to get a rough estimate of the uncertainties, we examined the change in the results caused by changing the region used for the Gaussian fits. This gives some indication of the sensitivity of the result to details of the measurement procedure. We used half-widths of 100 and 180 pixels instead of the default 150 pixels (see Section 4.1). From such fits on several filter settings representative of the dataset (FR418N+F375N, FR418N+F437N, FR533N+F502N, and FR533N18+F502N), we calculated the average positional differences between these two region widths and the default one. These

indicated approximately 1- and 2-pixel uncertainties for X and Y, respectively. The uncertainty in Y is larger, because the spots in that direction were generally closer to the field edge and had more irregular shapes. In cases where cross-correlation and visual estimates were used for Y, we obtained similar uncertainty estimates.

In the case where two images were available, FR418N+F375N for *Epoch 2,* comparison of the two images gives differences of 0.8 and 2 pixels, respectively, for ΔX and ΔY, which is consistent with the above error estimates. Hence we estimate 1- and 2-pixel uncertainties in X and Y positions, respectively. The corresponding uncertainties for position *change* would be approx. 1.4 and 2.8 pixels for ΔX and ΔY, respectively.

4.4. Converting Pixel Shifts to Wavelength Shifts

We obtained a conversion from pixel shift to wavelength shift using Figures 3.5 and 3.6 in the WFPC2 Instrument Handbook (McMaster & Biretta et al. 2008); The LRF calculator tool[a] could have been used. For un-rotated LRF settings, the conversion could be applied directly to ΔX to obtain Δλ. However, for rotated LRF settings, wavelength does not run along X, but is rotated, so we had to project the pixel shift on the ramp direction for an accurate Δλ. We used Equation 2 to do this:

$$\Delta\lambda = \sqrt{\Delta X^2 + \Delta Y^2} \times a_{conv} \times \cos\theta_{conv} \ , \qquad (2)$$

where a_{conv} is the conversion scale in Å/pix for that particular ramp and LRF, and θ_{conv} is the angle between shift and ramp directions. Values of a_{conv} range from ~0.18 Å/pix in the blue to ~0.42 Å/pix in the red. Resulting values of Δλ are given in Table 5.

The accuracy of Δλ, which is a relative comparison between 2 epochs, depends primarily on the accuracy of the pixel shift measurement. Even for rotated LRF settings, λ changes are mainly in the X-direction. Hence a 1.4 pixel uncertainty in ΔX (see Section 4.3) translates to Δλ uncertainty ~0.3 Å in the blue and ~0.6 Å in the red. The conversion scale a_{conv} does not contribute significant uncertainty, as any systematic error is eliminated in a relative comparison.

4.5. Filter Wheel Rotation Anomaly

As mentioned in Section 7.10 in the WFPC2 Instrument Handbook (McMaster & Biretta et al. 2008), WFPC2 suffers from an "*apparently randomly occurring offset in the filter position*" corresponding "*to one step in the filter rotation, or about 0.5 degrees*." Moreover, we note that most of the large ΔX (wavelength direction) offsets in Table 4 are also accompanied by a large ΔY offset in the spacial direction. This could be easily understood if the offsets were due to a rotation error in the filter wheel position, rather

[a] http://www.stsci.edu/hst/wfpc2/software/wfpc2_lrfcalc.html

Table 5: Wavelength shifts between *Epoch 1* and *Epoch 2*, before and after filter positional anomaly correction. Values of Δλ, θ, and Δλ′ are from Sections 4.4, 4.5, and 4.6, respectively.

Epoch 1 Image	*Epoch 2* Image	Ramp Filter	NB Filter	Δλ (Å)	θ (°)	Δλ′ (Å)	Notes
u2mm0101t	u9w10801m	FR418N	F375N	1.972	0.449	0.515	
u2mm0101t	u9w10802m	FR418N	F375N	1.849	0.476	0.392	
u2mm0301t	u9w10803m	FR418N	F437N	1.123	0.046	—	
u2mm0302t	u9w10804m	FR418N	F469N	1.025	0.443	1.078	
u2mm0401t	u9w10905m	FR533N	F487N	0.728	0.031	—	
u2mm0402t	u9w10907m	FR533N	F502N	0.039	0.023	—	
u2mm0501t	u9w11002m	FR533N18	F502N	0.788	0.412	0.152	
u2mm0403t	u9w11001m	FR533N	F588N	1.606	0.377	0.646	
u2mm0502t	u9w11003m	FR533N18	F588N	0.939	0.023	—	
u2mm0601t	u9w11004m	FR533N33	F588N	1.044	0.025	—	
u2mm0602t	u9w11005m	FR680N	F631N	0.076	0.045	—	
u2mm0603t	u9w11006m	FR680N	F656N	1.274	0.421	0.311	
u2mm0604t	u9w11007m	FR680N	F658N	0.875	0.479	0.089	
u2mm0605t	u9w11008m	FR680N	F673N	1.263	0.450	0.316	
u2mm0705t	u9w1100am	FR680N18	F673N	0.537	0.059	—	Spot #1
u2mm0705t	u9w1100am	FR680N18	F673N	0.473	0.034	—	Spot #2
u2mm0901p	u9w1100bm	FR680N33	F673N	0.100	0.035	—	
u2mm0701t	u9w11009m	FR680N	FQCH4N-C	1.508	0.313	1.832	
u2mm0903p	u9w1100fm	FR868N	F953N	3.848	0.041	—	

than an actual change in the filter central wavelength. Hence it is necessary consider the possibility of filter rotation errors, and their potential impacts on our results.

To investigate this possibility, we predicted the angle of filter wheel rotation offset needed to produce the observed shift, should the offset be the sole factor in the shift. We used the same filter wheel rotation axis with respect to image mosaic as Figure 7 in WFPC2 ISR 02-04 (Gonzaga, Baggett, & Biretta 2002). Instead of the simple trigonometry in the ISR, we used 2-D vector calculus for more accuracy.

We defined V_1 to be the vector from the filter wheel pivot to the *Epoch 1* spot and V_2 to be the vector from the *Epoch 1* spot to the *Epoch 2* position (with components ΔX and ΔY). Knowing the positions and lengths of the vectors, we projected V_2 onto components parallel and perpendicular to V_1. Then we obtained filter wheel rotation offset angle, θ, from Equation 3 below:

$$\theta = \tan^{-1} \frac{S}{R}, \qquad (3)$$

where S is the V_2 component perpendicular to V_1 and R is the length of V_1. These θ values are given in Table 5.

Most of the θ values were consistent with either zero rotation or a 0.5-degree step (within the errors), indicating the filter wheel rotation anomaly was a likely cause of the observed

position changes. Two cases, FR533N+F588N and FR680N+FQCH4N-C, could not be explained by this effect. We also attempted to correlate the filter used prior to an observation with the presence (or absence) of the 0.5-degree nominal rotation error (i.e. to see if the error only occurred when the filter wheel rotated in a particular direction) but no correlation was apparent.

4.6. Estimating Wavelength Shift after Filter Positional Anomaly Correction

WFPC2 ISR 02-04 (Gonzaga et al. 2002) attempted to measure the filter wheel rotation offset angle empirically, and reported an average angle of 0.42° ± 0.06°. To better understand how this might affect our results, we removed the 0.42° rotation effect and re-calculated wavelength shifts between *Epoch 1* and *Epoch 2,* in situations where we saw apparent offsets with $\theta > 0.3°$.

We defined an angle, β, to be the angle measured counter-clockwise between V_1 and the X-axis. Removing 0.42° from β would rotate V_1 to a new vector V_1' with the same length, R. This new angle would also change the values of X and Y components of V_2 to be $\Delta X'$ and $\Delta Y'$.

Trigonometry dictates that the spot position shift is solely in the Y-direction when cos β is zero, and similarly in the X-direction when sin β is zero. Knowing this and using small-angle approximation, we calculated the corrected shifts $\Delta X'$ and $\Delta Y'$ using Equation 4 below (also see Section 4.5).

$$\Delta X' = \Delta X + R \sin 0.42° \sin \beta \quad (4\text{ a})$$

$$\Delta Y' = \Delta Y - R \sin 0.42° \cos \beta \quad (4\text{ b})$$

We used the values of $\Delta X'$ and $\Delta Y'$ and Equation 2 to calculate the new wavelength shift, $\Delta\lambda'$, which is also presented in Table 5, where applicable. For cases where $\theta > 0.3°$, removing 0.42° decreased most wavelength shifts to ~1.0 Å or less, except for two cases: FR680N+FQCH4N-C (1.8 Å) and FR868N+F953N (3.8 Å).

It is important here to emphasize that removal of the 0.42° rotation error is primarily motivated by a desire to eliminate shift in the Y (spatial) direction, which is otherwise unexplainable. Removing the rotation error, as a secondary effect, also reduces the measured shifts in X (wavelength) direction.

4.7. VISFLAT Lamp Stability

The lamp used for the VISFLATs is known to be evolving (becoming dimmer) with time (O'Dea, Mutchler, & Wiggs 1999), so we were concerned whether this might somehow impact our wavelength measurements. The lamp assembly contains multiple bulbs with

different properties, so it is conceivable the illumination pattern might change over time. For example, if some region in the field of view were fading more quickly, it could shift our measured spot positions. To make sure that this was not the case, we checked broadband VISFLAT exposures (F336W, F555W, and F814W) taken near *Epoch 1* and *Epoch 2*. These exposures were not from our LRF proposals, but were selected to be close in time to the LRF measurements.

We utilized exposures that were as close to the epochs as possible and had similar exposure times for the same filters. For exposures with less than 10 seconds, we used only those with same the shutters due to the shutter shading effect, as discussed on page WFPC2:3-13 in WFPC2 Data Handbook (Baggett et al. 2002). The broadband exposures used are given in Table 6.

Table 6: Broadband exposures used to check VISFLAT lamp stability.

Image Name	Broadband Filter	Observation Date (YYYY-MM-DD)	Exposure Time (s)	Shutter
u2fd0n01t	F336W	1994-06-16	600	A
u2fd0p01t	F336W	1994-06-15	600	A
u2fd0x01t	F336W	1994-06-21	600	A
u2fd0z01t	F336W	1994-06-22	600	A
ub030801m	F336W	2008-04-03	600	A
ub030802m	F336W	2008-04-03	600	B
ub030803m	F336W	2008-04-03	600	A
ub030804m	F336W	2008-04-03	600	B
u2fd0f02t	F555W	1994-06-08	1.2	A
u2fd0p03t	F555W	1994-06-15	1.2	A
u2fd0z03t	F555W	1994-06-22	1.2	A
u2fd1j03t	F555W	1994-07-15	1.2	A
u9jae203m	F555W	2006-06-26	1.6	A
u9jaeh03m	F555W	2006-06-29	1.6	A
u9uncn03m	F555W	2007-05-30	1.6	A
u9unen03m	F555W	2007-09-04	1.6	A
u2fd5q03t	F814W	1995-02-07	0.5	A
u2fd6003t	F814W	1995-02-14	0.5	A
u2fd6a03t	F814W	1995-03-06	0.5	A
u2fd6k03t	F814W	1995-03-13	0.5	A
u9jae207m	F814W	2006-06-26	0.6	A
u9jaeh07m	F814W	2006-06-29	0.6	A
u9uncn07m	F814W	2007-05-31	0.6	A
u9unen07m	F814W	2007-09-04	0.6	A

For each broadband filter, we combined 4 exposures per epoch with IRAF task "*crrej*" and divided the combined image from the newer epoch by the older one, taking their exposure times into account. We mosaicked the ratio and median-smoothed it with a 10×150-pixel box. The larger Y-dimension was selected to be consistent with averaging about that many pixels for X-position measurement, as described in Section 4.1. As a

result, we had one mosaicked ratio image per broadband filter. For each chip region, we performed the IRAF task "*imstat*" on an area 160 and 50 pixels away from the X and the Y borders, respectively.

The standard deviations from the F555W regions mentioned above are 0.2% for all WF chips. (PC1 is not used for our analysis.) Values for F336W and F814W are essentially identical. The position error caused by such a brightness fluctuation across the ~150 pixel spot size is approximately 0.1 pixel[b] (i.e., 0.2%×150/2.36), and is not important. The VISFLAT lamp is thus sufficiently stable and does not significantly contribute to the observed spot position shifts.

4.8. EARTH-CALIB Exposures

We attempted to analyze spot positions for EARTH-CALIB cross-filter exposures in a similar fashion as their VISFLAT counterparts. However, we found the measurements unreliable because most of the images were affected by the changing Earth features (streaks) due to their short exposure times. Some images with longer exposure times were affected by saturation. Thus we were unable to compare the spot positions for different epochs for EARTH-CALIB exposures, and for EARTH-CALIB and VISFLAT exposures for the same epochs.

5. Discussion

We present spot position shifts from Table 4 and Section 4.6 as vector plots in Figure 2 and Figure 3 for un-rotated and rotated LRFs, respectively. Dashed lines are the approximate border positions of the 4 chips on a WFPC2 image mosaic. The black dots mark the measured X and Y position for *Epoch 1*. The blue vectors indicate the position change between 1995 and 2008, and has ΔX and ΔY as its components. The red vectors, if present, are our best attempts to correct the position change for the filter wheel rotation anomaly (with components $\Delta X'$ and $\Delta Y'$). Each vector length is multiplied by 15 on the plots for clarity. The number next to each vector corresponds to that in the respective legend, which indicates the filters, actual length of the blue vector, and if available, actual length of the red vector.

The observed spot position changes (blue vectors) are primarily of two types. Firstly, there are small vectors approximately pointing in the +X or –X direction, which are likely to represent small changes in the filter wavelengths. And secondly, there are large vectors pointing in the direction of the filter wheel rotation – these are apparently cases which have been impacted at one epoch by the filter wheel rotation anomaly. Removing

[b] The position error is approximately the intensity error divided by the local derivative of the observed intensity, which we approximate here as a Gaussian function with FWHM of 150 pixels.

the mean filter wheel rotation error of 0.42° (Gonzaga et al. 2002; see Section 4.6) from these later cases produces the red vectors, which have nearly zero component in the Y (spatial) direction. Importantly, removing the filter wheel rotation error also reduces the X position or wavelength change to near-zero in most cases.

Of the twelve unique filter pairs measured[c], all but two have a wavelength change, $\Delta\lambda$, less than 1.1 ± 0.6 Å (see Sections 4.4 and 4.6). The filter combination with the largest change is FR868N+F953N ($\Delta\lambda = 3.8$ Å), but this is also the longest wavelength filter

Figure 2: Vector plot for un-rotated LRF crossed with NB filters. See Section 5 for explanation.

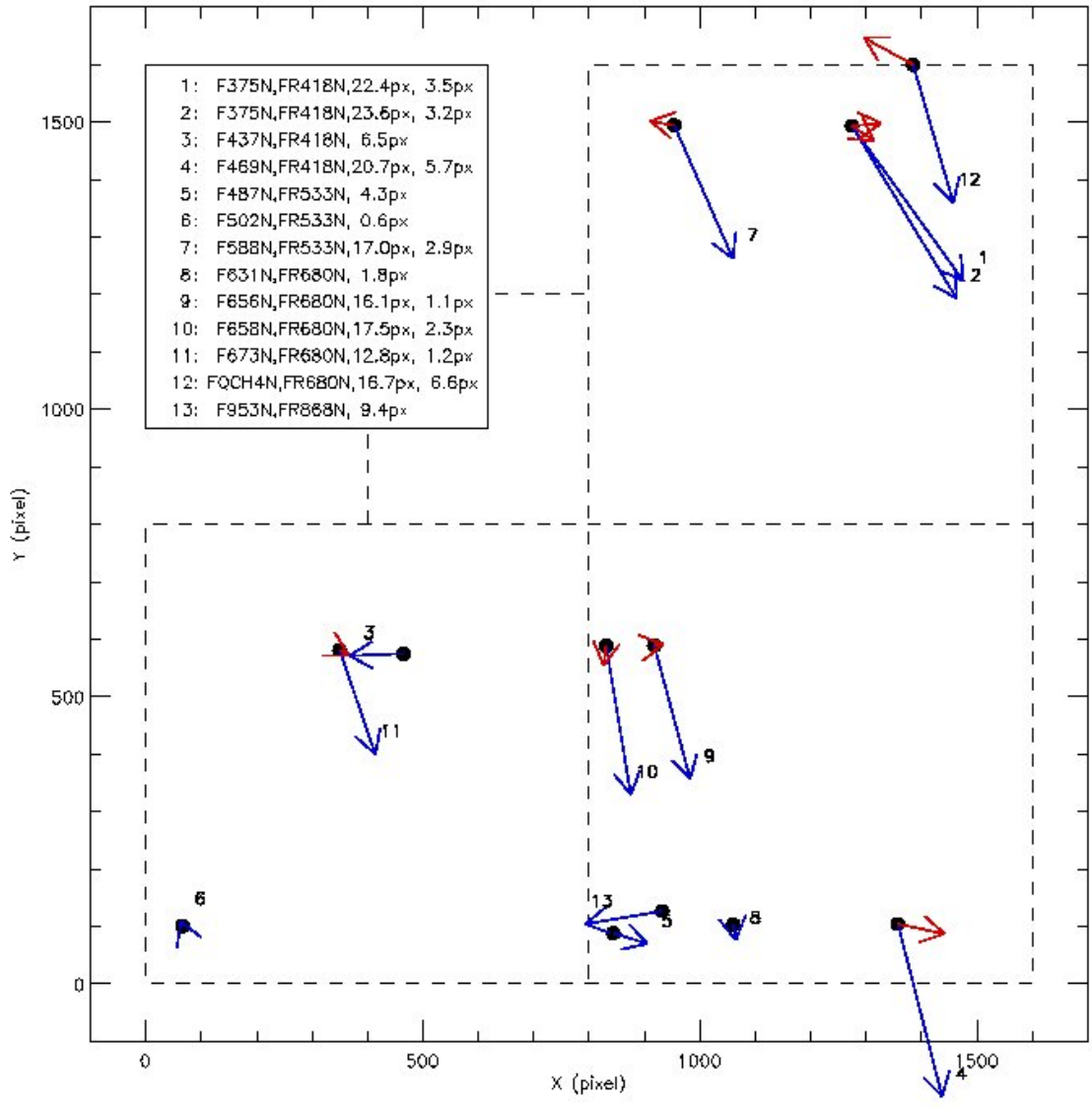

[c] Counting multiple datasets and filter rotations together.

Figure 3: Same as Figure 2, but for rotated LRF.

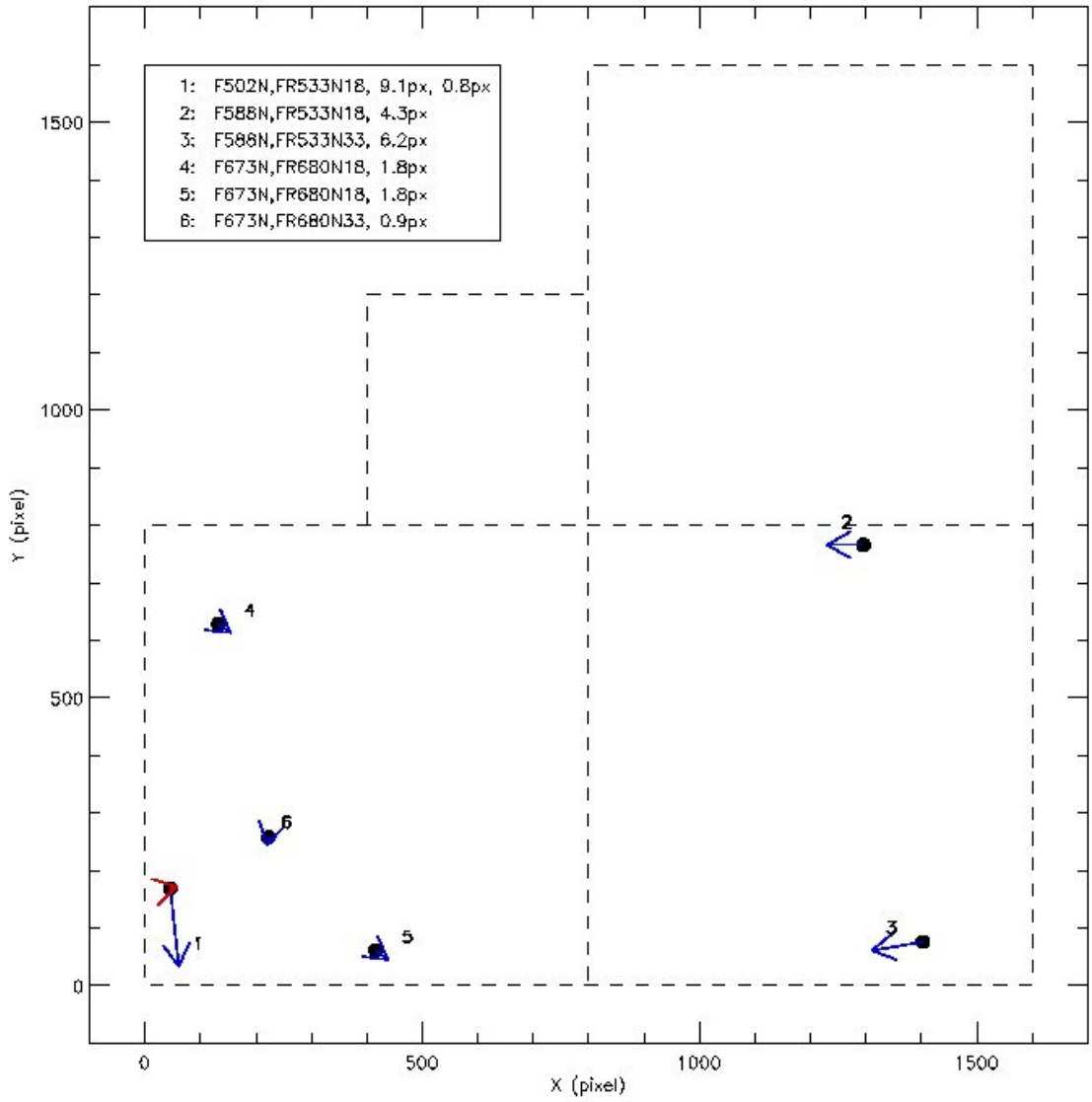

pairing. The second largest change is for FR680N+FQCH4N-C, for which Δλ is 1.8 Å after correcting for the filter wheel rotation anomaly. Expressed as a fractional change in the central wavelength, the largest change is 1 part in 2500 for the FR868N+F953N, followed by 1 part in 3900 for FR418N+F437N. In several cases there are multiple observations (e.g. FR418N+F375N) or pairings with several rotations of the LRF filters (e.g. F588N and F673N), and these results are always consistent within the measurement uncertainties.

In all cases the measured wavelength change is much smaller than the filter bandwidths, so should have little or no consequence for most science observations. The largest change in the central wavelength expressed as a fraction of the bandwidth (effective width) is for

the FR868N+F953N pairing, where the change is 7% of the bandwidth. The next largest changes are for the FR418N+F437N, FR418N+F469N, and FR680N+FQCH4N-C pairings, where the respective change is 4% to 5% of the bandwidth. Pairings involving the narrow band filters used most often – F502N, F656N, F658N, and F673N – all showed fractional changes less than about 1% ± 1%[d].

The twelve filter pairings measured here all appear to be relatively stable during the 13 years between our test epochs, and this is excellent news for observers. There are, however, nine other narrow band filters which are not amenable to these measurement methods – F343N, F390N, four quads of FQUVN, and three remaining quads of the FQCH4N filter. One of these in particular, F343N, is known to have undergone a large throughput reduction during the WFPC2 mission (Gonzaga & Biretta 2009), so we cannot infer from the present results that all of the WFPC2 filters are stable. Ultimately it would be highly valuable to test all the filters after the de-orbit of WFPC2, if funding can be found to support this activity.

6. Summary

We have used VISFLAT images observed through LRFs crossed with NB filters taken 13 years apart to test the stability of the filter central wavelengths. In total, twelve pairings were tested. Of these, ten were found to be stable to better than 1.1 ± 0.6 Å. The largest change was for FR868N+F953N ($\Delta\lambda$ = 3.8 Å) and the second largest change was for FR680N+FQCH4N-C ($\Delta\lambda$ = 1.8 Å). Expressed as a fraction of the bandwidth of the filters, the largest wavelength change was again for FR868N+F953N of 7%, with several other filters showing changes that were 4% to 5% of the bandwidth.

In general, these changes are small enough to have no impact on most science observations. The narrow band filters most often used for science observations – F502N, F656N, F658N, and F673N – were among those tested, and all showed changes in central wavelength of $\lesssim$1% ± 1% of their bandwidth. There are many other WFPC2 filters, however, which are not amenable to this testing method, and post-mission laboratory tests remain highly desirable.

Acknowledgements

We would like to thank Dr. John Trauger (PI of the WFPC2 instrument team at JPL) for his encouragement on this project. We also thank Dr. Ralph Bohlin and Dr. Van Dixon for their helpful comments.

[d] Fractional change uncertainty is calculated using approximate $\Delta\lambda$ uncertainties and WFPC2 Instrument Handbook filter bandwidths.

References

Baggett, S., et al. 2002, in HST WFPC2 Data Handbook, v. 4.0, ed. B. Mobasher, Baltimore, STScI

Biretta, J., Ritchie, C., Baggett, S., & MacKenty, J. 1996, "Wavelength/Aperture Calibration of the WFPC2 Linear Ramp Filters," WFPC2 Instrument Science Report 96-05

Gonzaga, S., Baggett, S., & Biretta, J. 2002, "An Analysis of WFPC2 Filter Positional Anomalies," WFPC2 Instrument Science Report 02-04

Gonzaga, S., & Biretta, J. 2009, "WFPC2 F343N Filter Throughput Decline," WFPC2 Instrument Science Report 09-02

Koekemoer, A. M., Biretta, J., & Mack, J. 2002, "Updated WFPC2 Flatfield Reference Files for 1995 - 2001," WFPC2 Instrument Science Report 02-02

McMaster, M., Biretta, J., et al. 2008, WFPC2 Instrument Handbook, Version 10.0 (Baltimore: STScI)

O'Dea, C., Mutchler, M., & Wiggs, M. 1999, "Internal Flat Field Monitoring II. Stability of the Lamps, Flat Fields, and Gain Ratios," WFPC2 Instrument Science Report 99-01

Potter, J. R., & Simons, J. C. 1993, "Stability of IAD Refractory Oxide Narrowband Interference Filters," Proc. SPIE 1952, 186

Appendix A: VISFLAT Spot Position/Shift Measurement Plots

The figures in this section show spot position fits for VISFLAT exposures, as explained in Sections 4.1 and 4.2 and tabulated in Table 3 and Table 4. Gaussian fitting is primarily used, but cross-correlation or visual measurement, if applied, is shown as well. The order shown is same as the tables. Prefixes *u2mm* and *u9w1* correspond to *Epoch 1* and *Epoch 2* respectively.

For each Gaussian fit plot, the upper panel shows the spot profile (blue dashed line) along X (λ direction) and the lower panel Y (spatial direction). The fit itself is the red curve, with its peak (the measured spot position) marked by a red line. The yellow dotted region is the profile area used for fitting, a default half-width of 150 pixels adjusted for edge truncation. The plot title gives the image name with a spot number in parenthesis. Only images for FR680N18+F673N have more than one spot on the mosaic.

For each cross-correlation or visual measurement plot, only spot profiles along Y (blue curve being *Epoch 1* and red curve *Epoch 2*) are shown. The dashed lines are borders for the manually selected region used for shift measurement. Profiles in this region are normalized and displayed in the lower panel. Plot title names the images involved. The dashed curve in the lower panel is the blue profile shifted to match the red. Measured shift is labeled in the lower left corner of the lower panel, with "*C-CORR*" meaning cross-correlation and "*BY EYE*" visual measurement.

I. FR418N + F375N

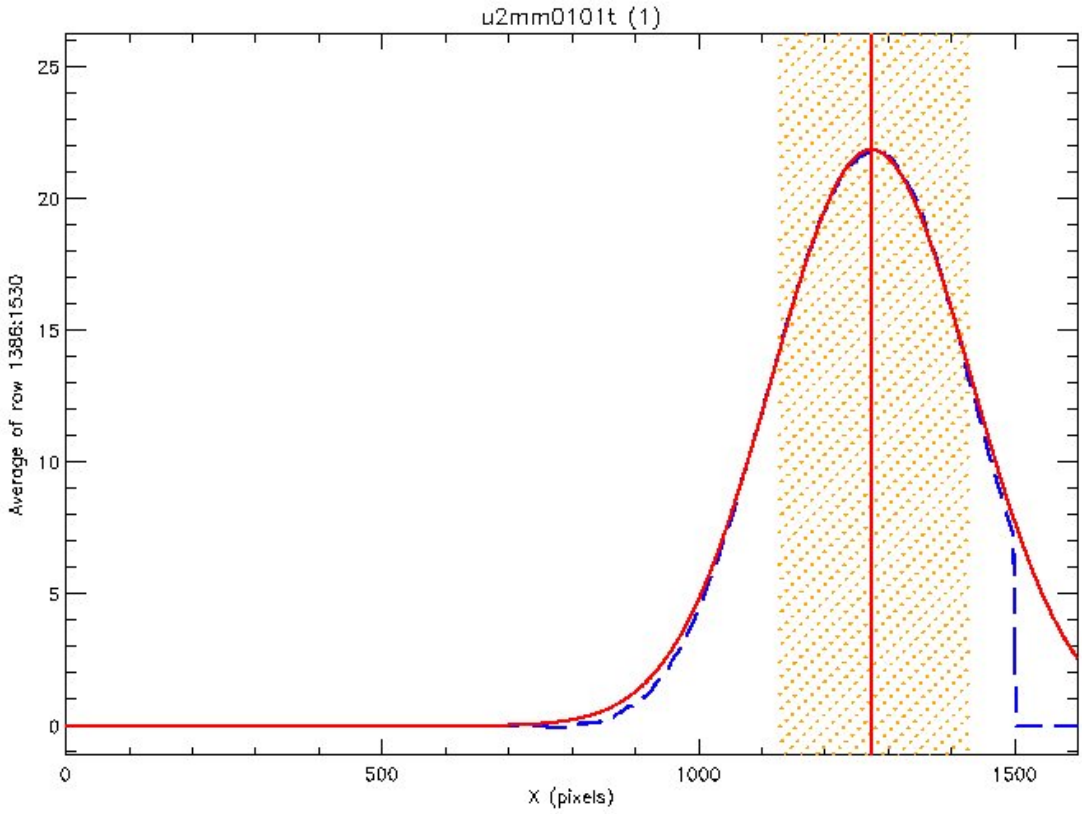

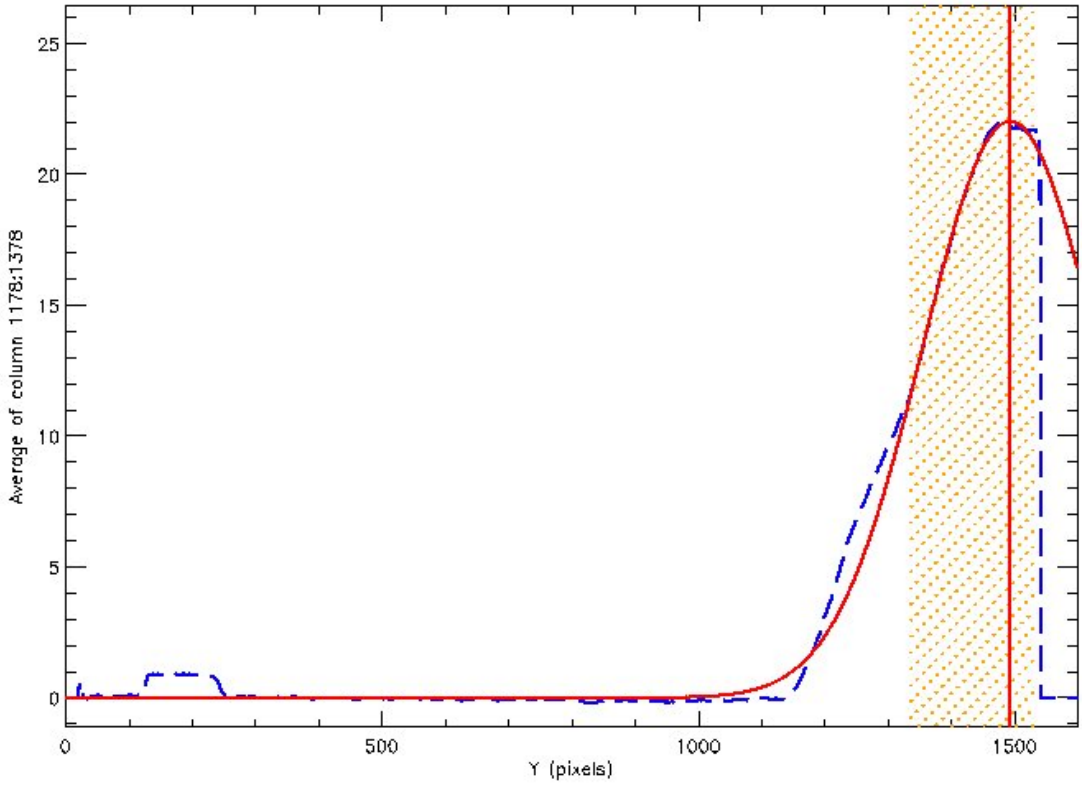

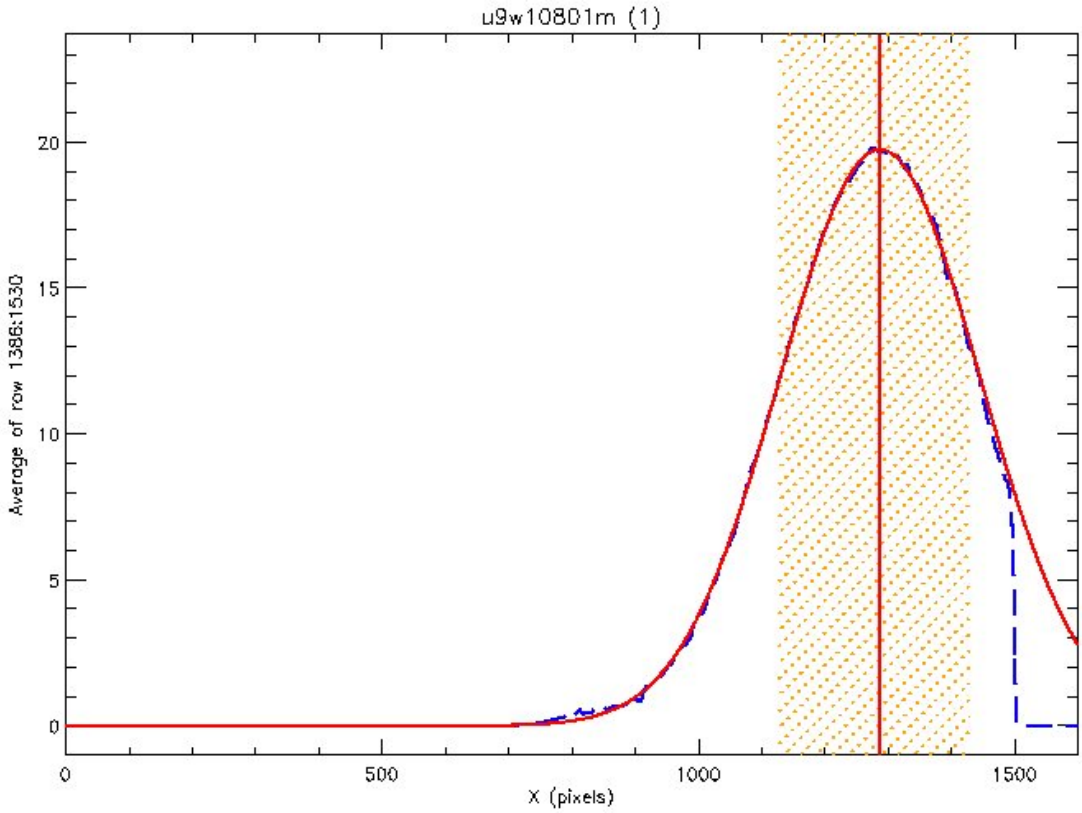
u9w10801m (1)
Average of row 1386:1530
X (pixels)
0
500
1000
1500
0
5
10
15
20

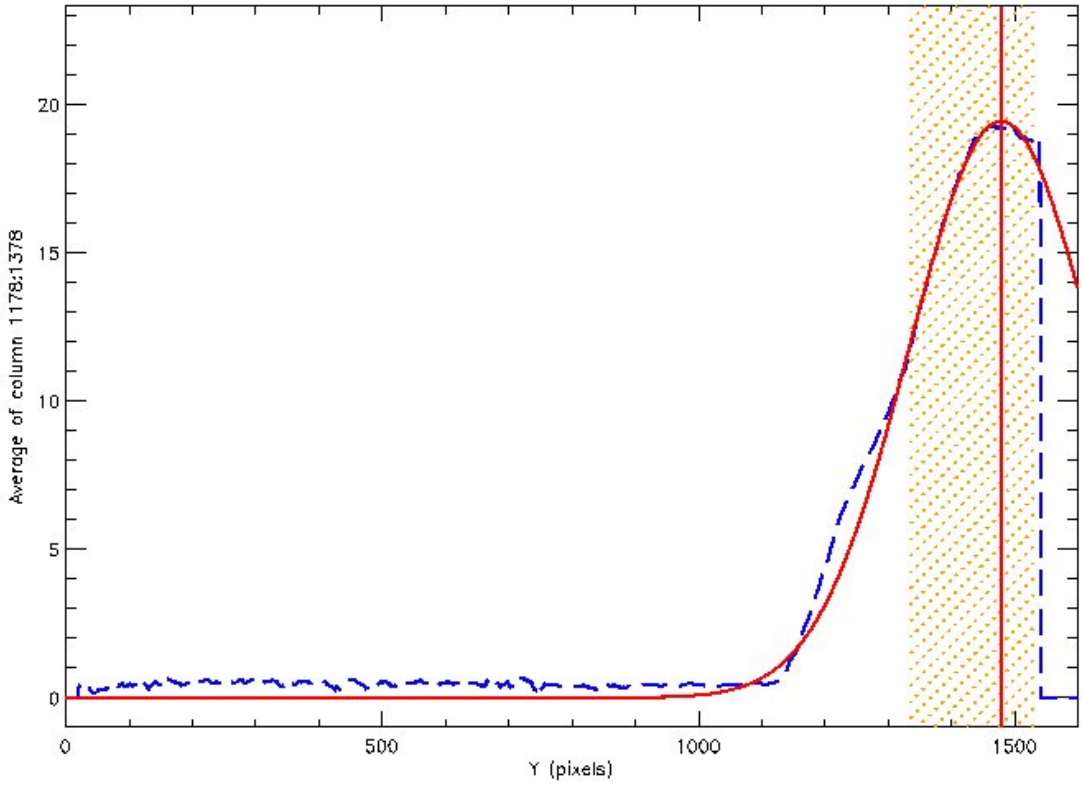
Average of column 1178:1378
Y (pixels)
0
500
1000
1500
0
5
10
15
20

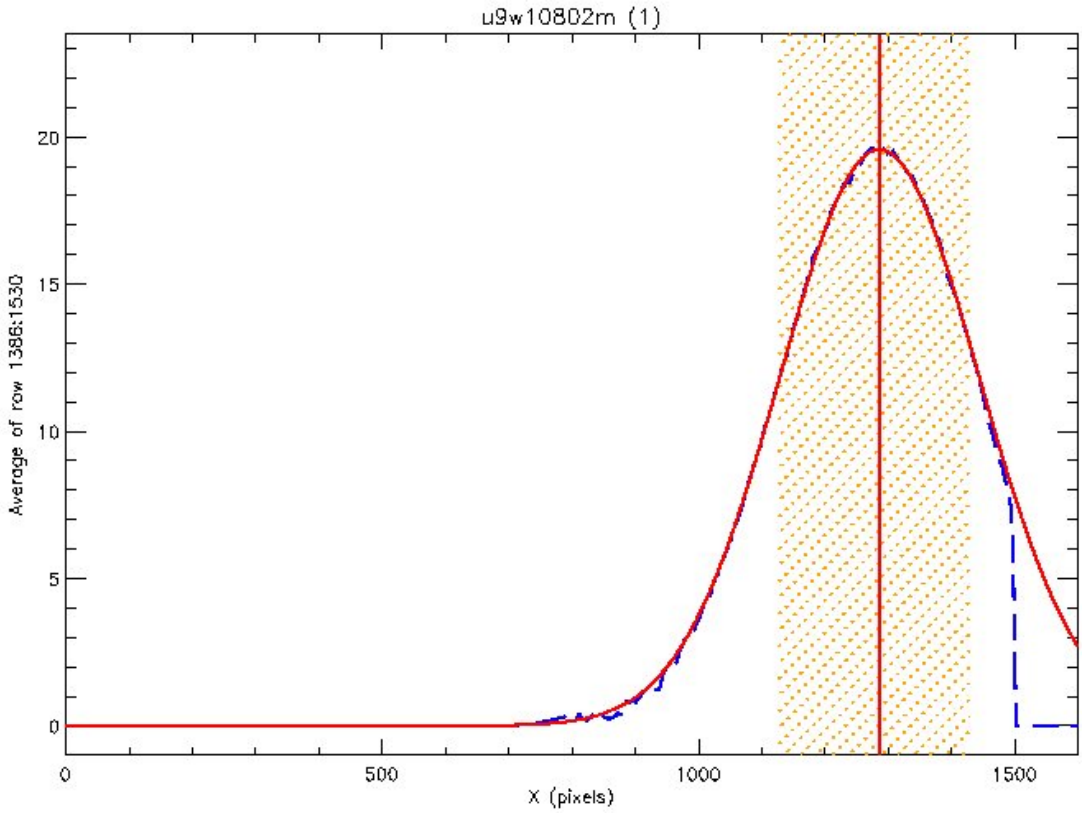
u9w10802m (1)
Average of row 1386:1530
X (pixels)
0
5
10
15
20
0
500
1000
1500

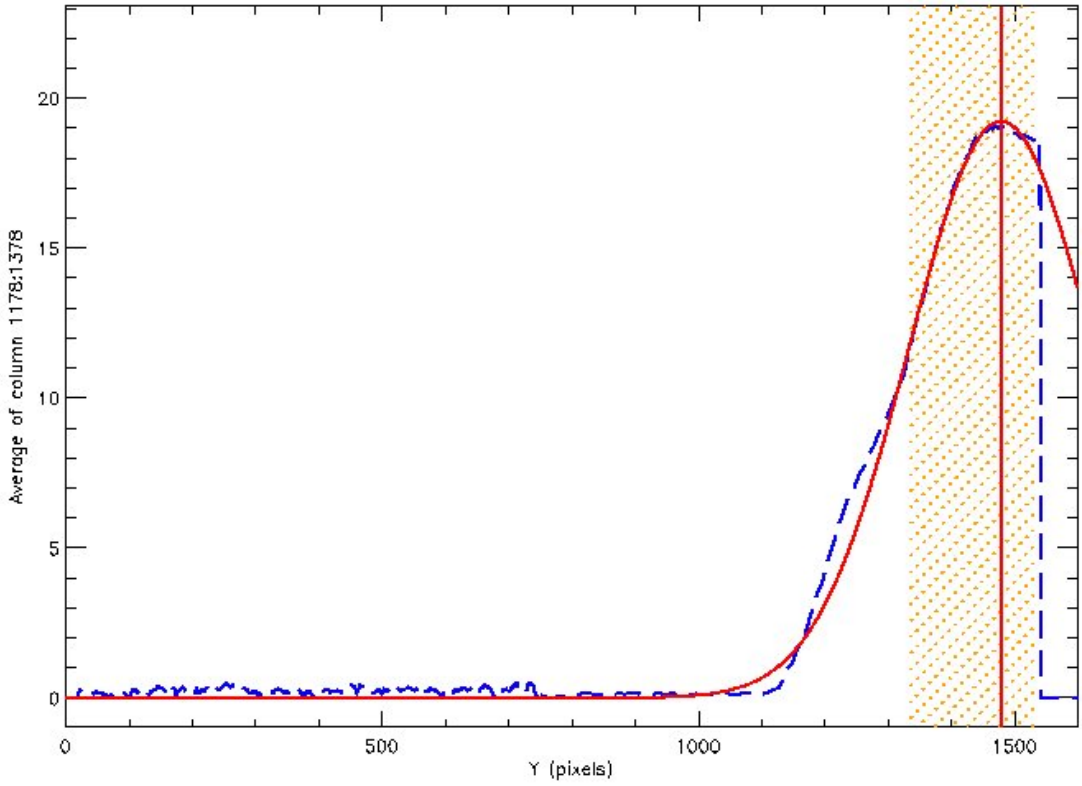
Average of column 1178:1378
Y (pixels)
0
5
10
15
20
0
500
1000
1500

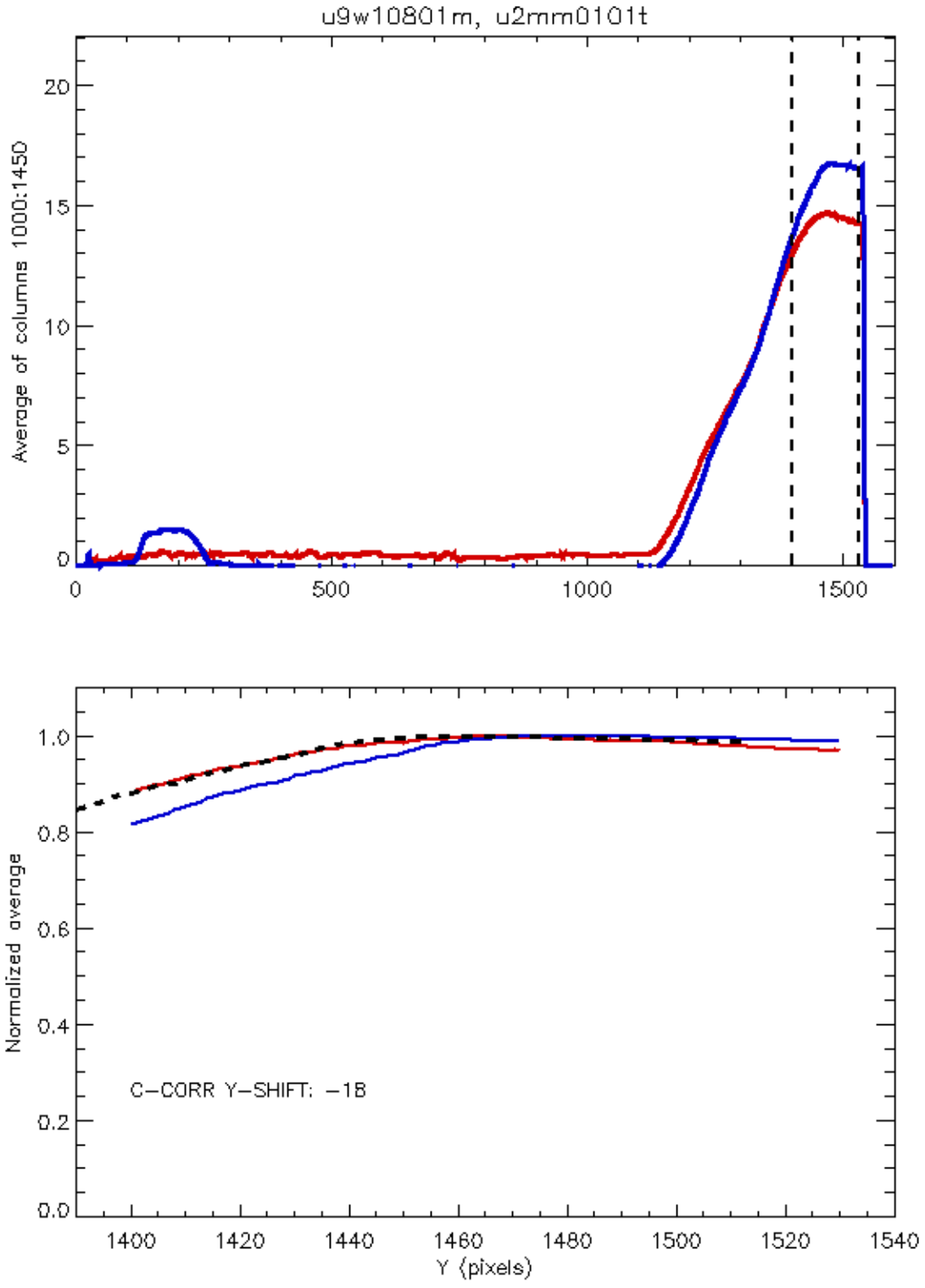
u9w10801m, u2mm0101t
Average of columns 1000:1450
0
5
10
15
20
0
500
1000
1500
Normalized average
0.0
0.2
0.4
0.6
0.8
1.0
C-CORR Y-SHIFT: -18
1400
1420
1440
1460
1480
1500
1520
1540
Y (pixels)

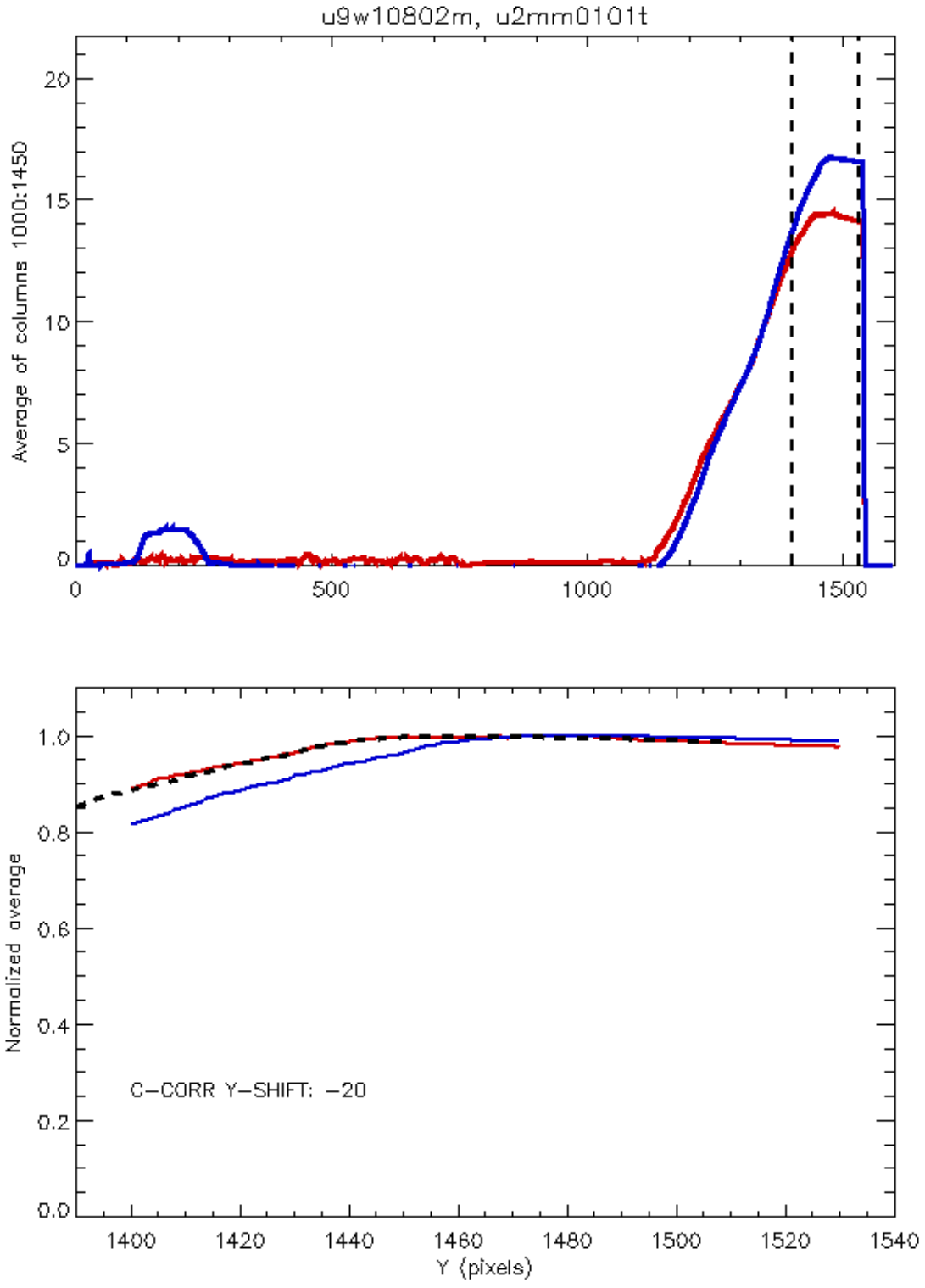
u9w10802m, u2mm0101t
Average of columns 1000:1450
0
5
10
15
20
0
500
1000
1500
Normalized average
0.0
0.2
0.4
0.6
0.8
1.0
C-CORR Y-SHIFT: -20
1400
1420
1440
1460
1480
1500
1520
1540
Y (pixels)

II. FR418N + F437N

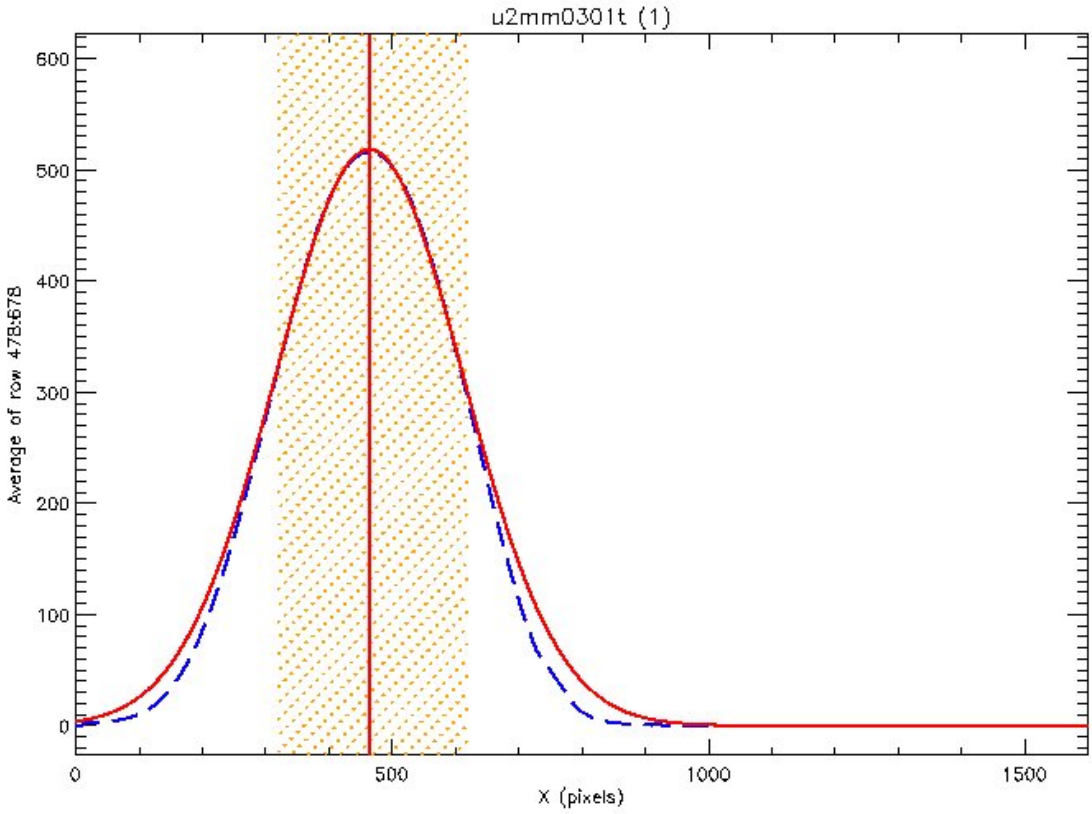

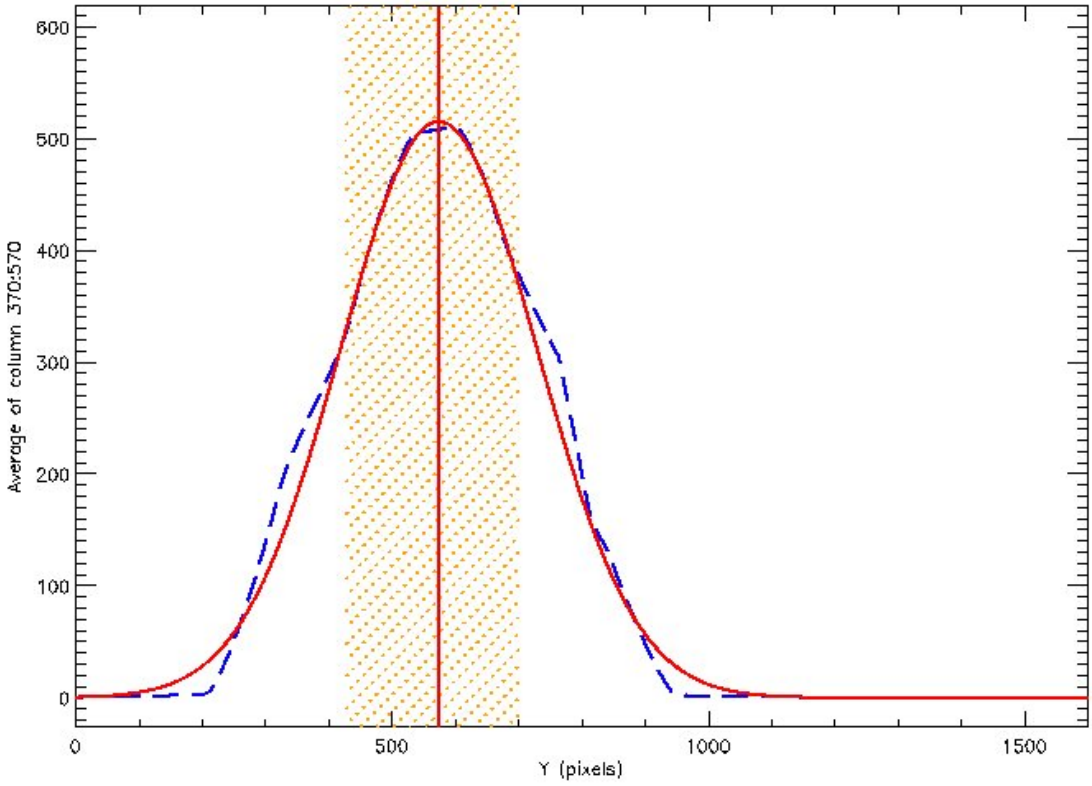

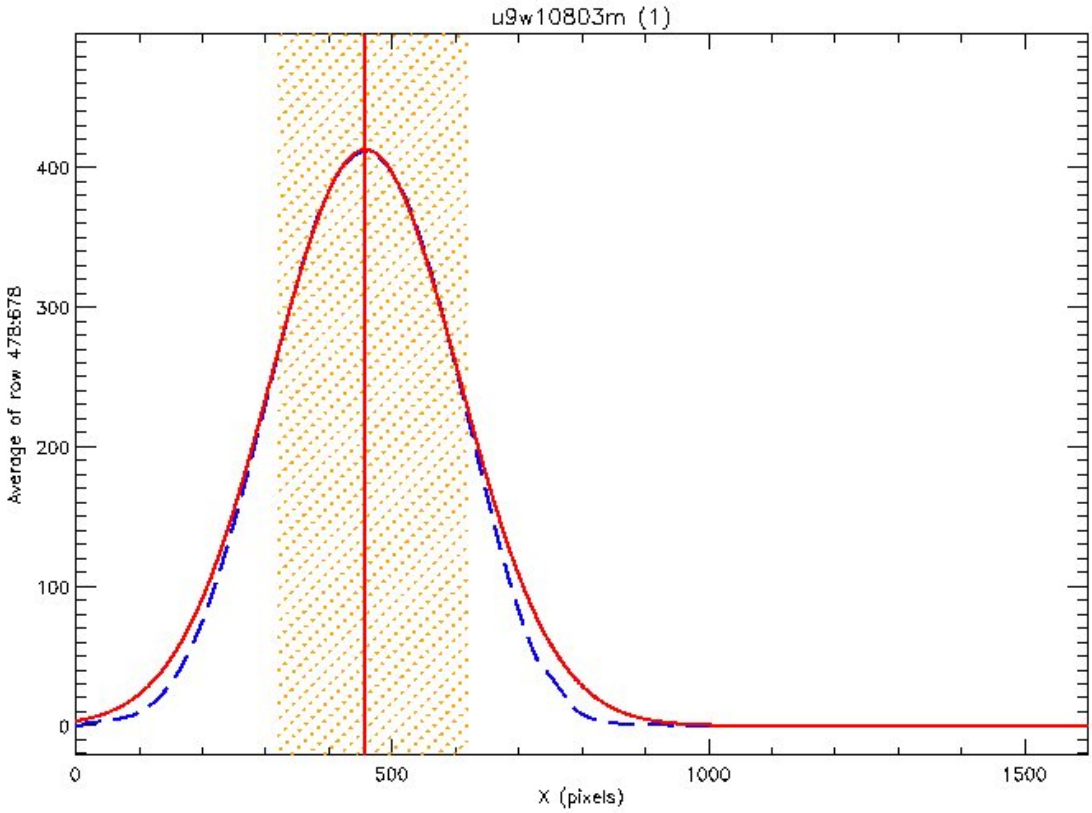
u9w10803m (1)
Average of row 478:678
X (pixels)
0
100
200
300
400
0
500
1000
1500

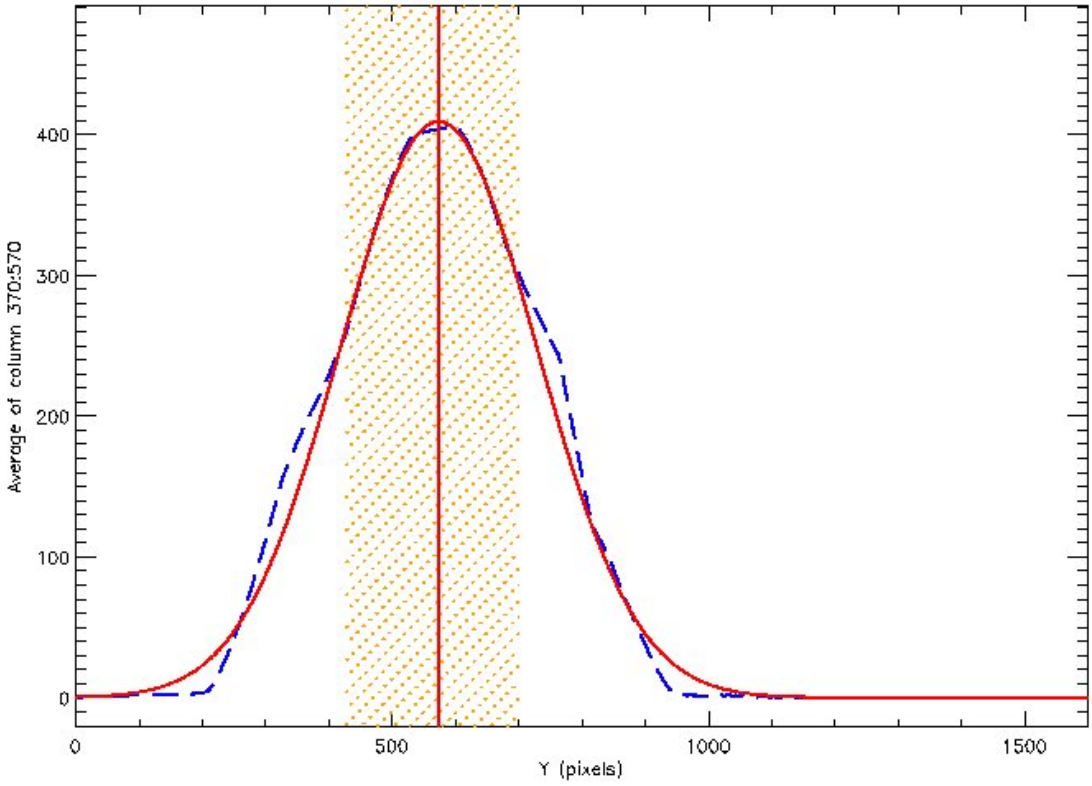
Average of column 370:570
Y (pixels)
0
100
200
300
400
0
500
1000
1500

III. FR418N + F469N

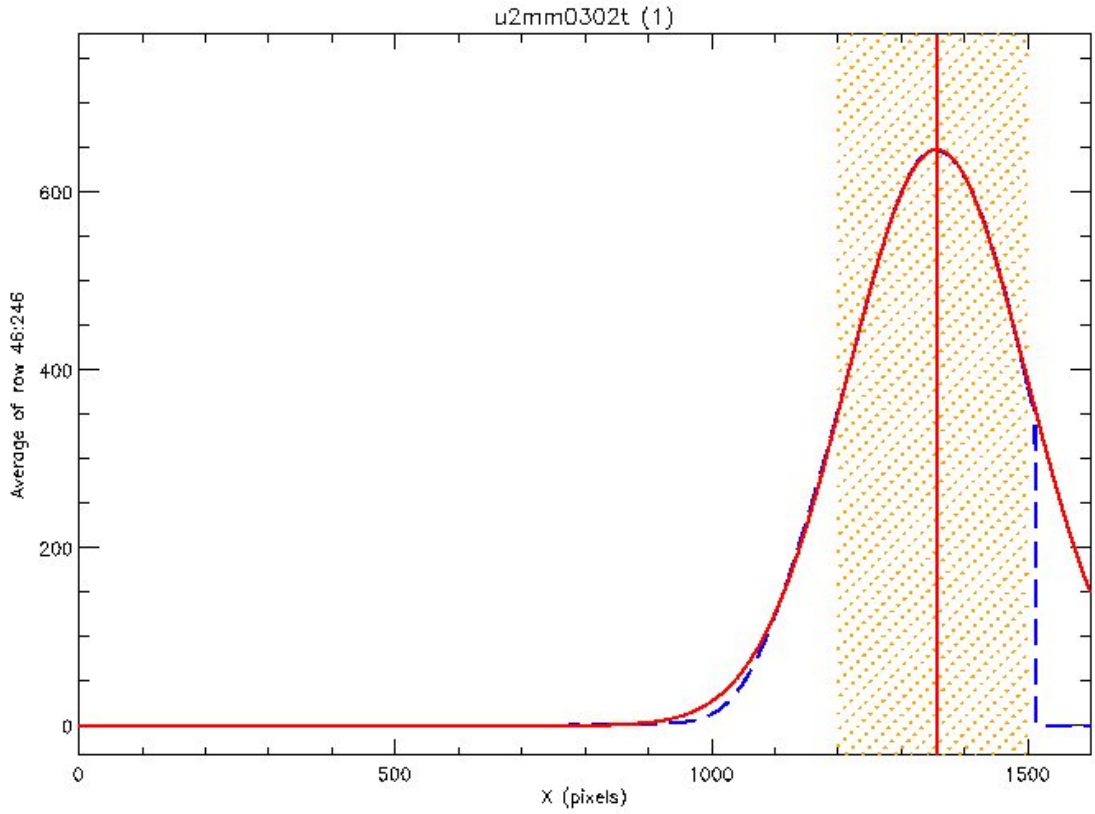

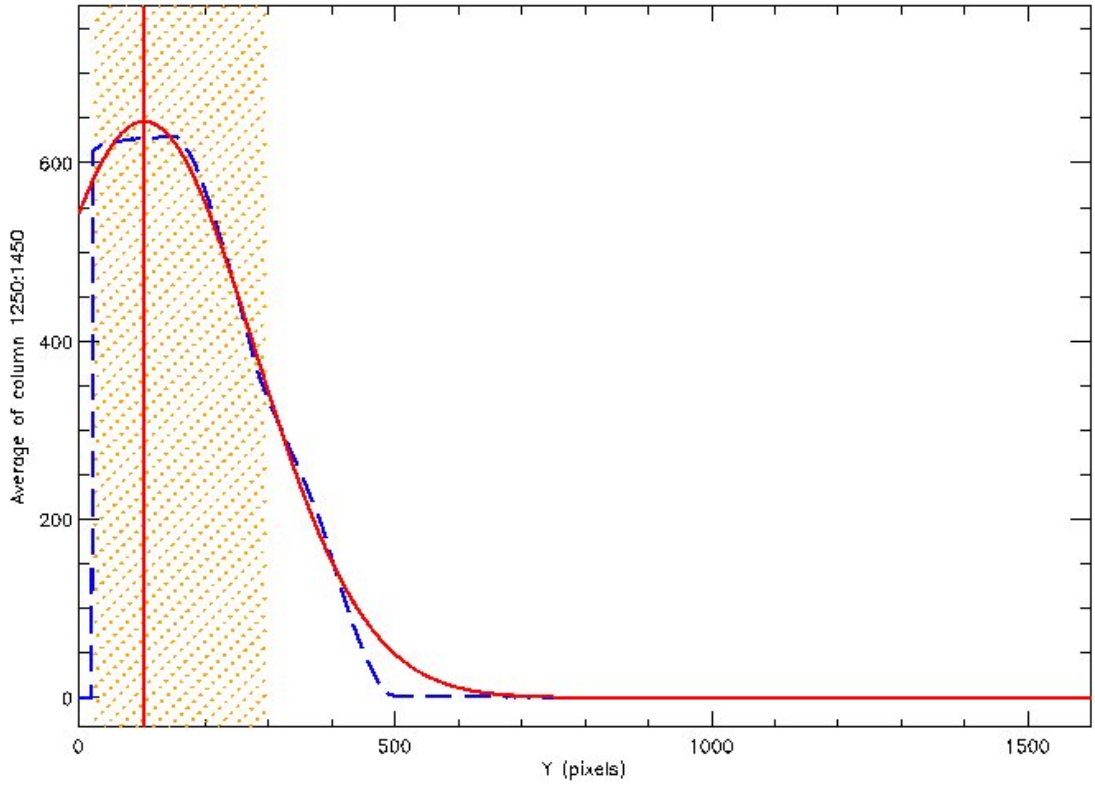

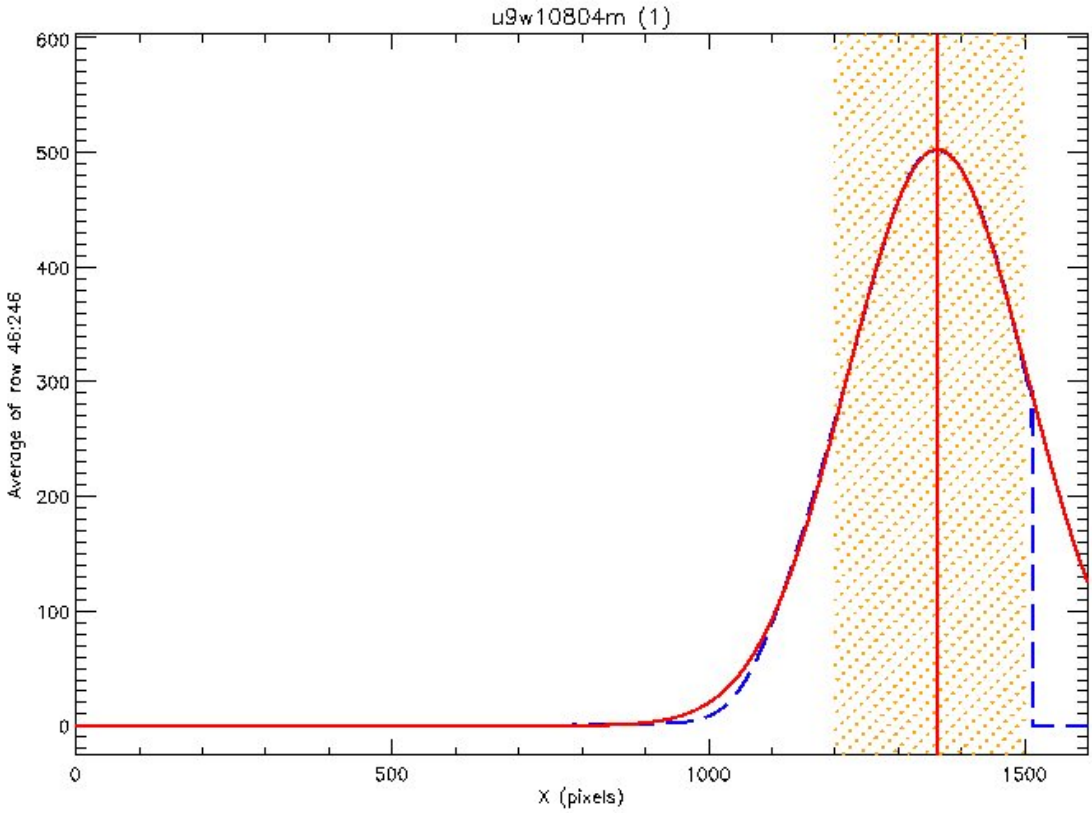
u9w10804m (1)
Average of row 46:246
X (pixels)
0
100
200
300
400
500
600
0
500
1000
1500

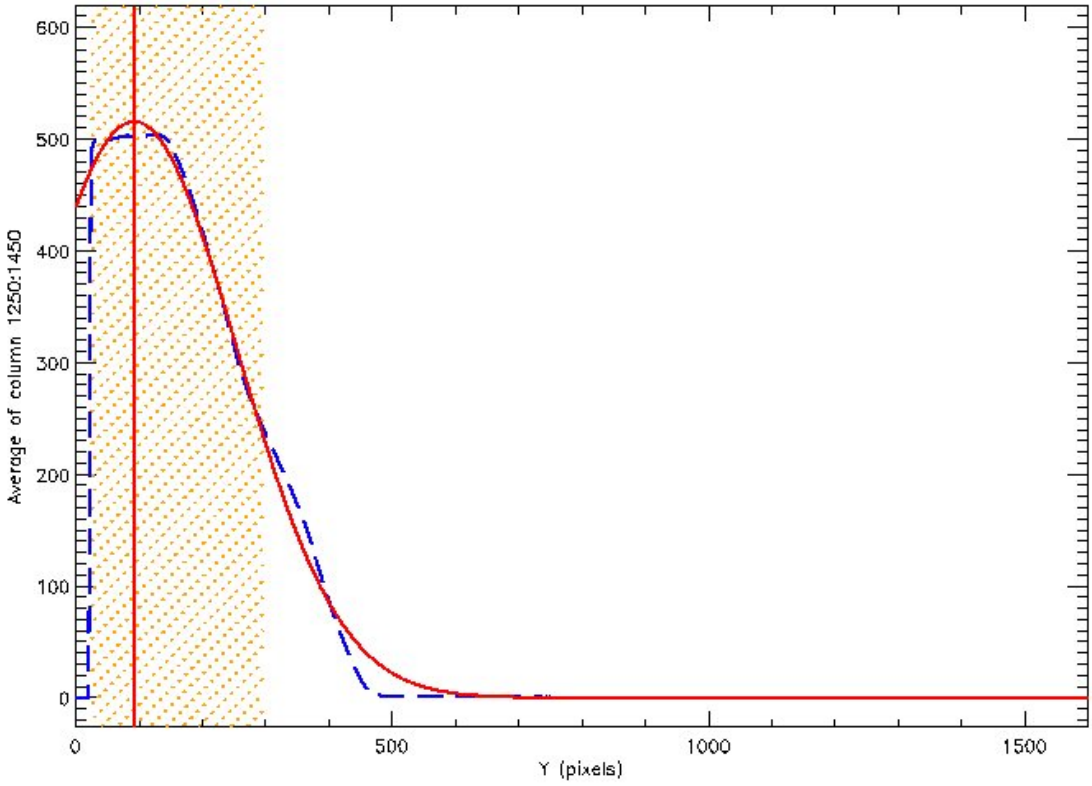
Average of column 1250:1450
Y (pixels)
0
100
200
300
400
500
600
0
500
1000
1500

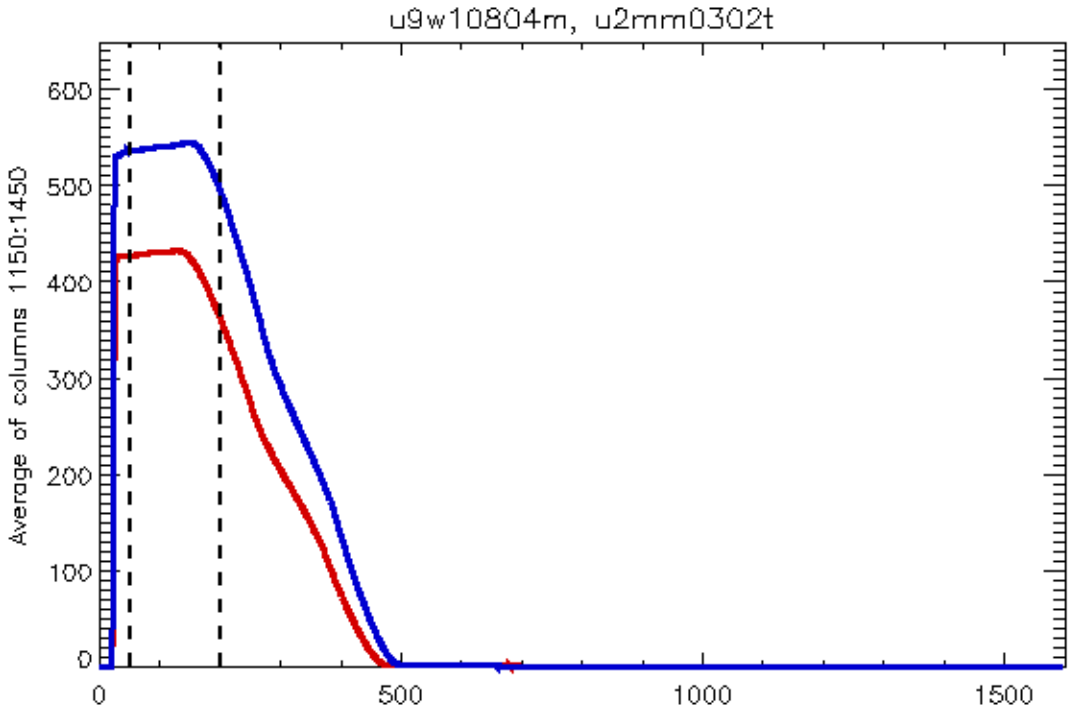
u9w10804m, u2mm0302t
Average of columns 1150:1450
600
500
400
300
200
100
0
0
500
1000
1500

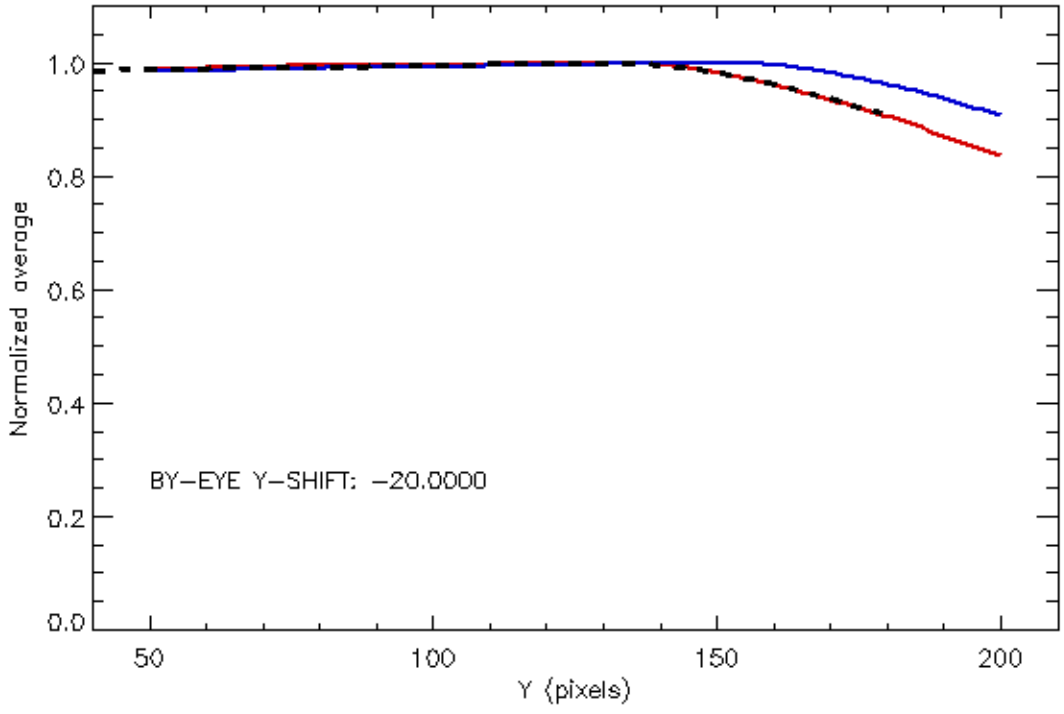
Normalized average
1.0
0.8
0.6
0.4
0.2
0.0
BY-EYE Y-SHIFT: -20.0000
50
100
150
200
Y (pixels)

IV. FR533N + F487N

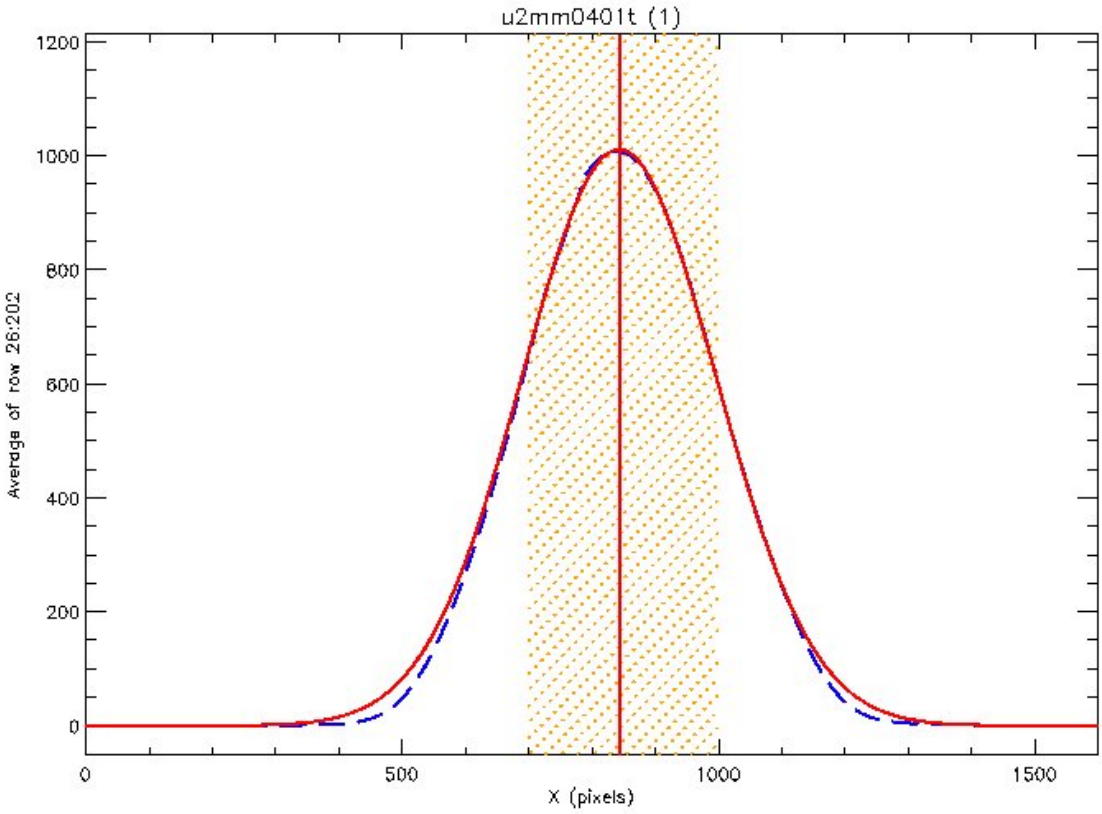

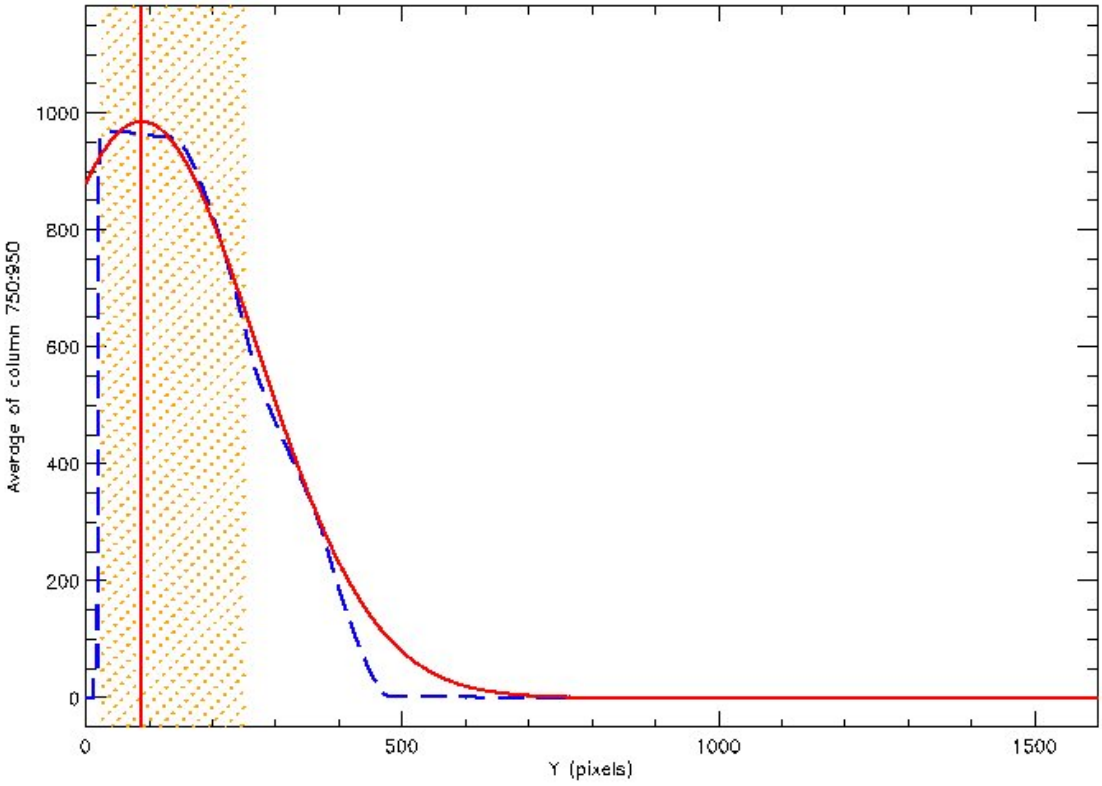

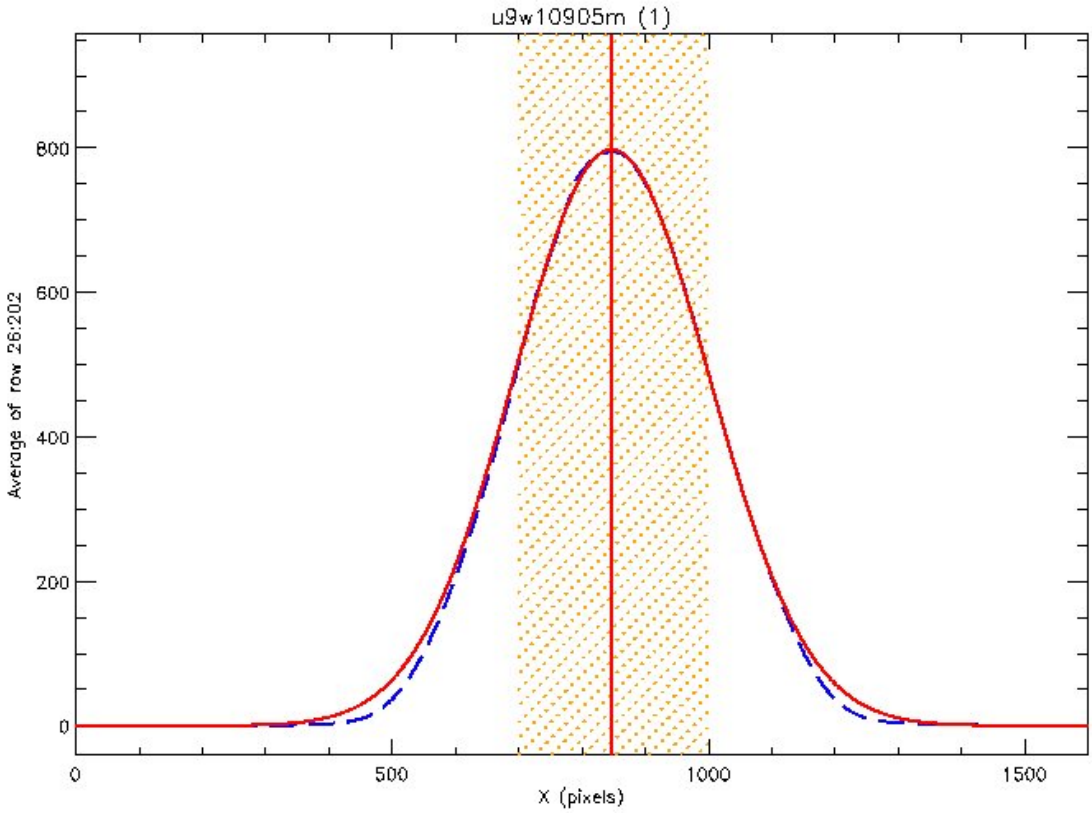
u9w10905m (1)
Average of row 26:202
X (pixels)
0
200
400
600
800
0
500
1000
1500

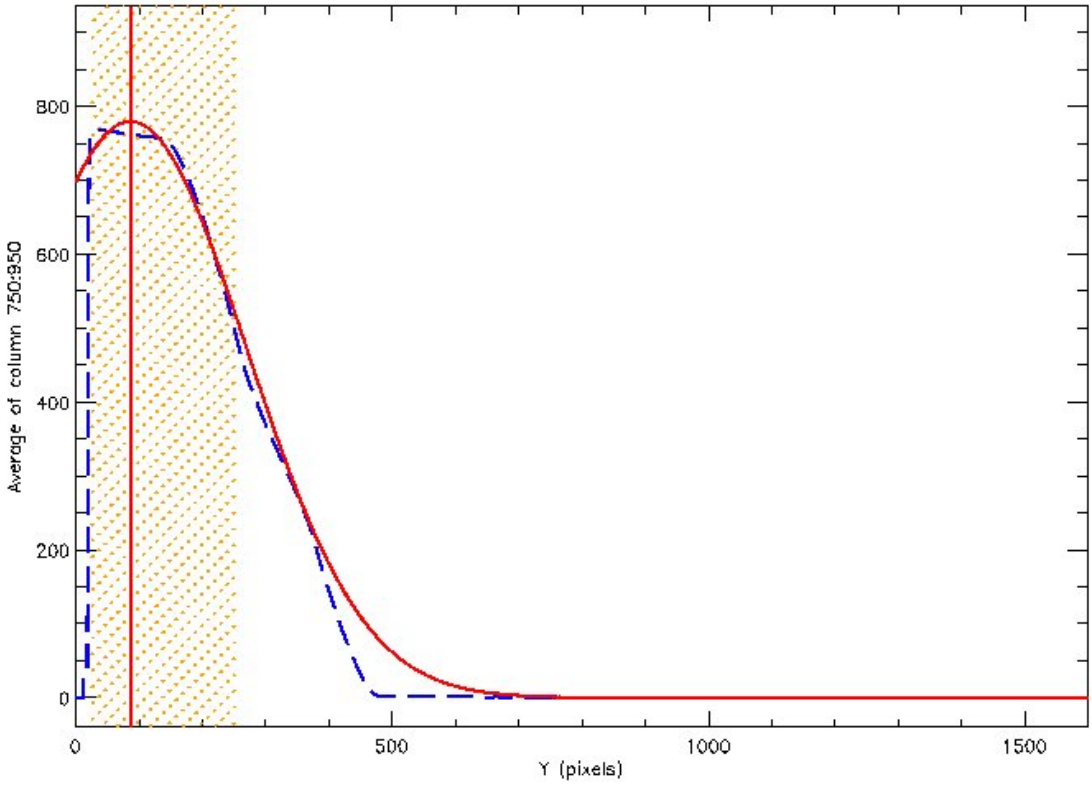
Average of column 750:950
Y (pixels)
0
200
400
600
800
0
500
1000
1500

V. FR533N + F502N

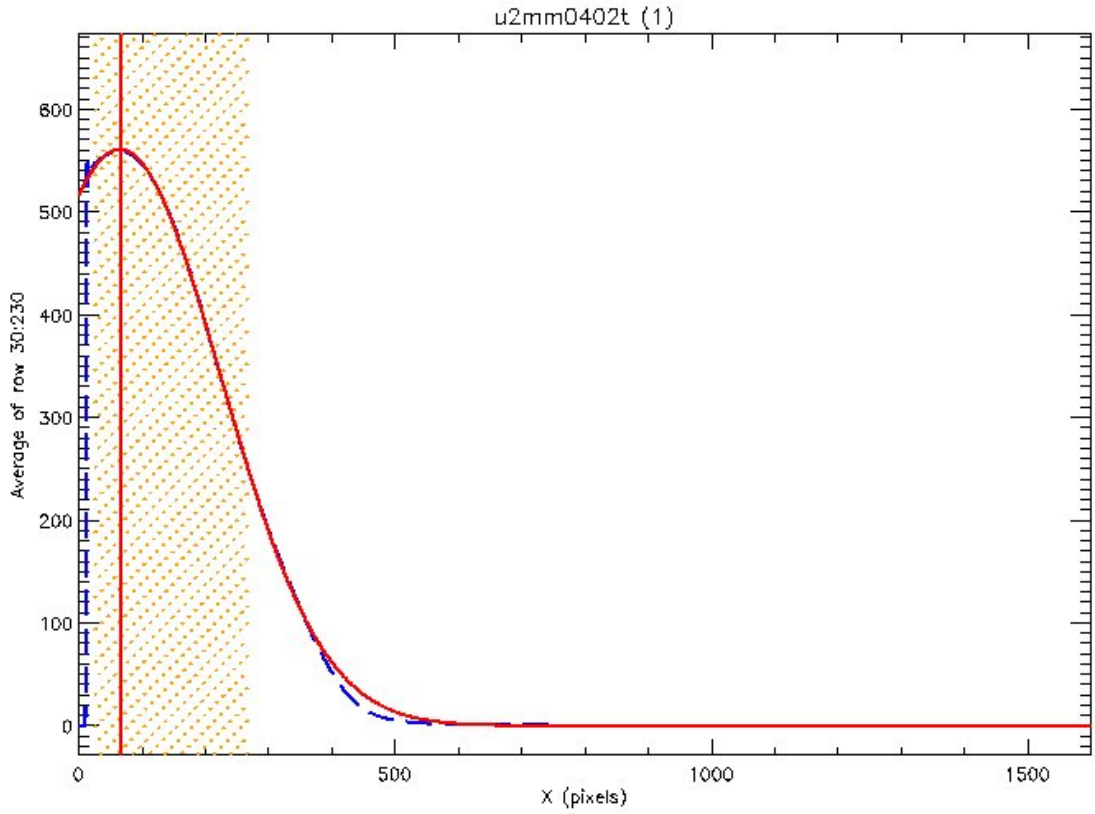

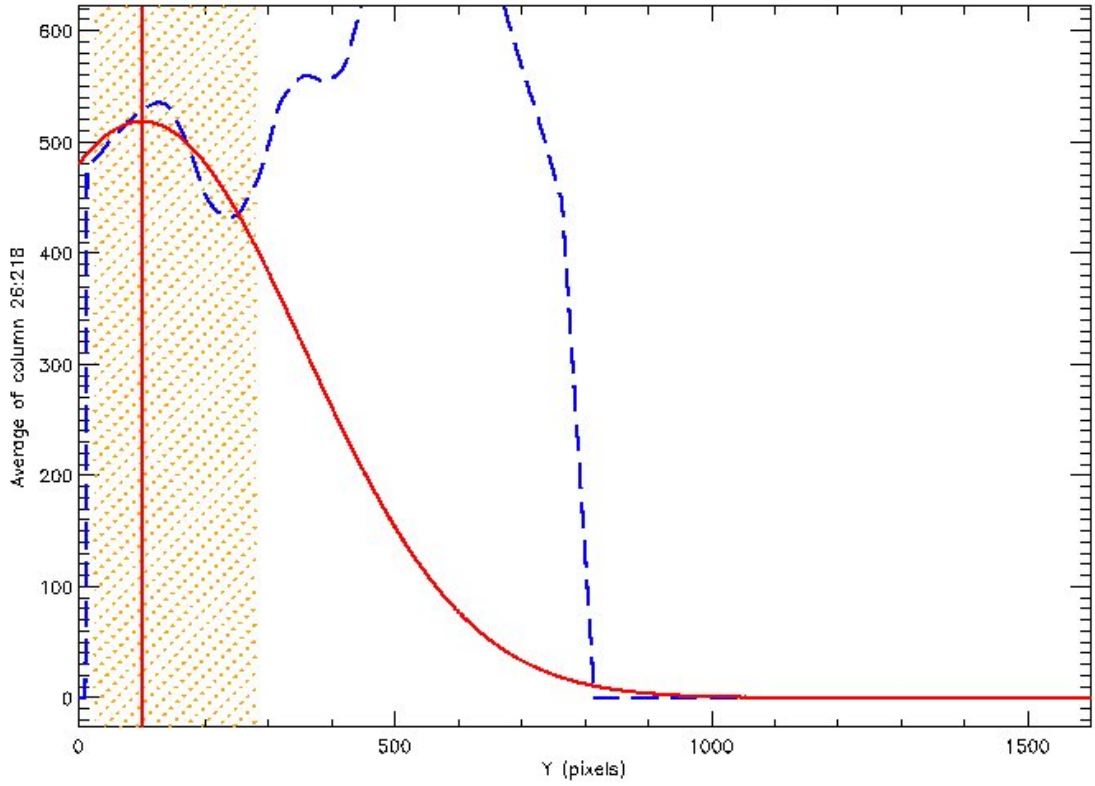

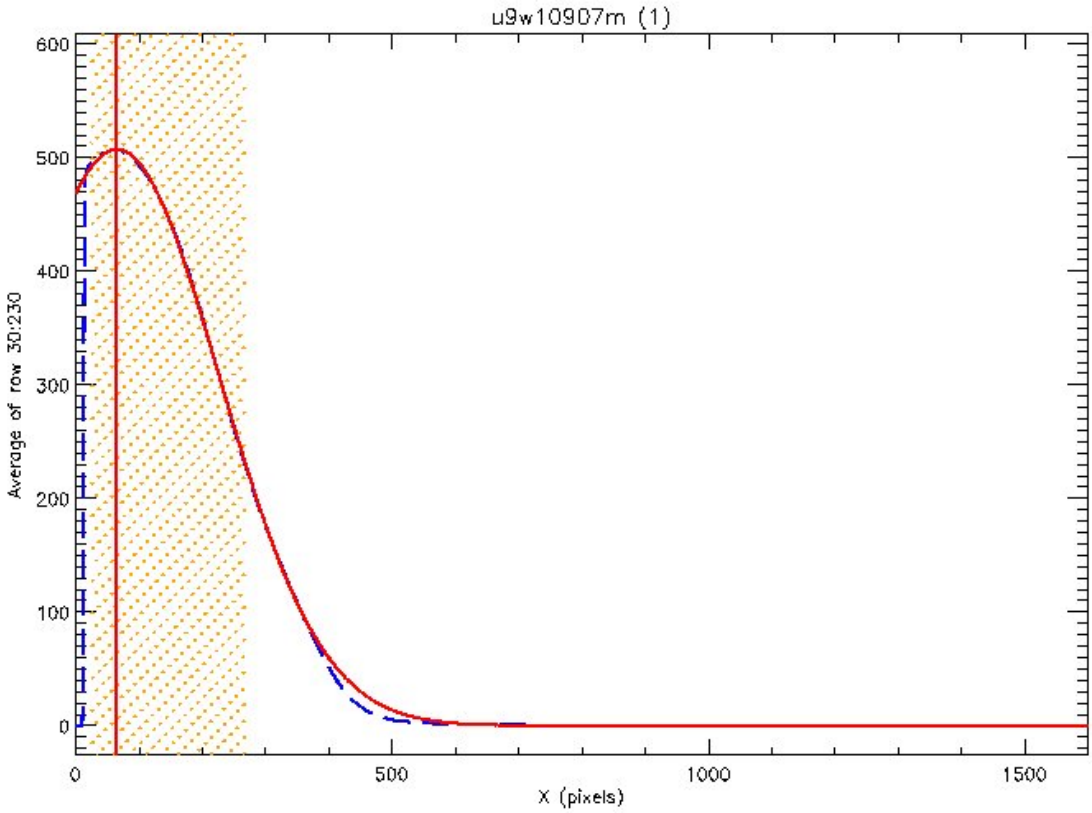
u9w10907m (1)
Average of row 30:230
X (pixels)
0
100
200
300
400
500
600
0
500
1000
1500

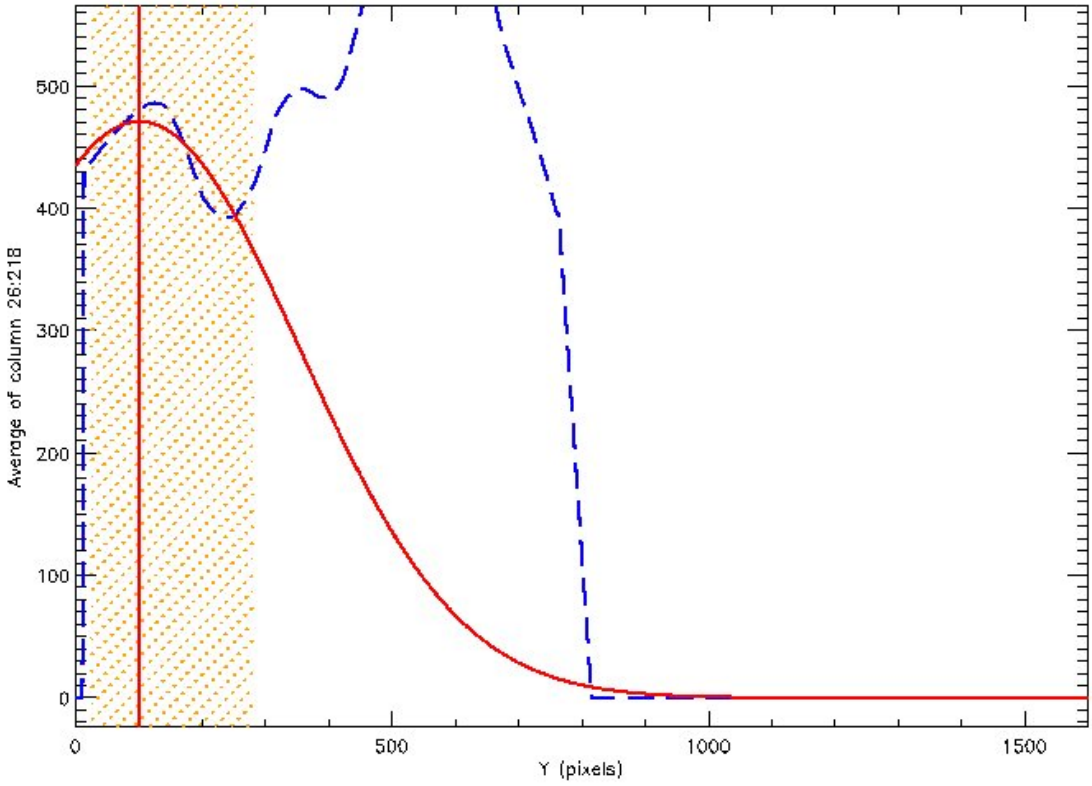
Average of column 26:218
Y (pixels)
0
100
200
300
400
500
0
500
1000
1500

VI. FR533N18 + F502N

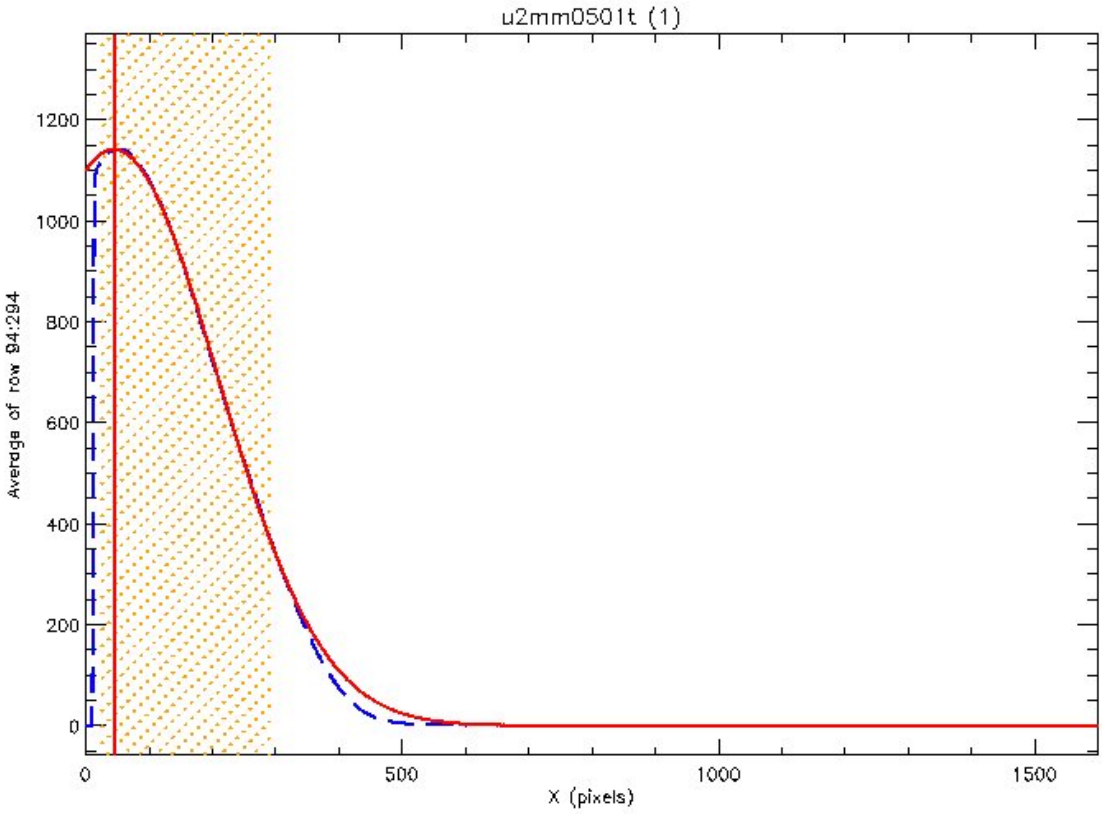

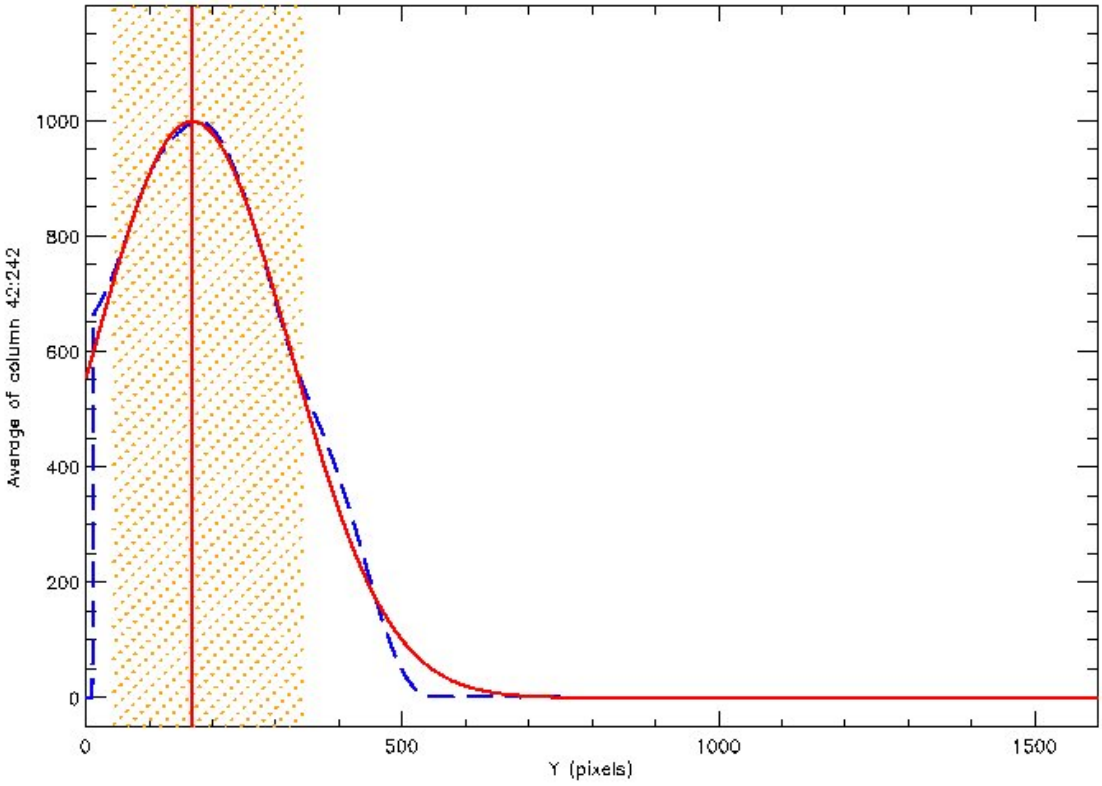

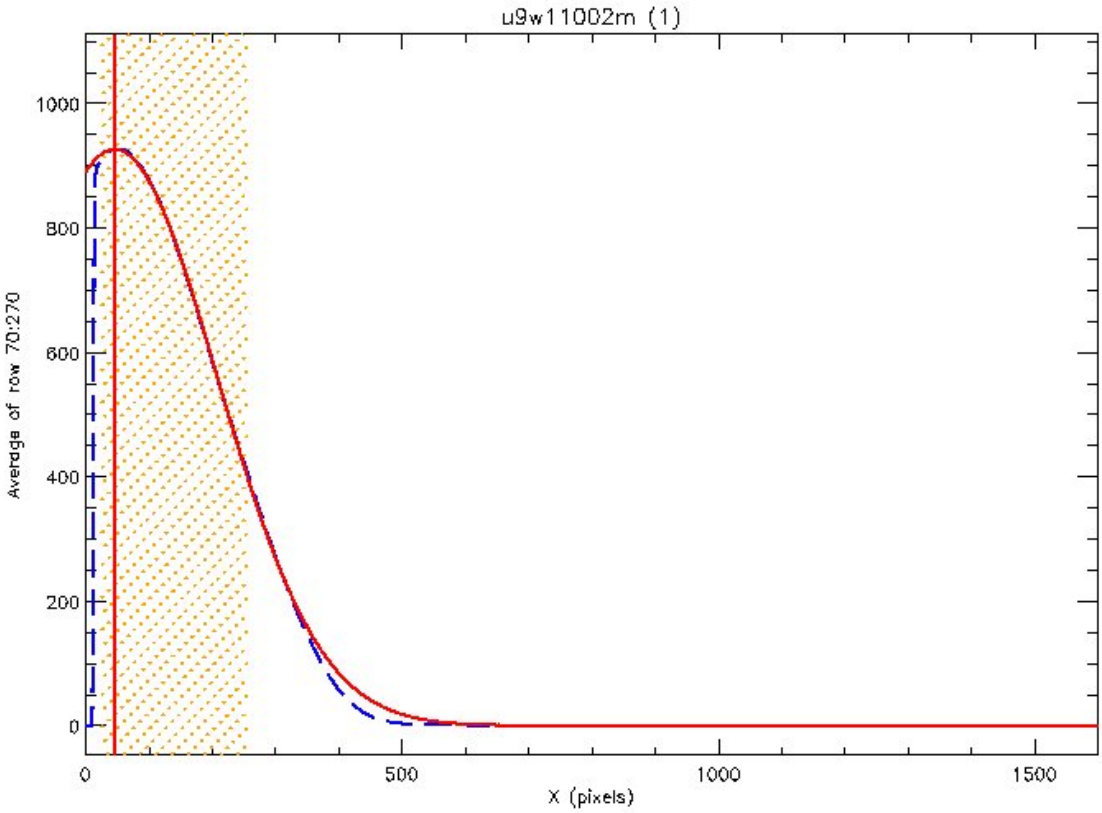
u9w11002m (1)
Average of row 70:270
X (pixels)
0
200
400
600
800
1000
0
500
1000
1500

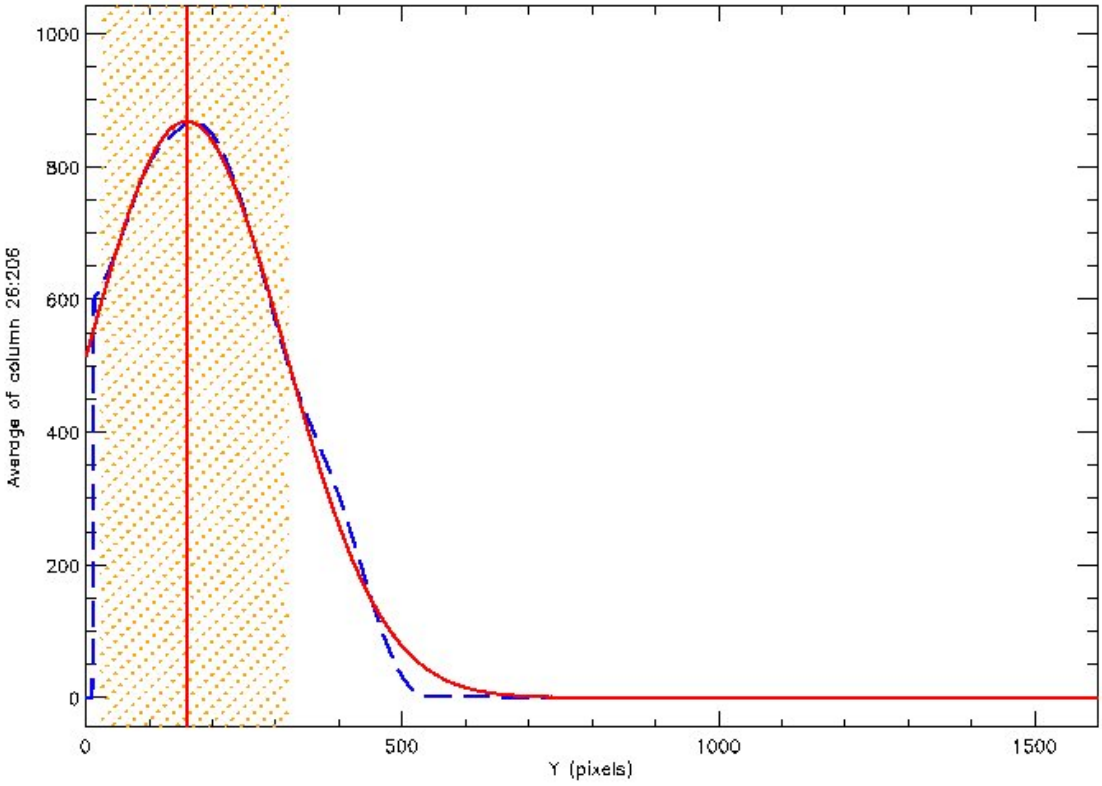
Average of column 26:206
Y (pixels)
0
200
400
600
800
1000
0
500
1000
1500

VII. FR533N + F588N

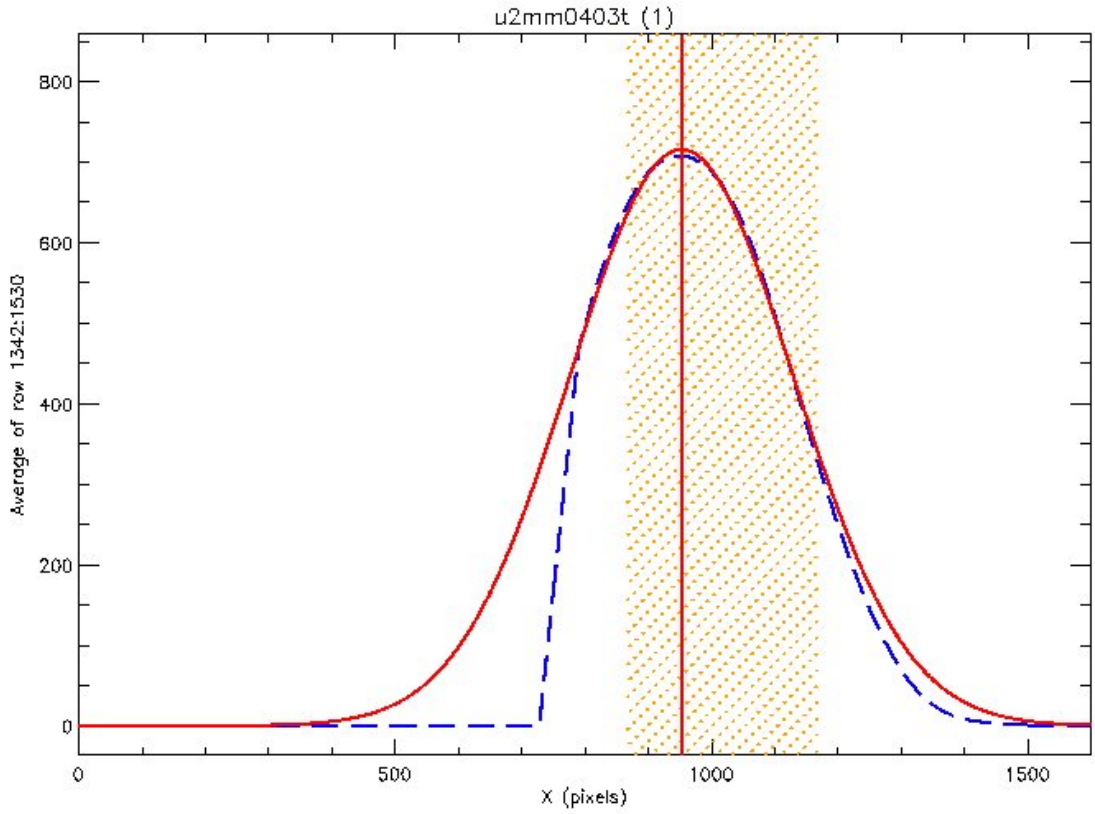

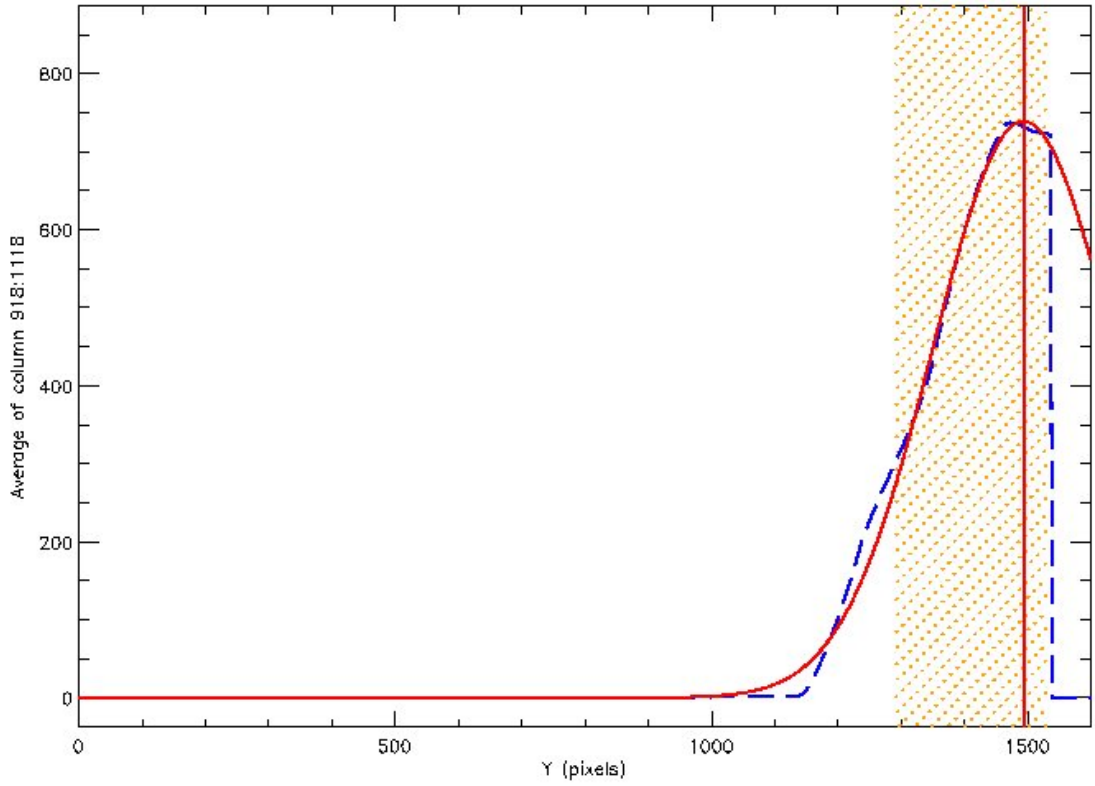

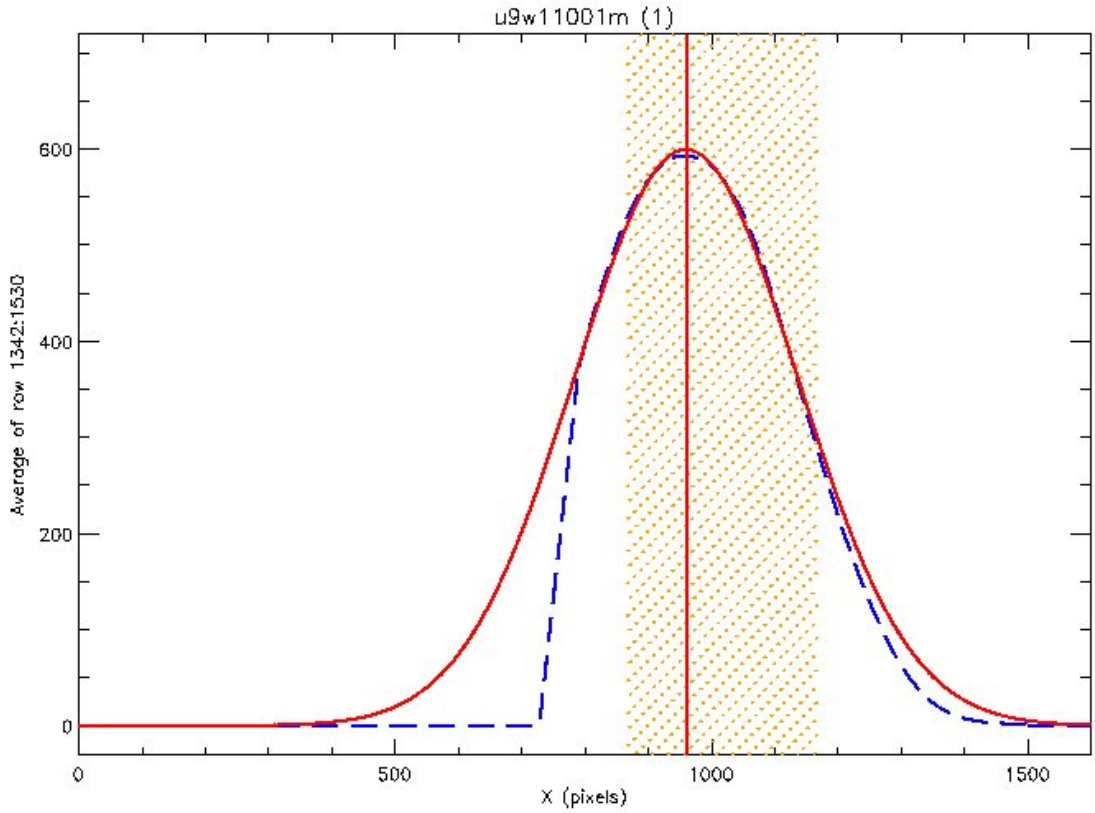
u9w11001m (1)
Average of row 1342:1530
X (pixels)
0
200
400
600
0
500
1000
1500

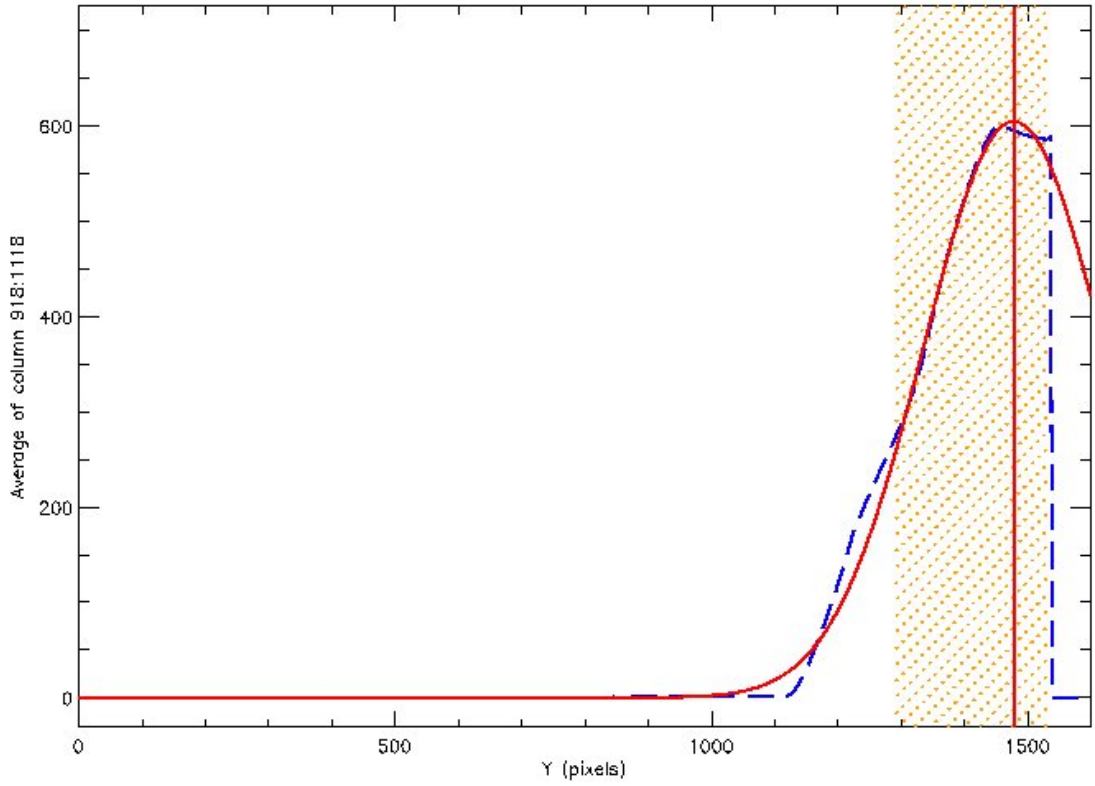
Average of column 918:1118
Y (pixels)
0
200
400
600
0
500
1000
1500

VIII. FR533N18 + F588N

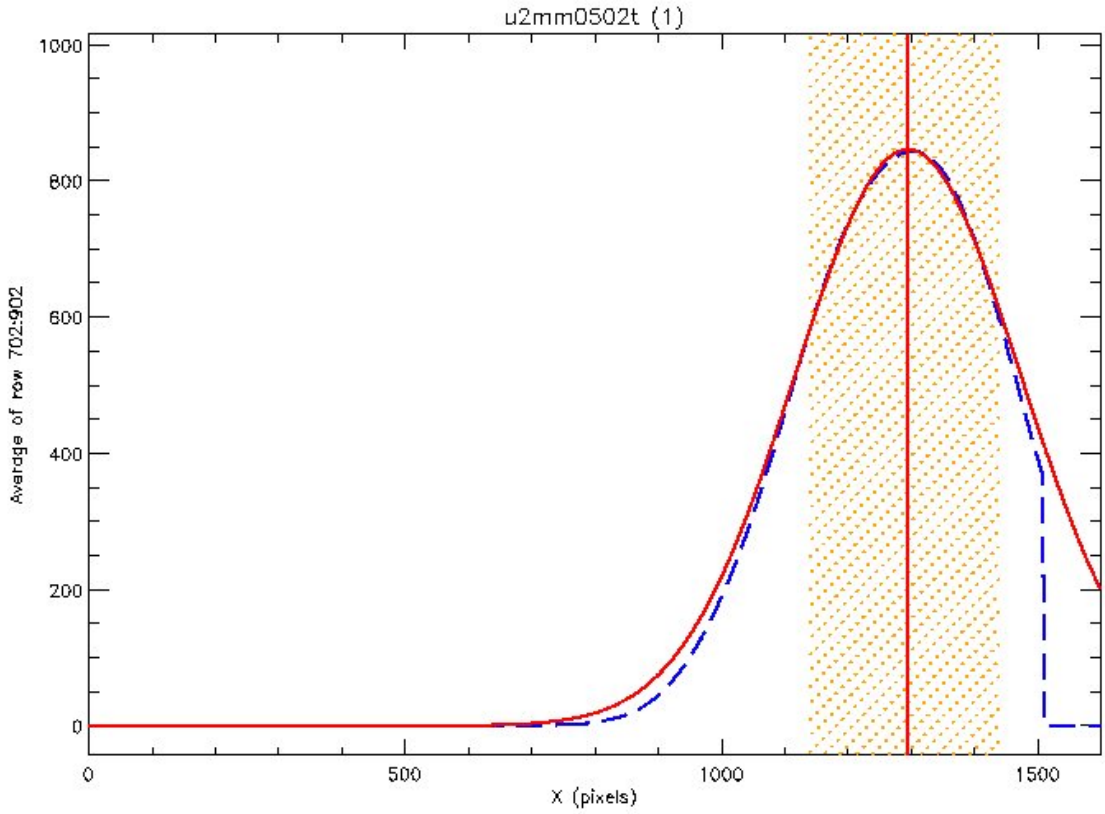

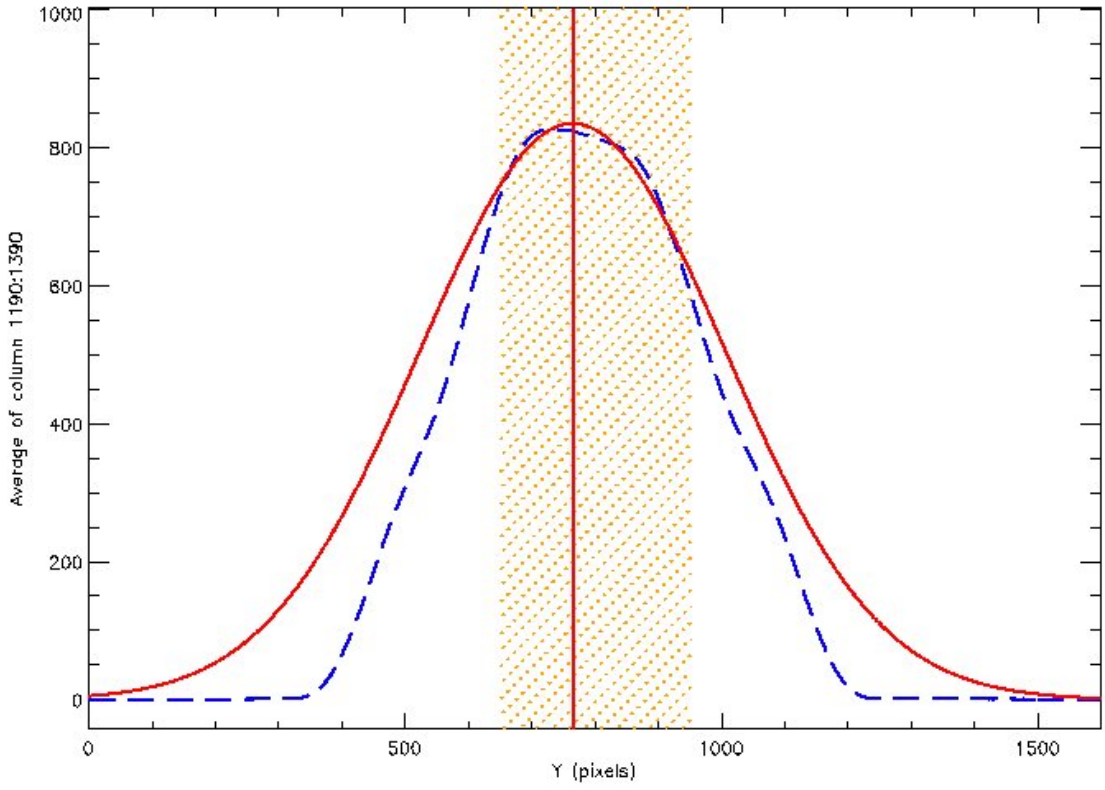

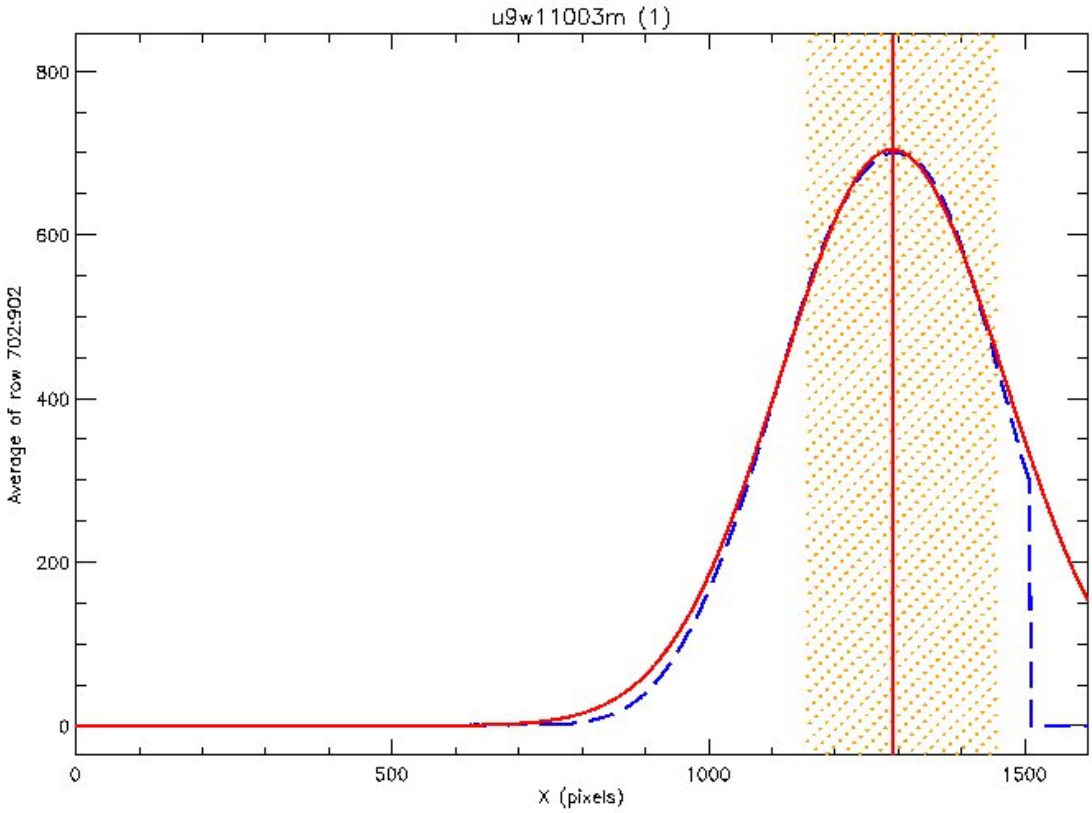
u9w11003m (1)
Average of row 702:902
X (pixels)
0
200
400
600
800
0
500
1000
1500

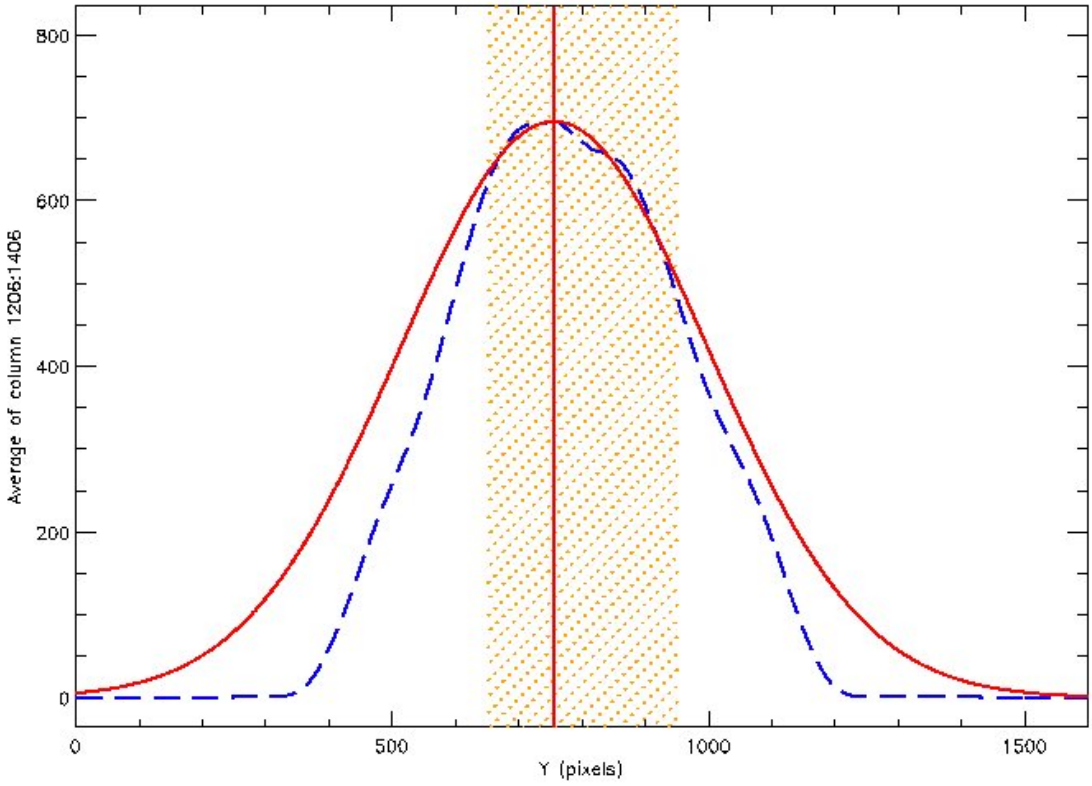
Average of column 1206:1406
Y (pixels)
0
200
400
600
800
0
500
1000
1500

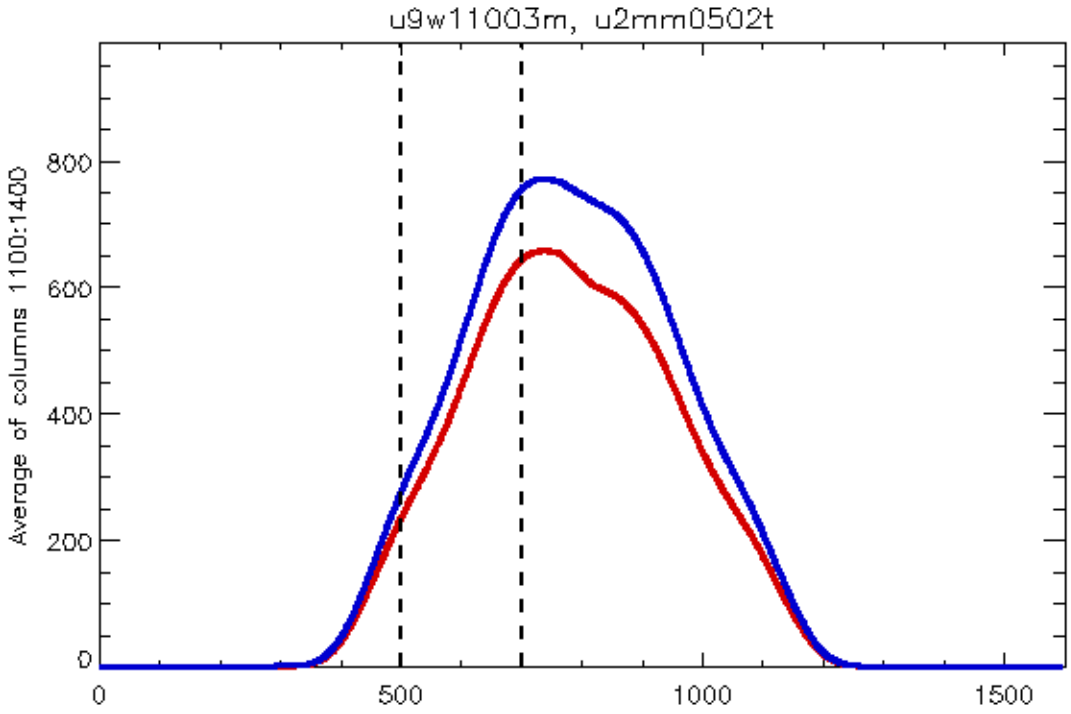
u9w11003m, u2mm0502t
Average of columns 1100:1400
800
600
400
200
0
0
500
1000
1500

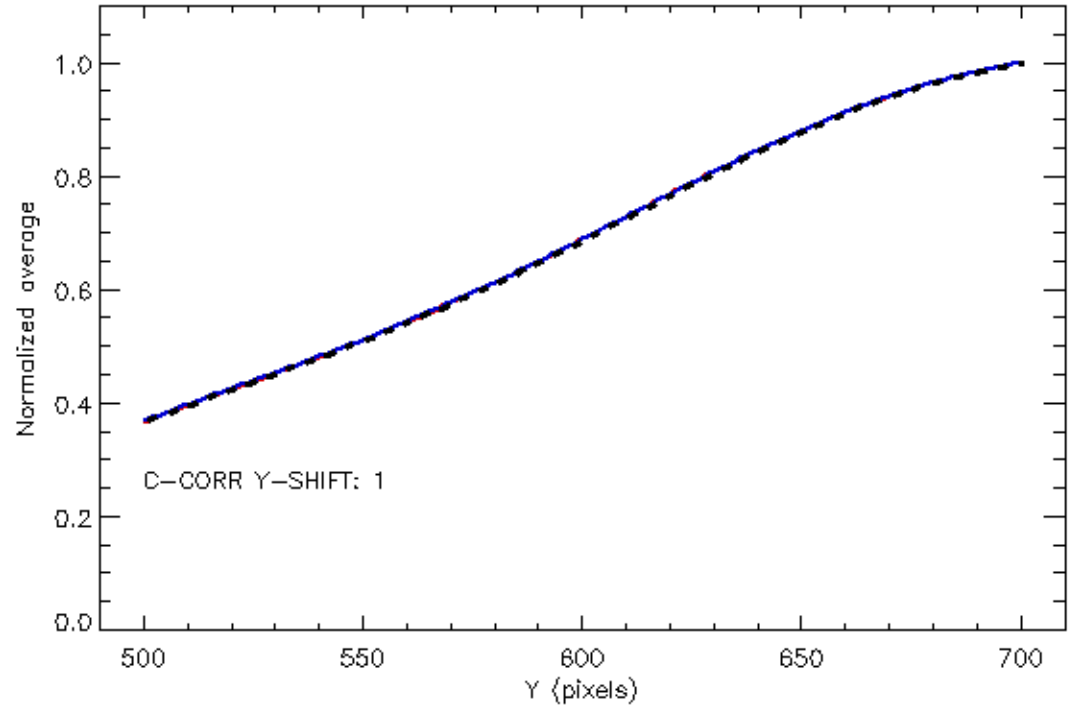
Normalized average
1.0
0.8
0.6
0.4
0.2
0.0
C-CORR Y-SHIFT: 1
500
550
600
650
700
Y (pixels)

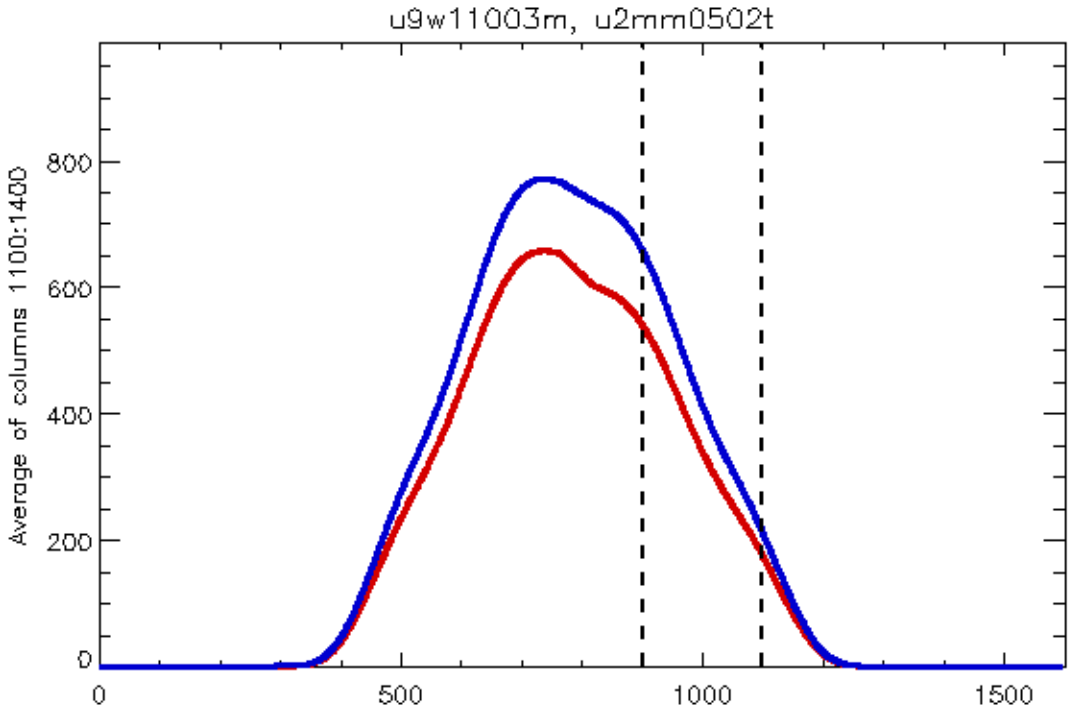
u9w11003m, u2mm0502t
Average of columns 1100:1400
800
600
400
200
0
0
500
1000
1500

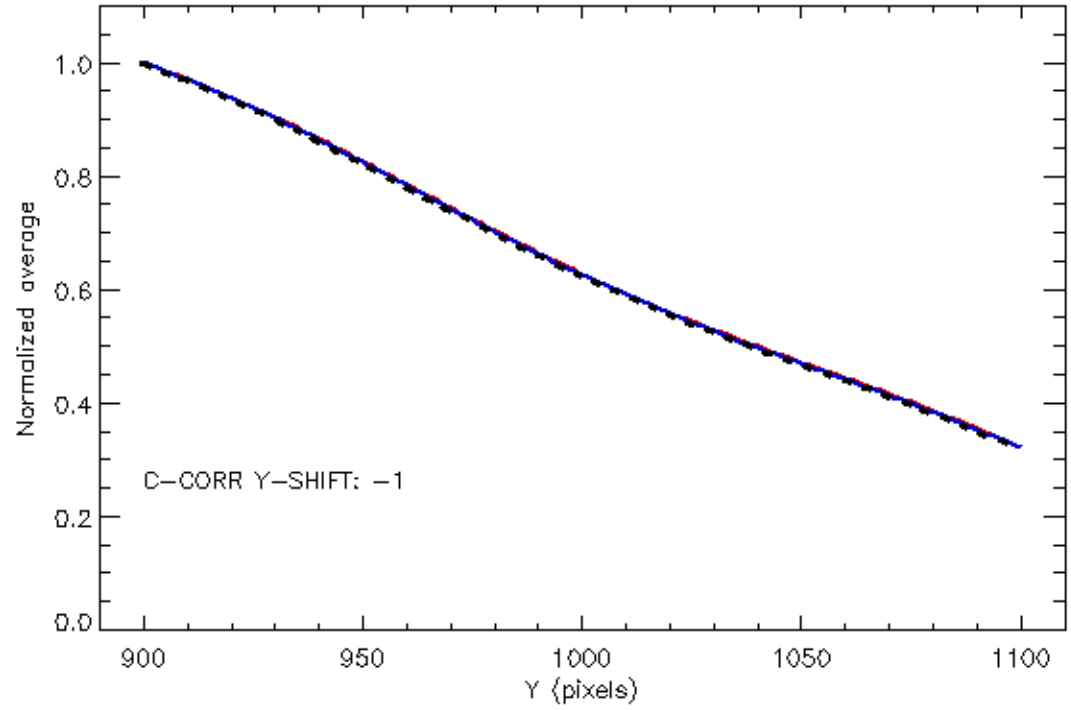
Normalized average
1.0
0.8
0.6
0.4
0.2
0.0
C-CORR Y-SHIFT: -1
900
950
1000
1050
1100
Y (pixels)

IX. FR533N33 + F588N

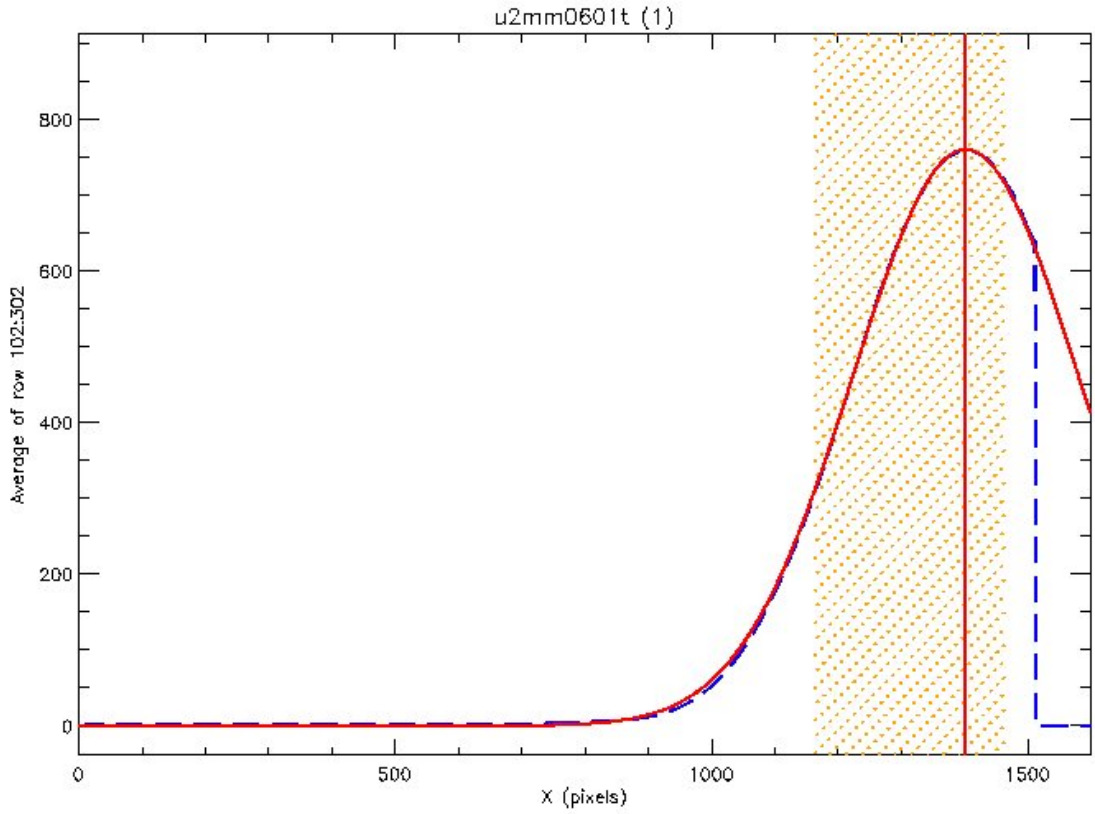

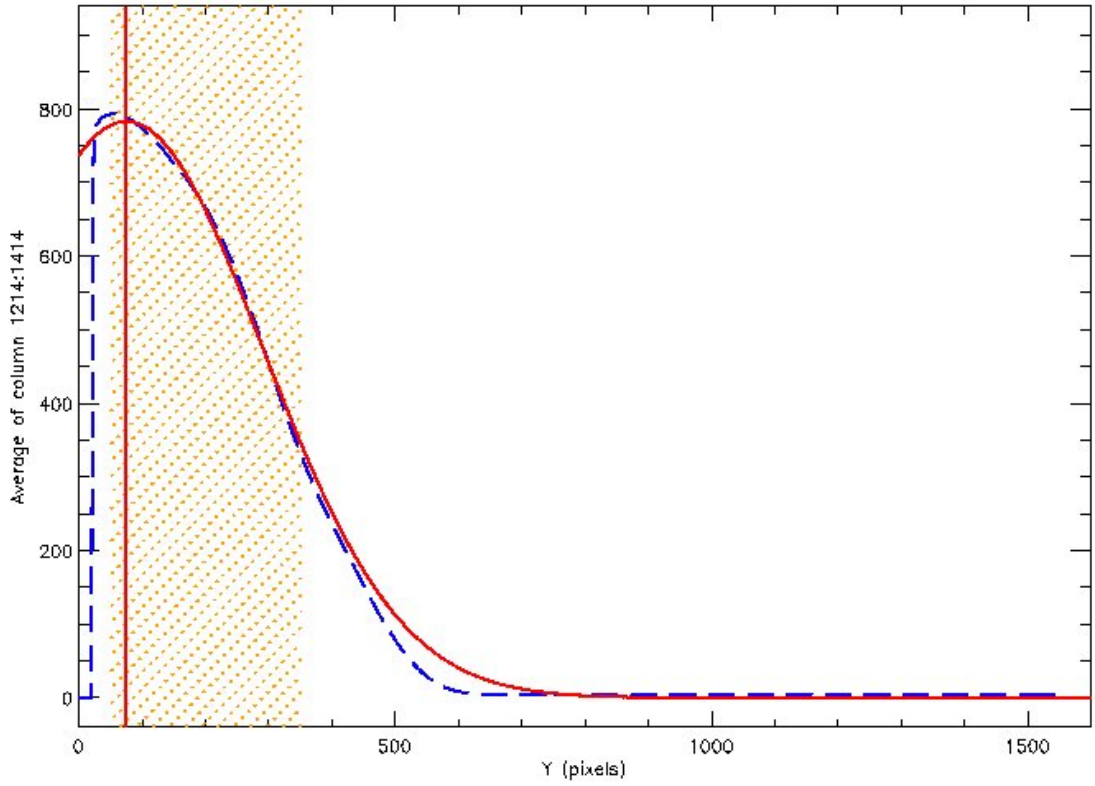

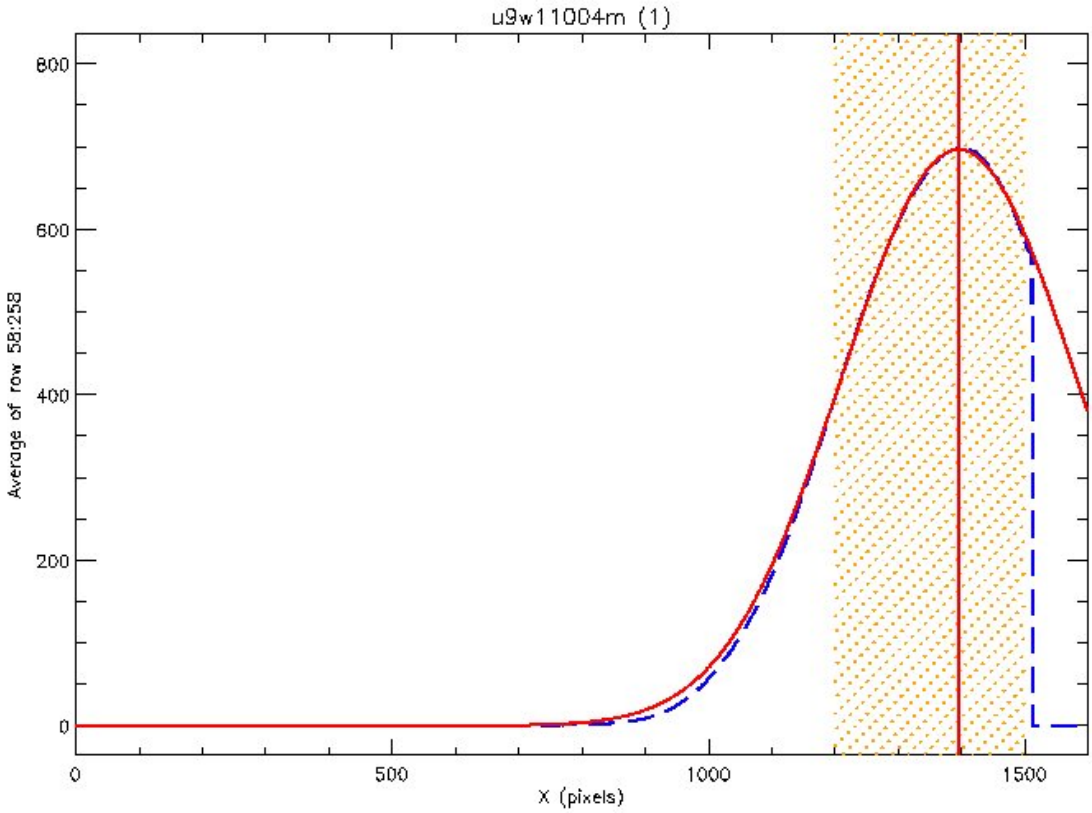
u9w11004m (1)
Average of row 58:258
X (pixels)
0
200
400
600
800
0
500
1000
1500

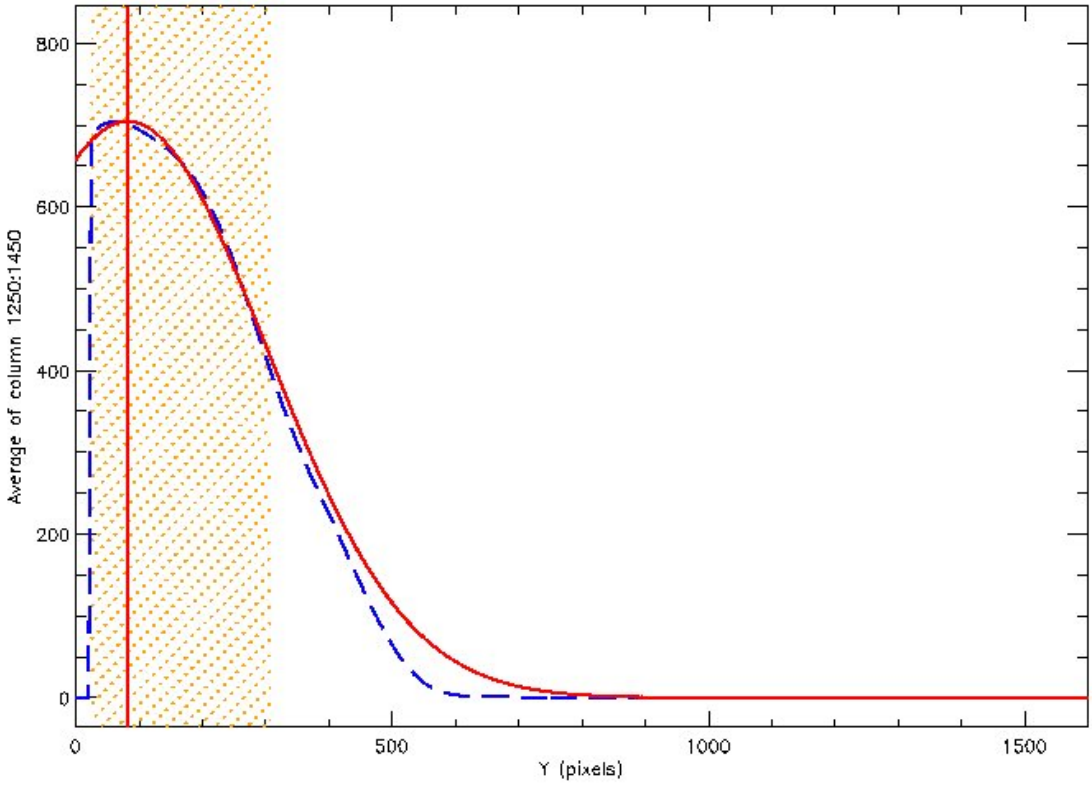
Average of column 1250:1450
Y (pixels)
0
200
400
600
800
0
500
1000
1500

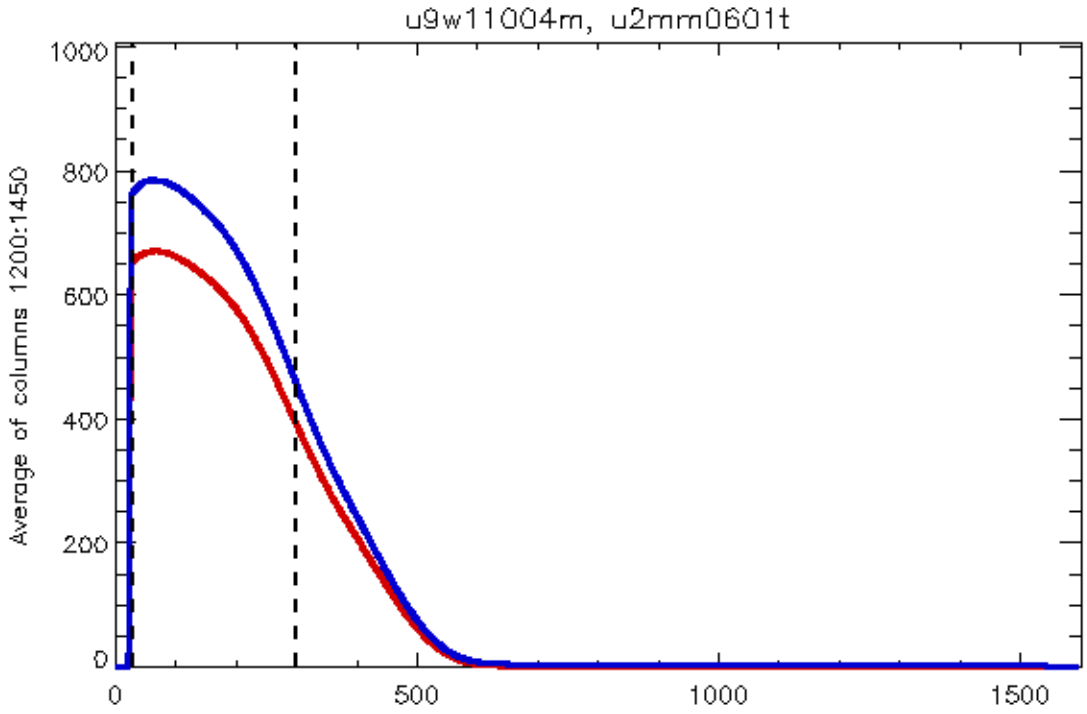
u9w11004m, u2mm0601t
Average of columns 1200:1450
1000
800
600
400
200
0
0
500
1000
1500

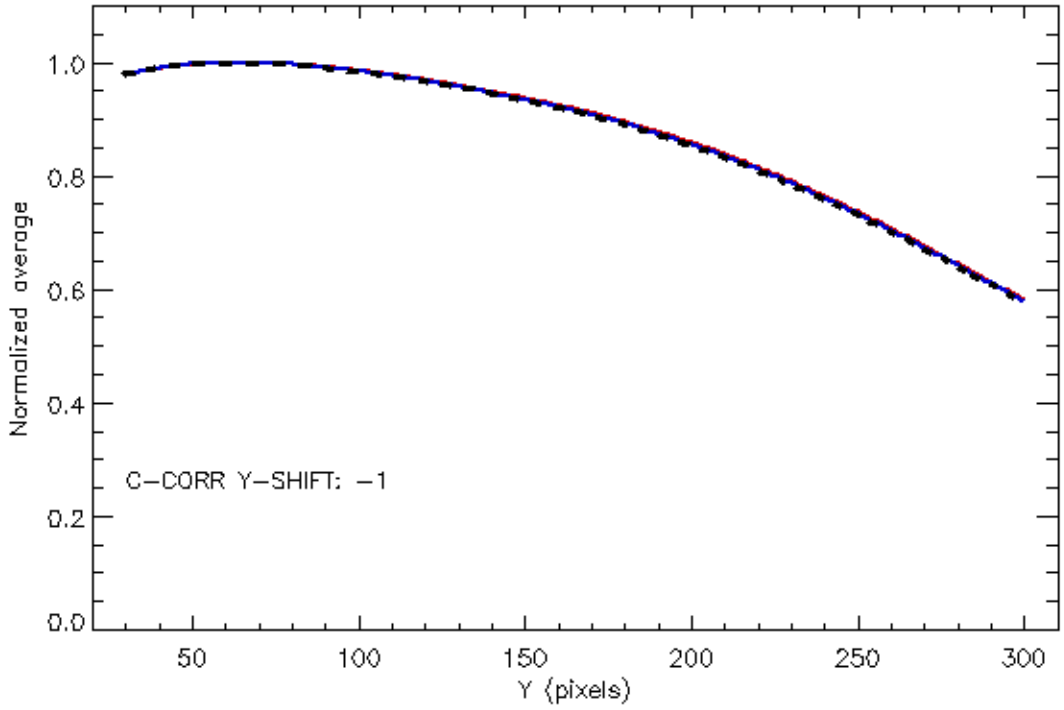
Normalized average
1.0
0.8
0.6
0.4
0.2
0.0
C-CORR Y-SHIFT: -1
50
100
150
200
250
300
Y (pixels)

X. FR680N + F631N

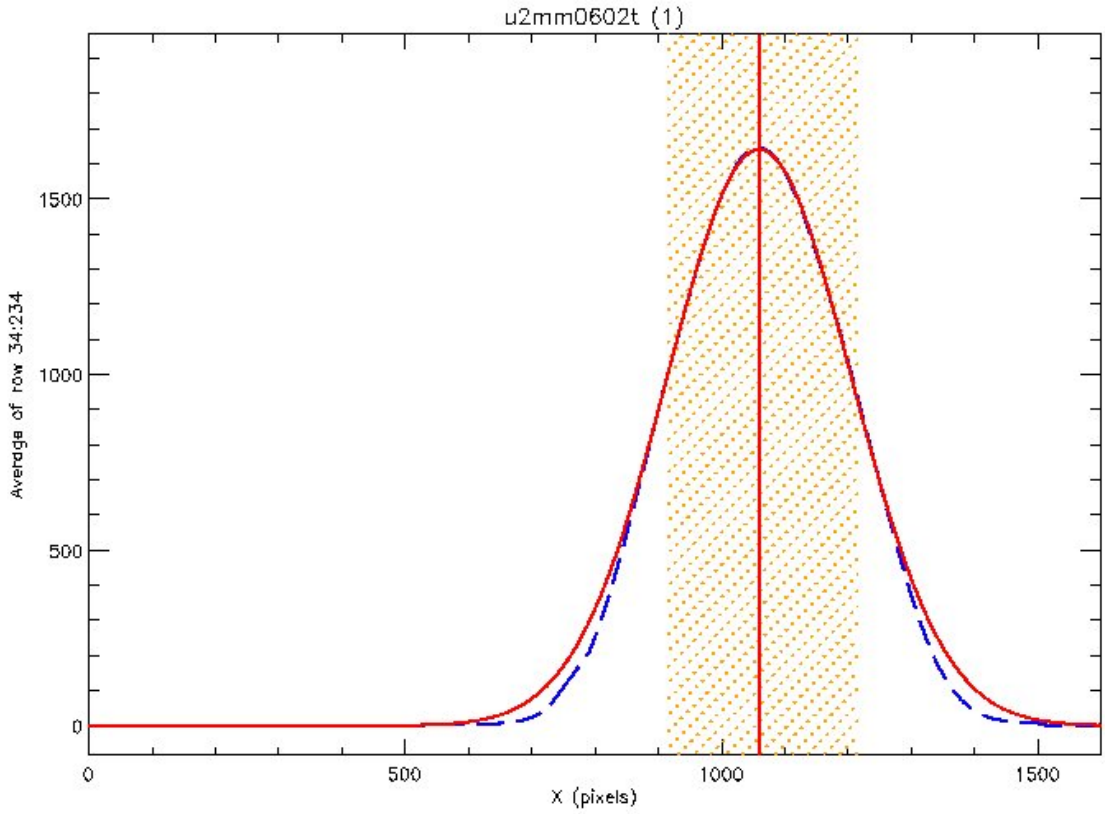

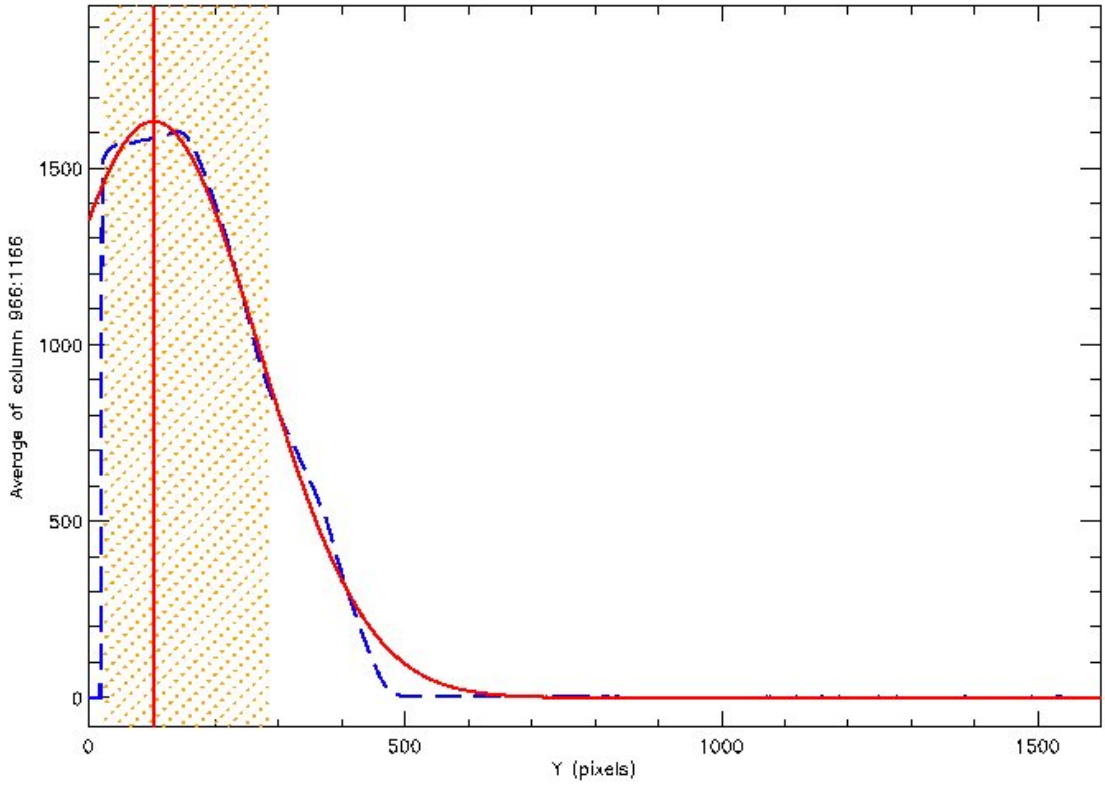

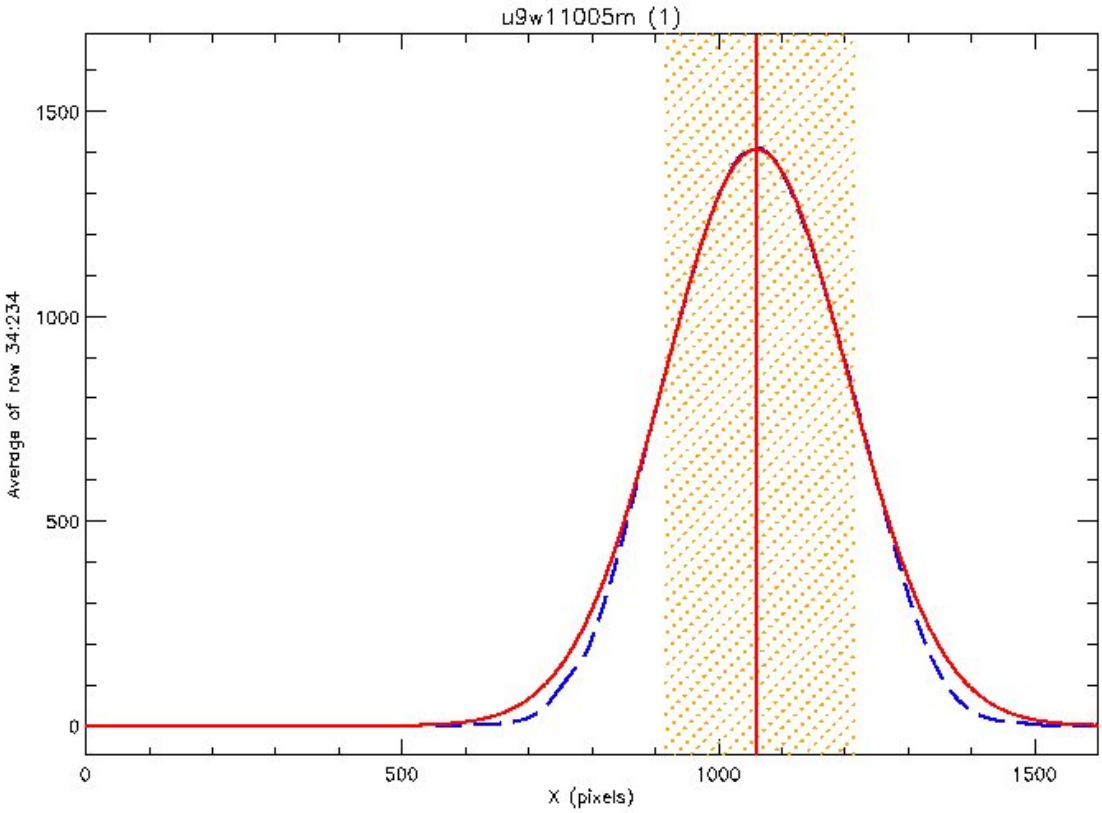
u9w11005m (1)
Average of row 34:234
X (pixels)
0
500
1000
1500

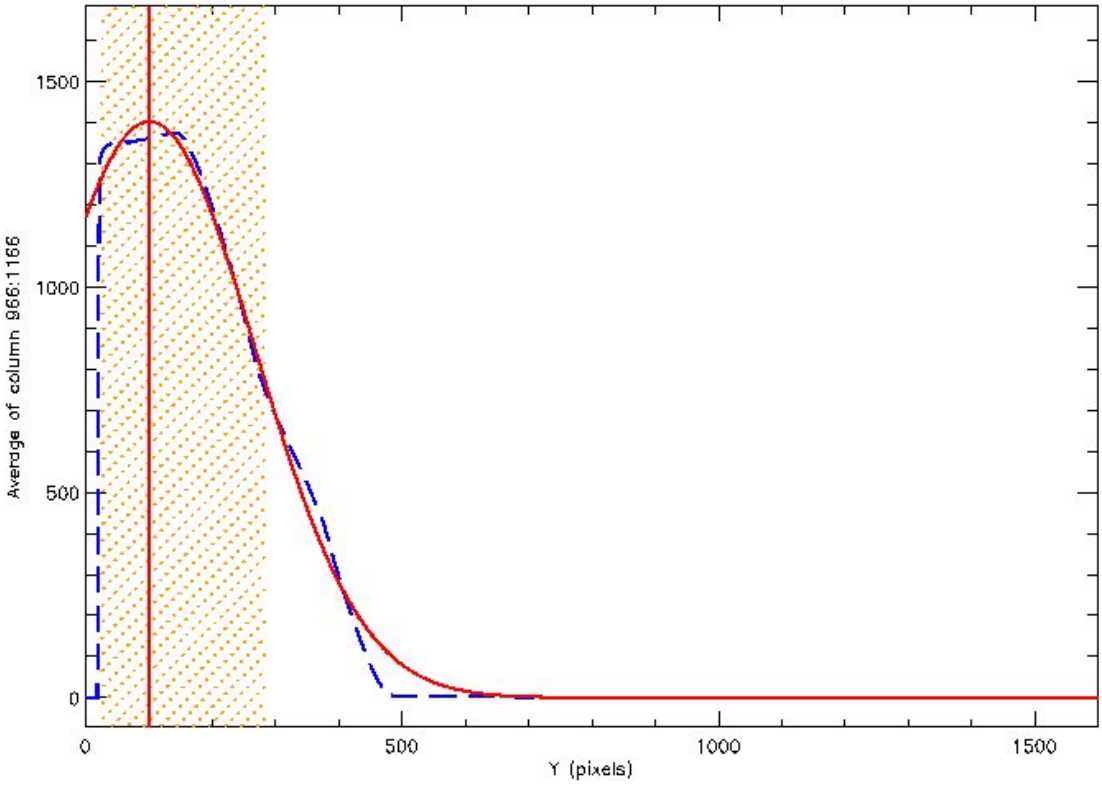
Average of column 966:1166
Y (pixels)
0
500
1000
1500

XI. FR680N + F656N

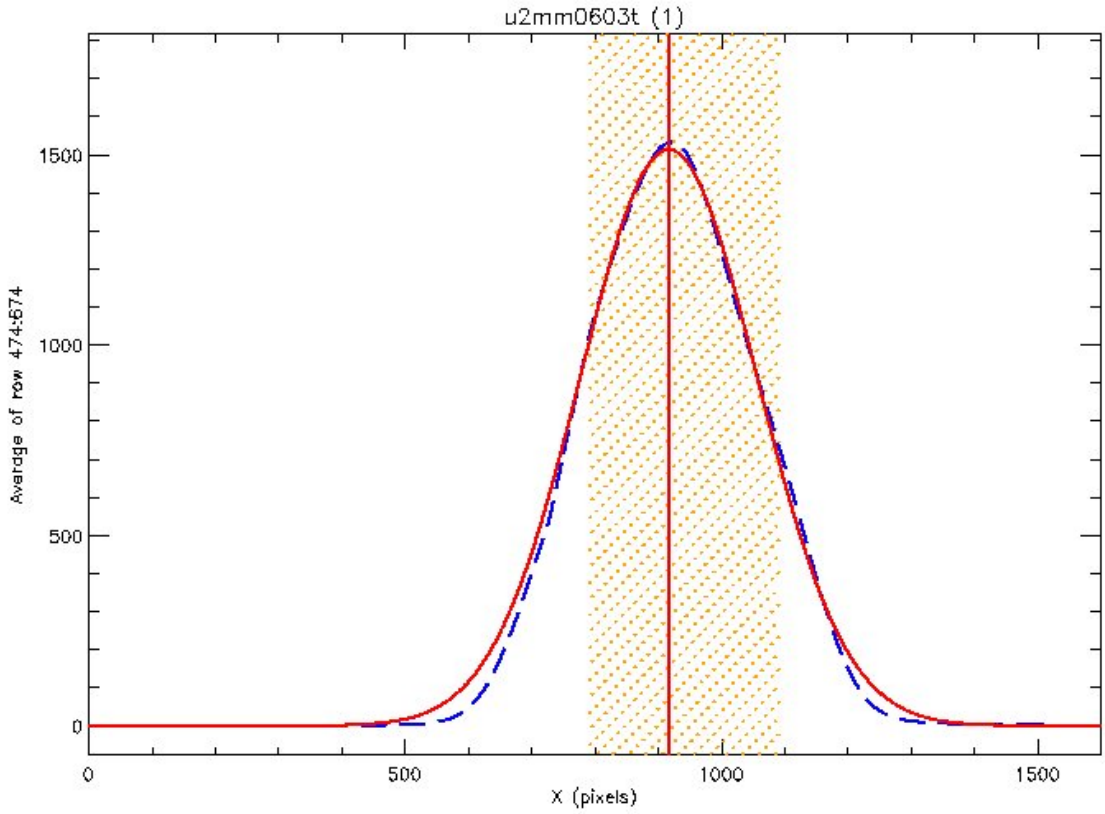

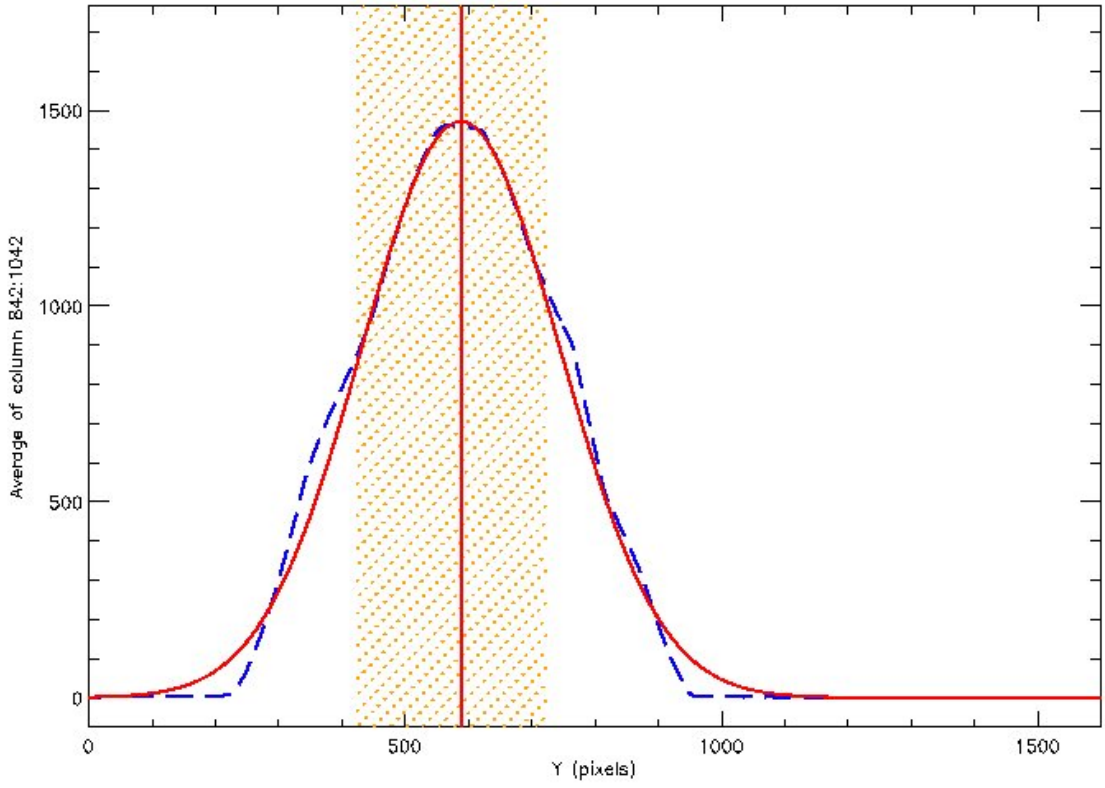

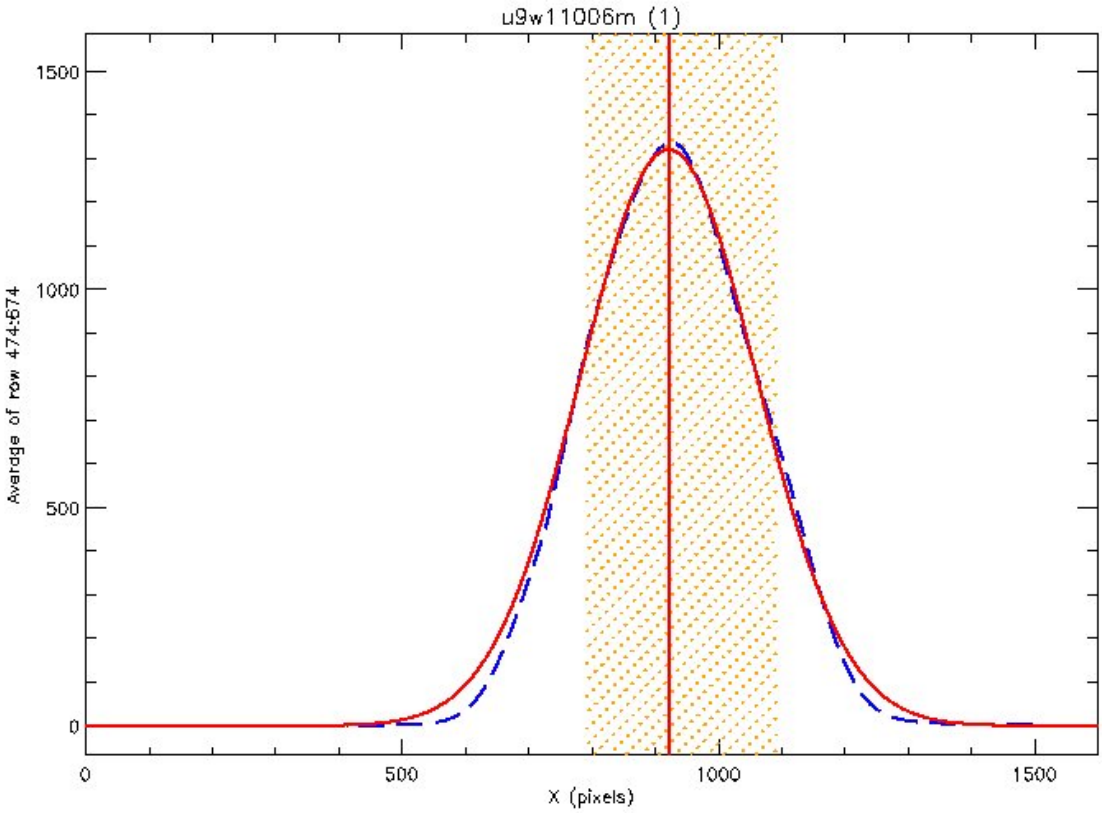
u9w11006m (1)
Average of row 474:674
X (pixels)
0
500
1000
1500

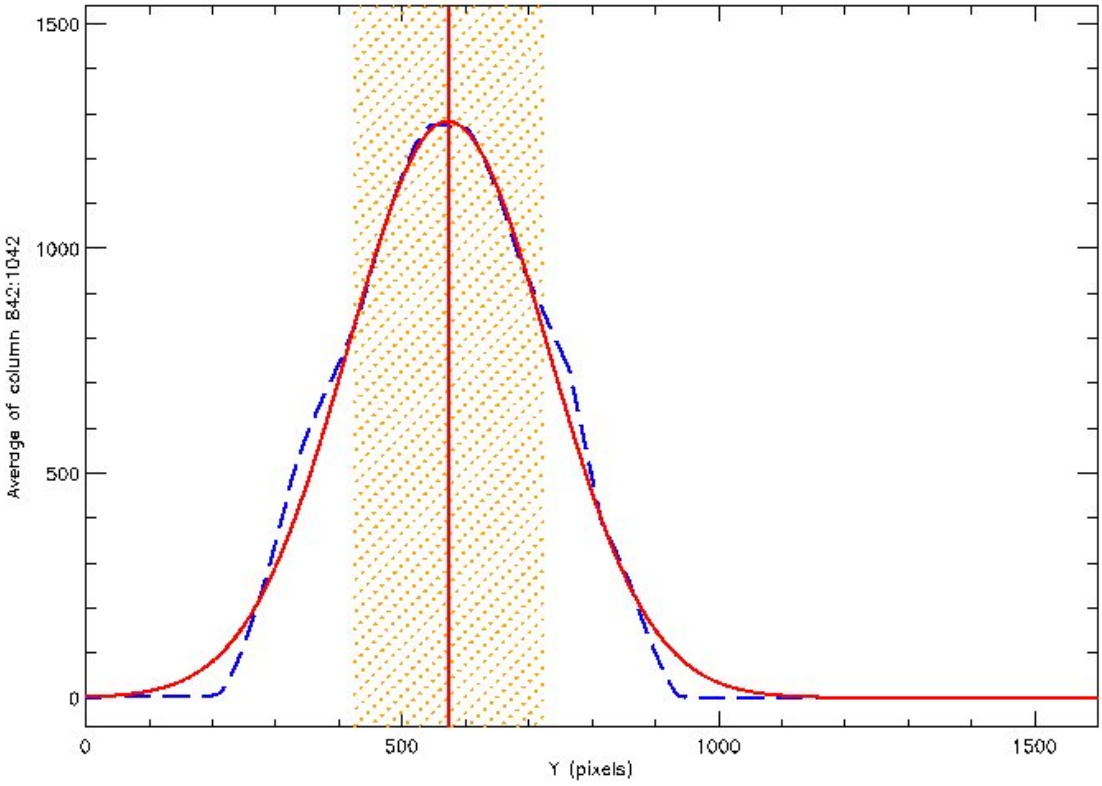
Average of column 842:1042
Y (pixels)
0
500
1000
1500

XII. FR680N + F658N

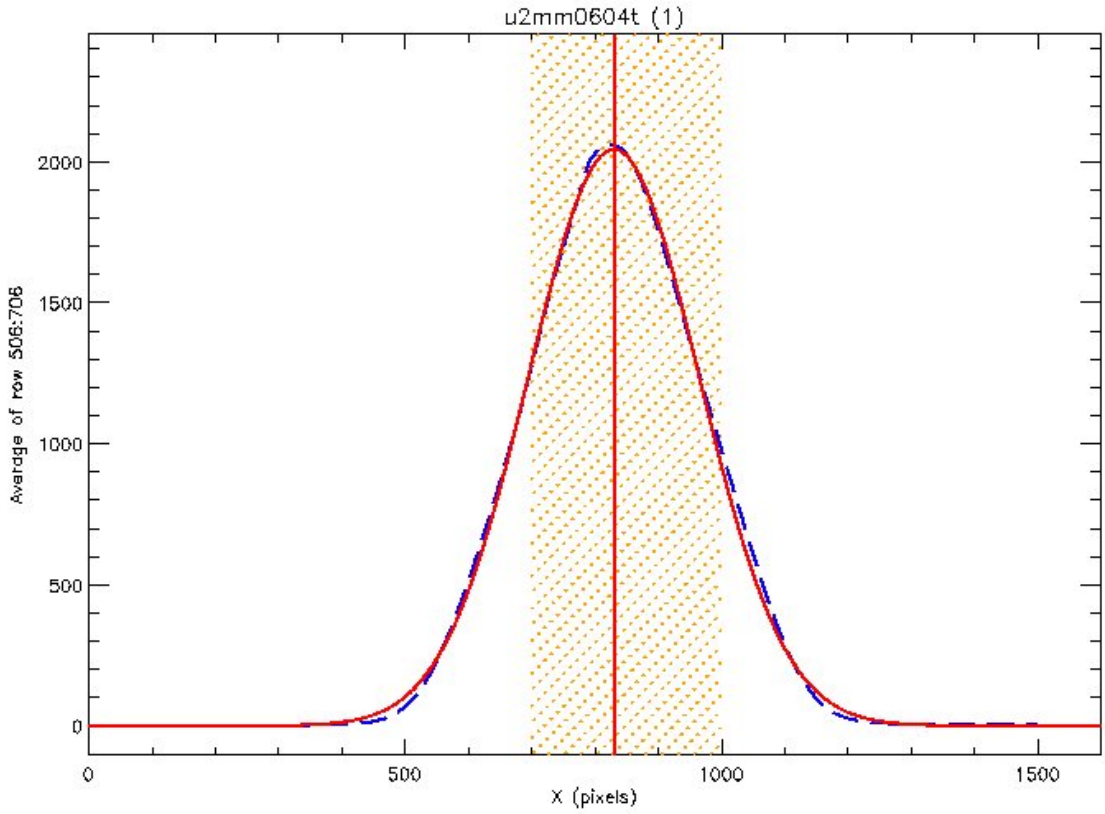

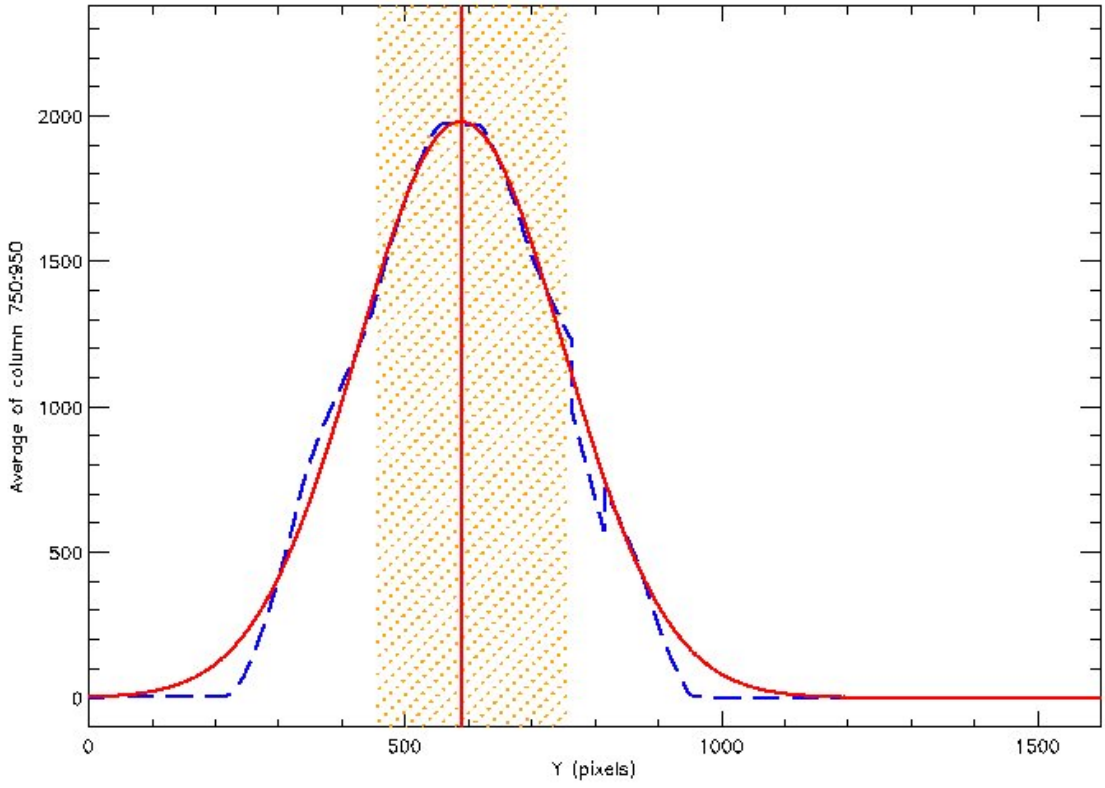

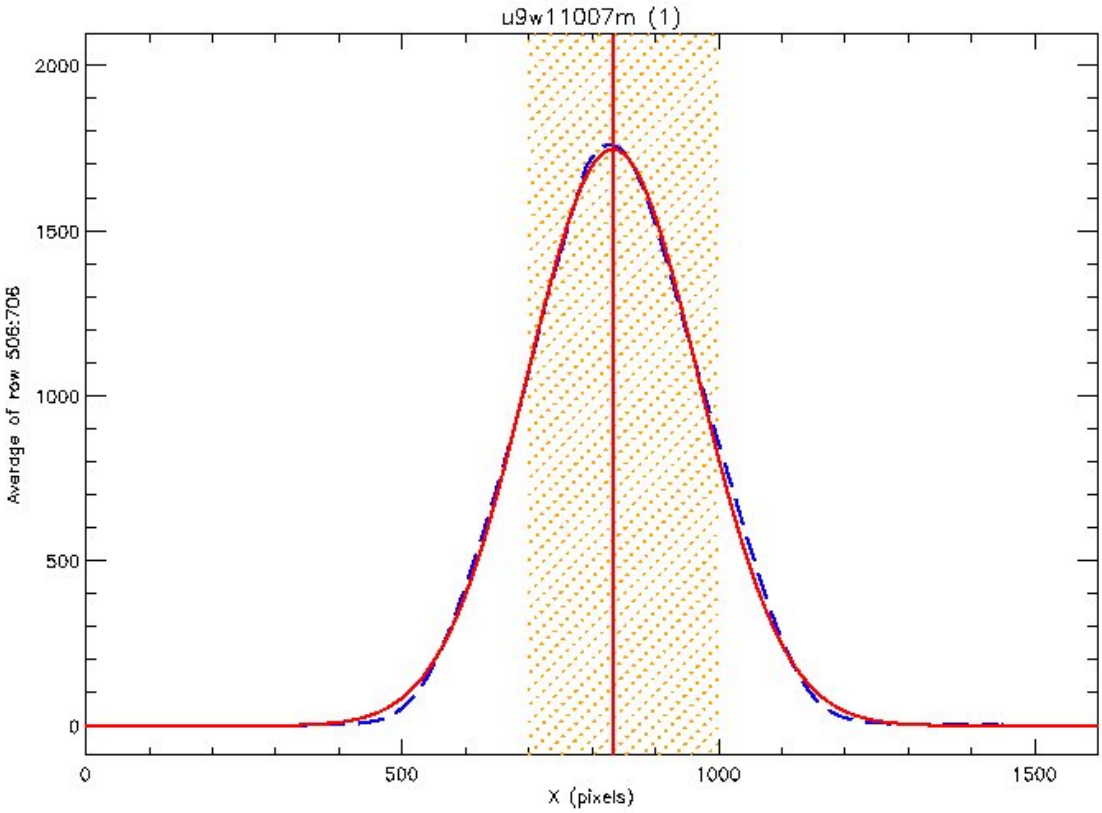
u9w11007m (1)
Average of row 506:706
X (pixels)
0
500
1000
1500
2000

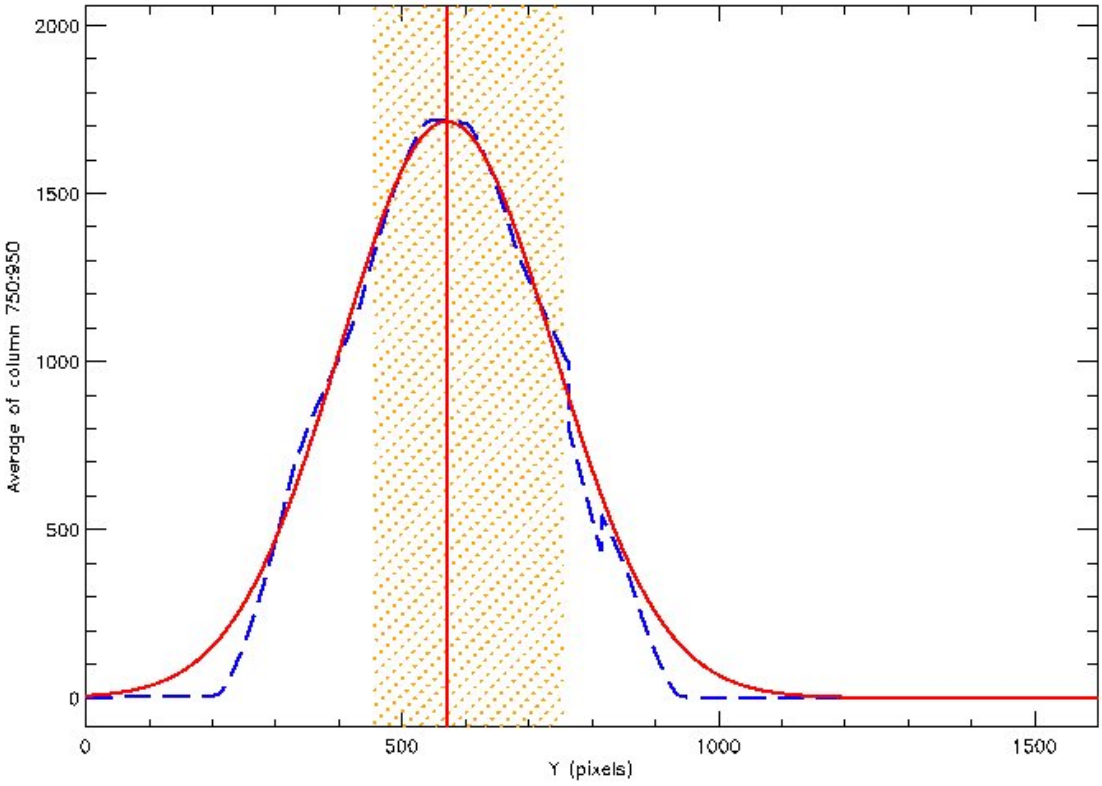
Average of column 750:950
Y (pixels)
0
500
1000
1500
2000

XIII. FR680N + F673N

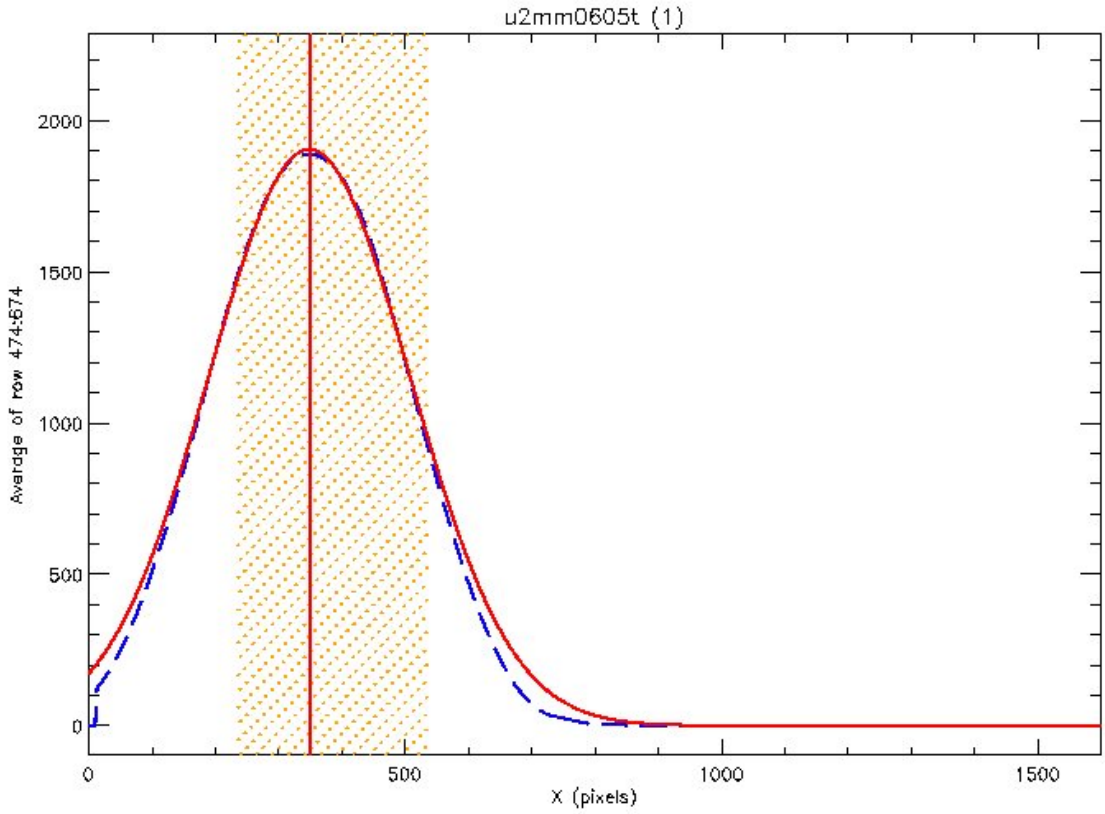

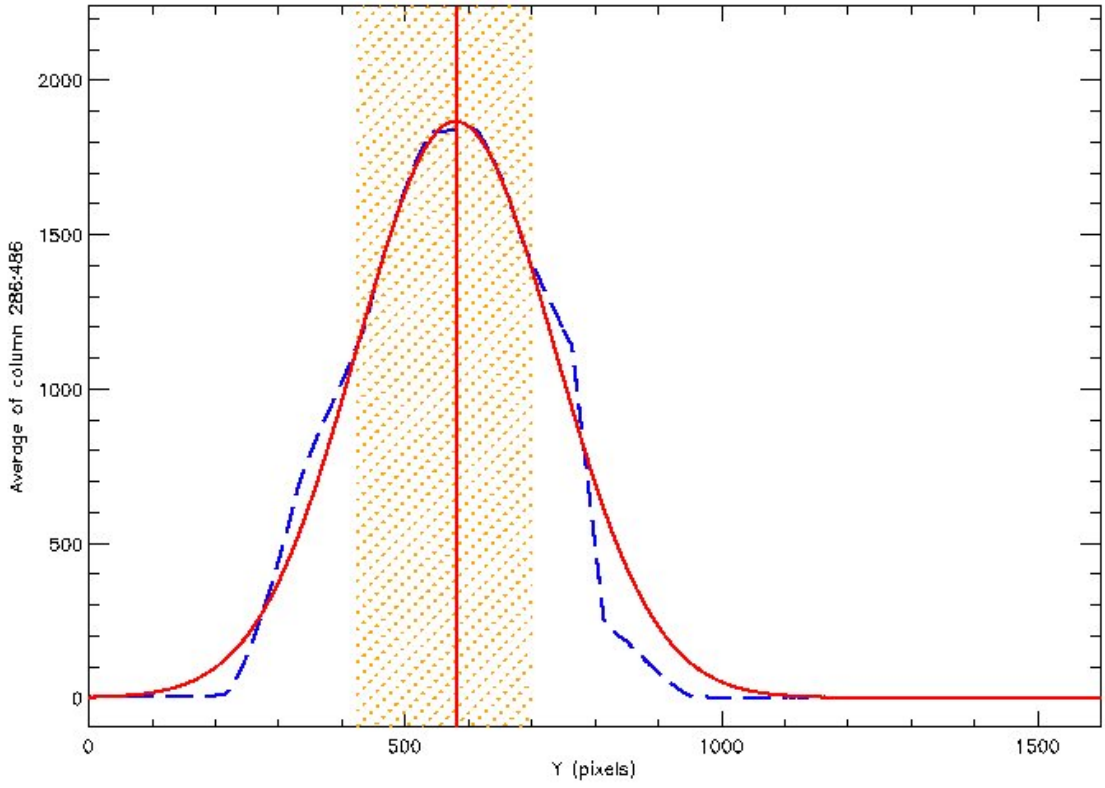

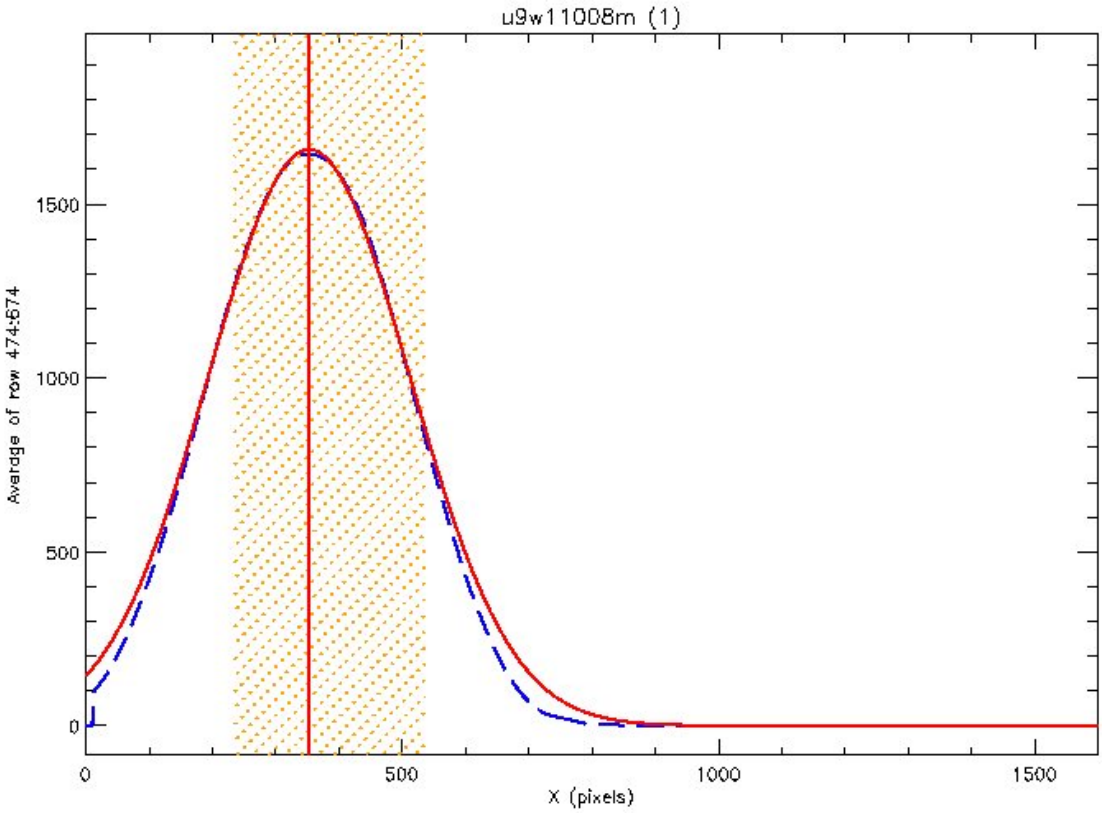
u9w11008m (1)
Average of row 474:674
X (pixels)
0
500
1000
1500

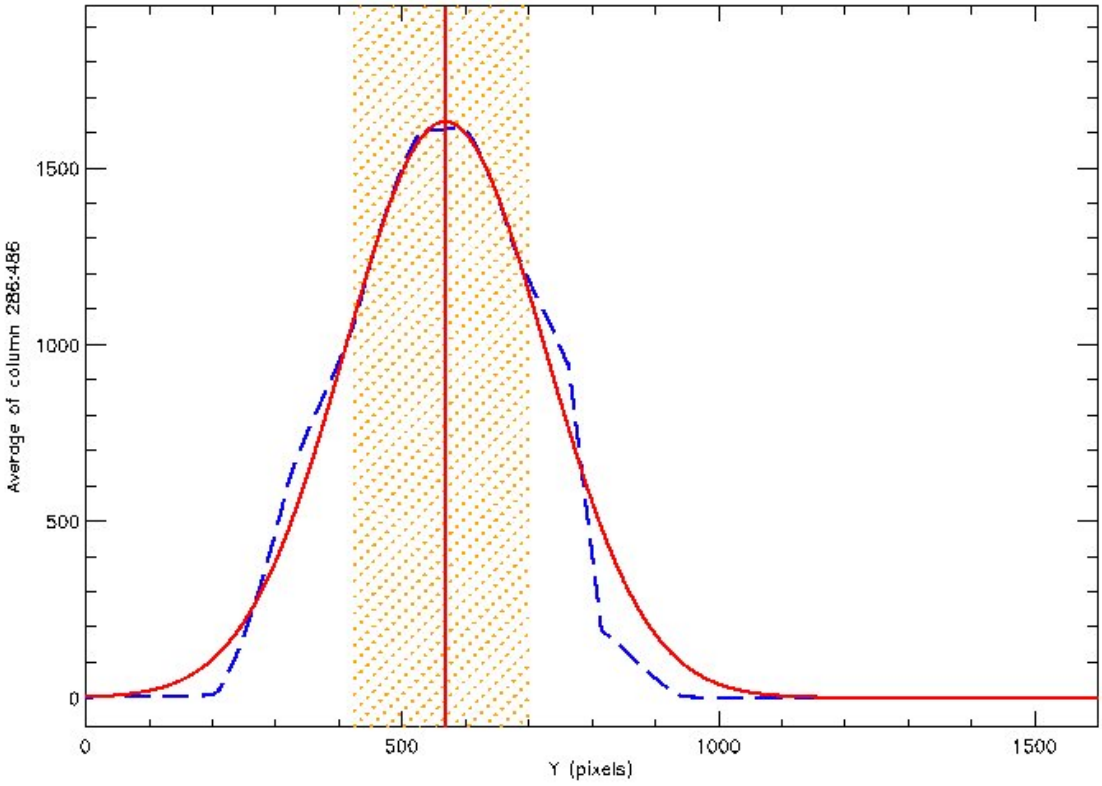
Average of column 286:486
Y (pixels)
0
500
1000
1500

XIV. FR680N18 + F673N

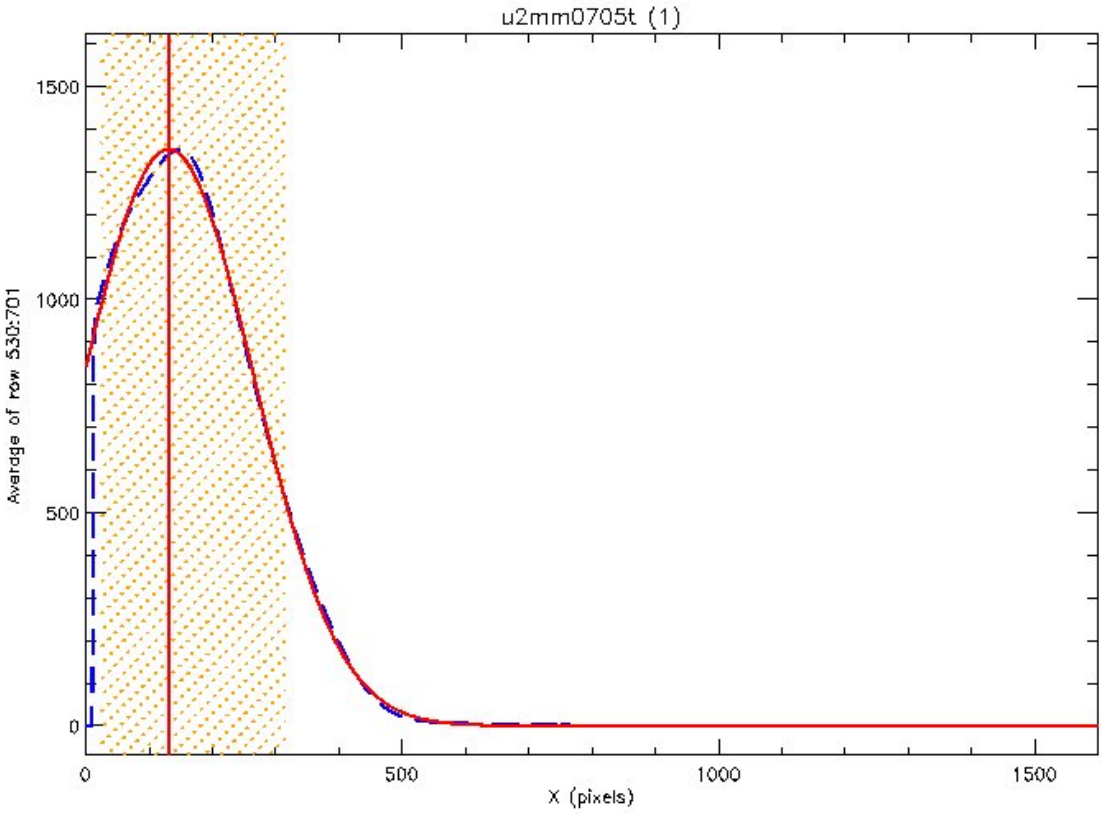

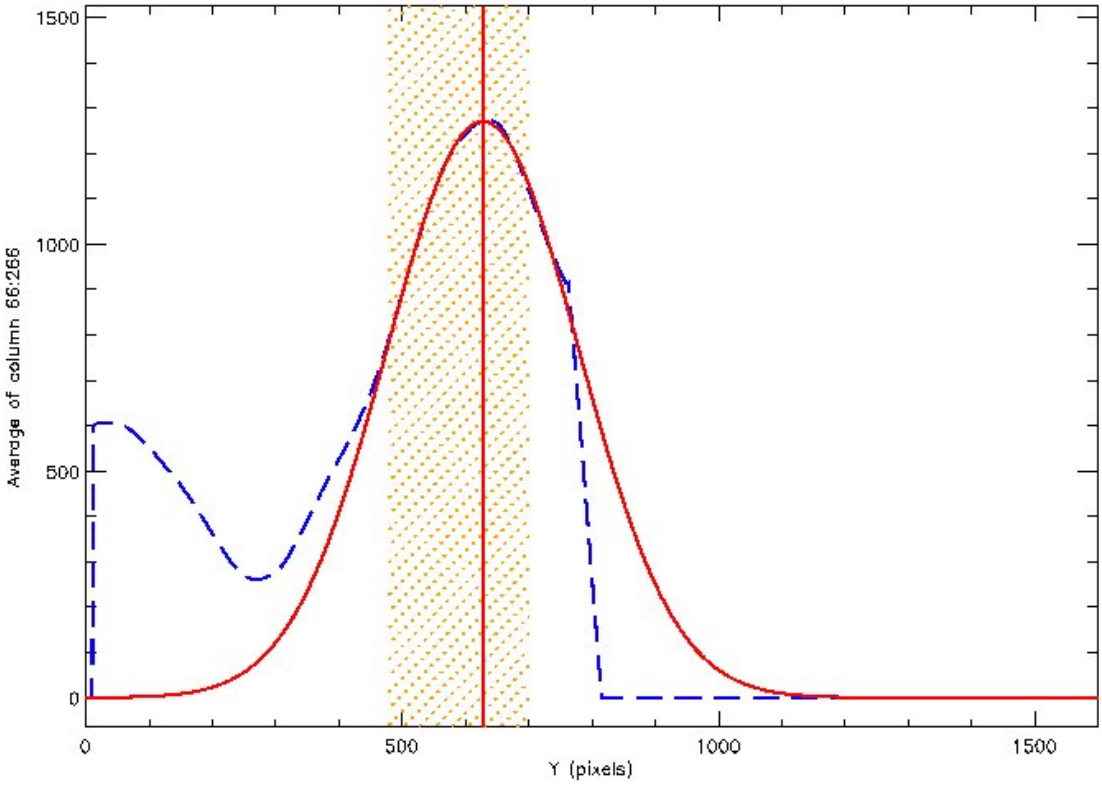

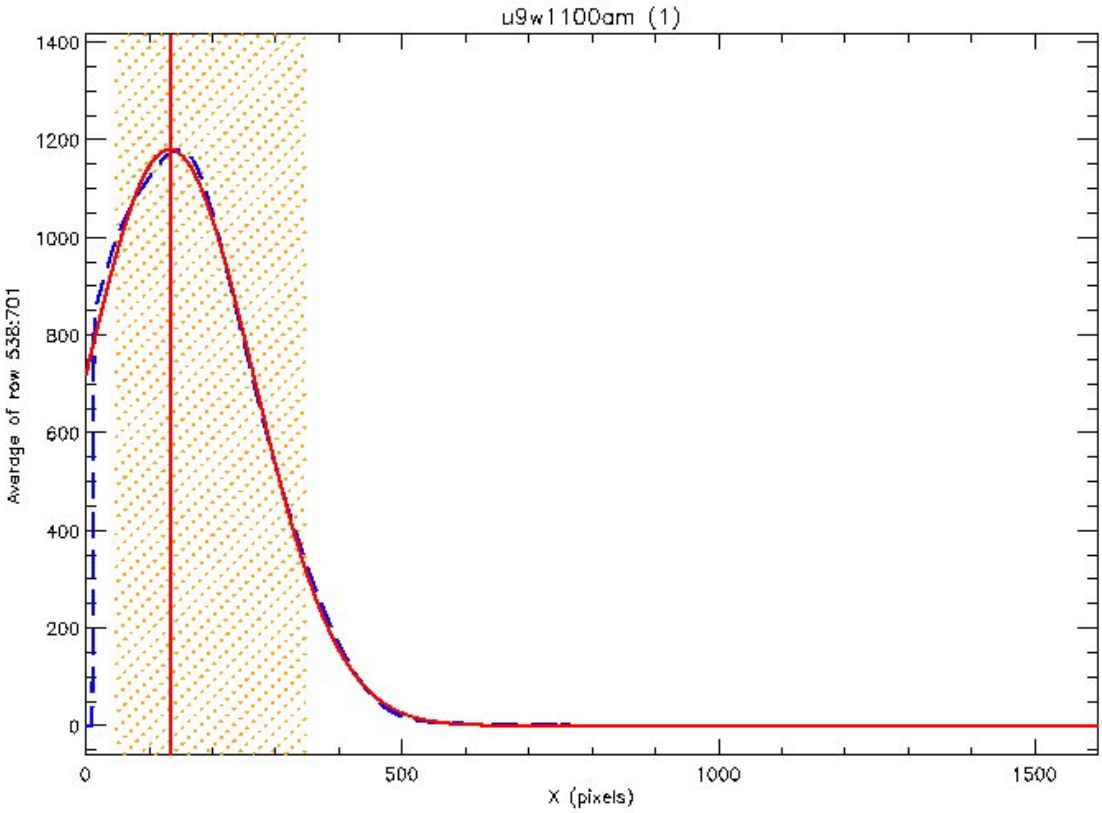
u9w1100am (1)
Average of row 538:701
X (pixels)
0
200
400
600
800
1000
1200
1400
0
500
1000
1500

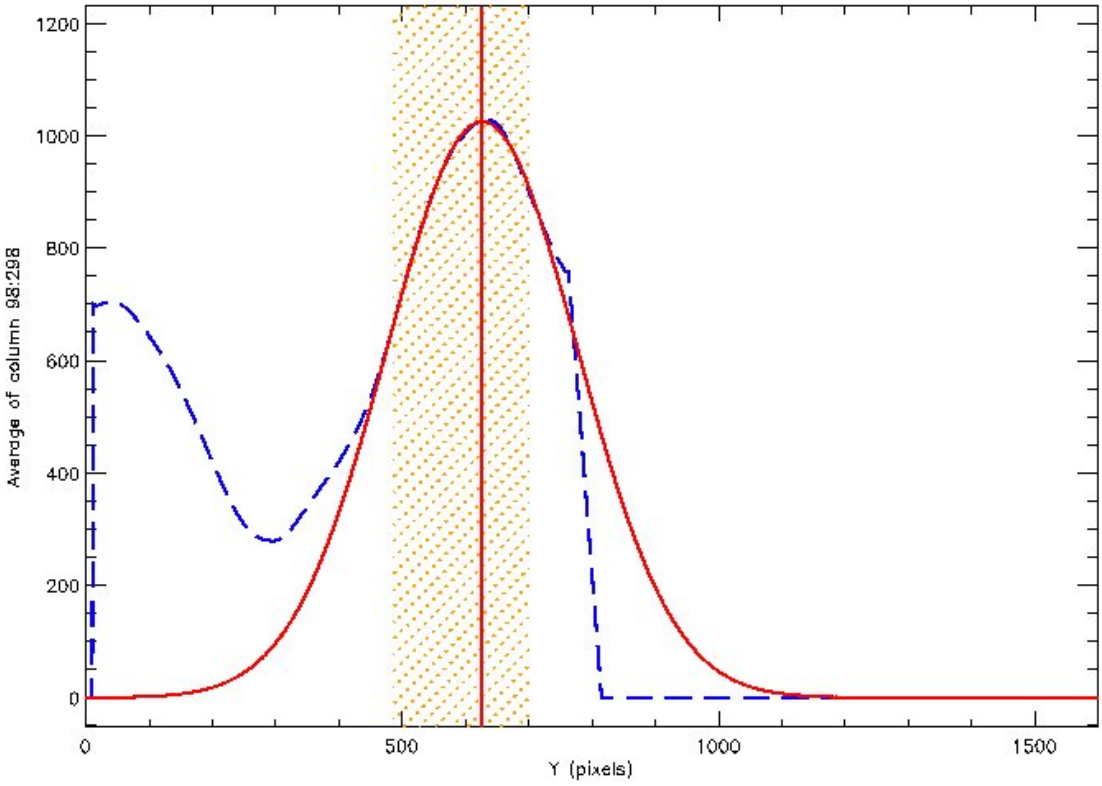
Average of column 98:298
Y (pixels)
0
200
400
600
800
1000
1200
0
500
1000
1500

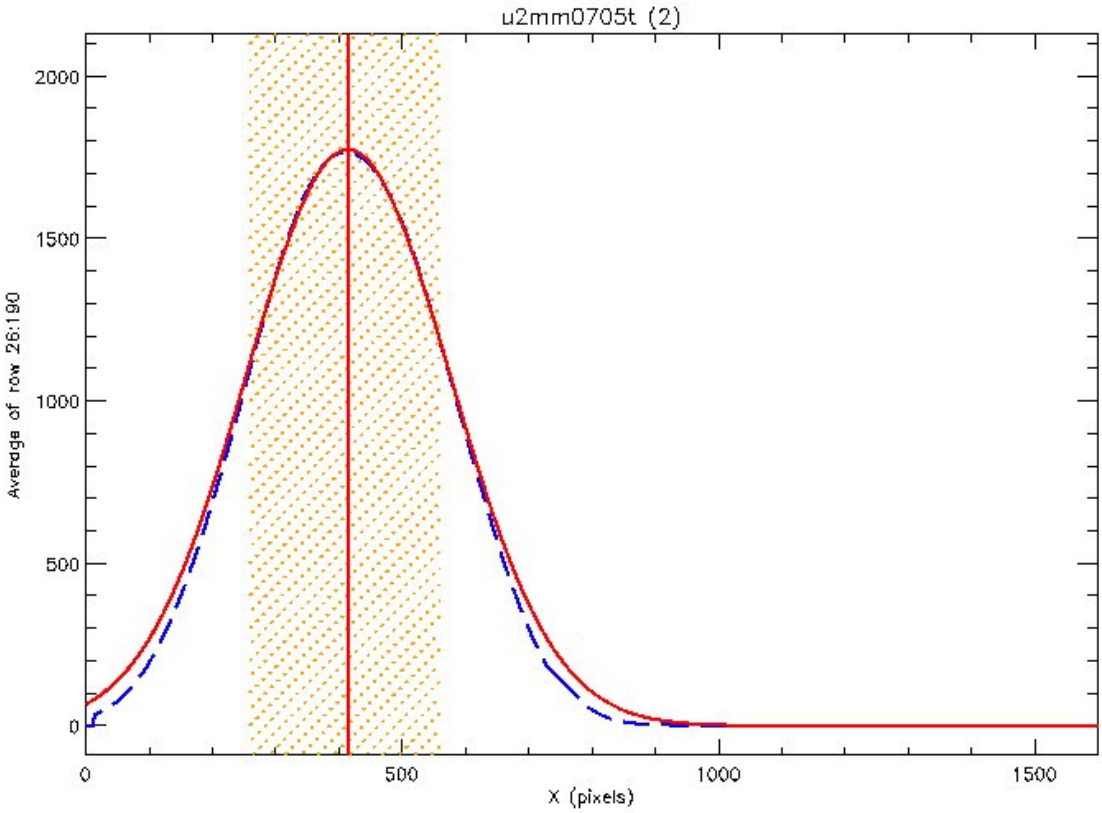
u2mm0705t (2)
Average of row 26:190
X (pixels)
0
500
1000
1500
2000

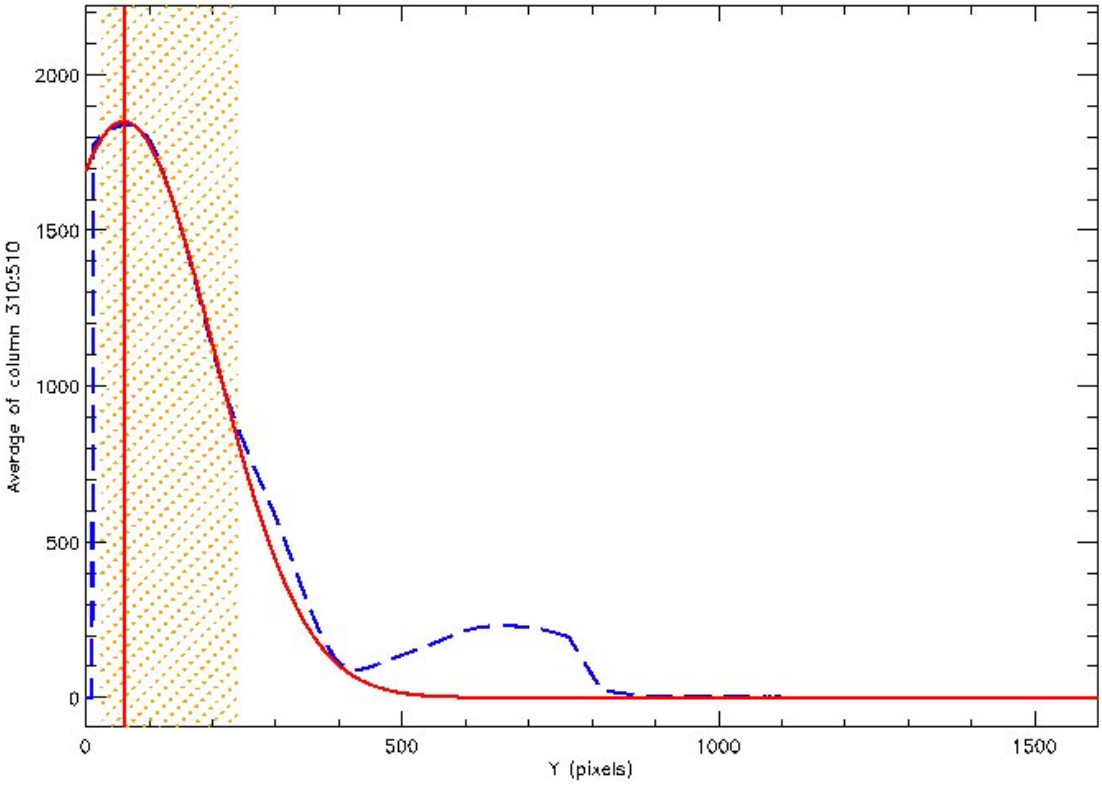
Average of column 310:510
Y (pixels)
0
500
1000
1500
2000

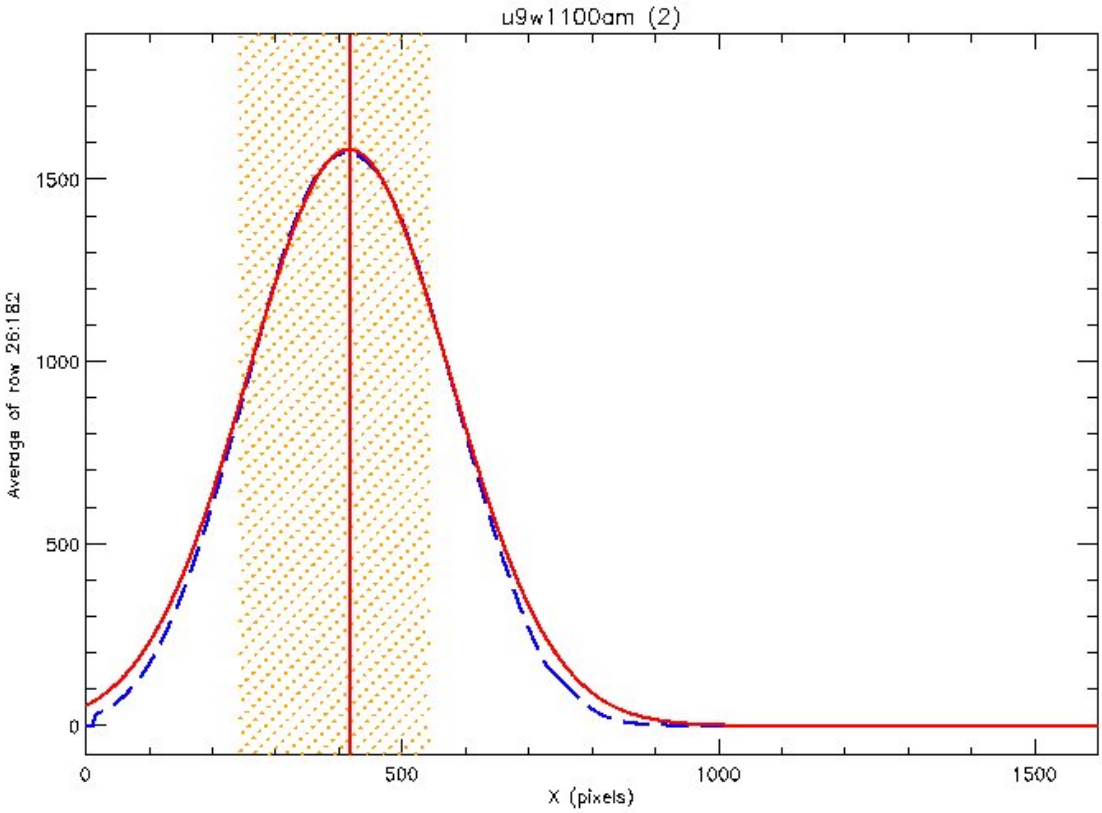
u9w1100am (2)
Average of row 26:182
X (pixels)
0
500
1000
1500

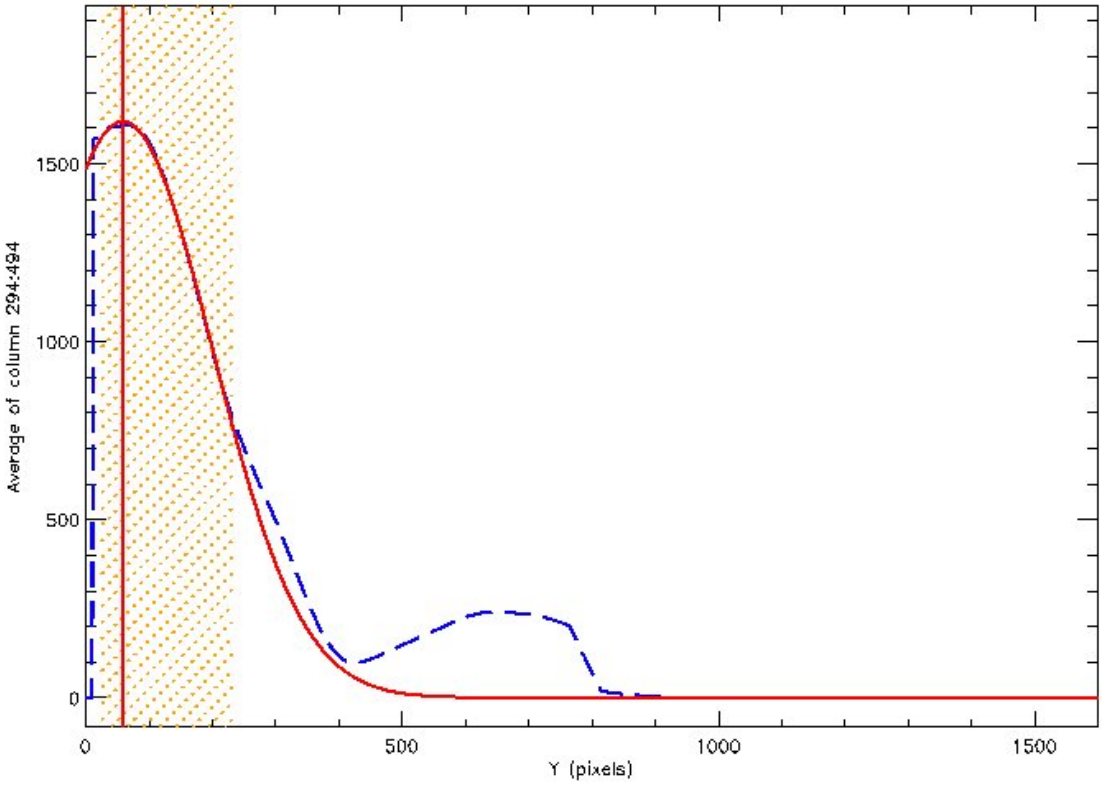
Average of column 294:494
Y (pixels)
0
500
1000
1500

XV. FR680N33 + F673N

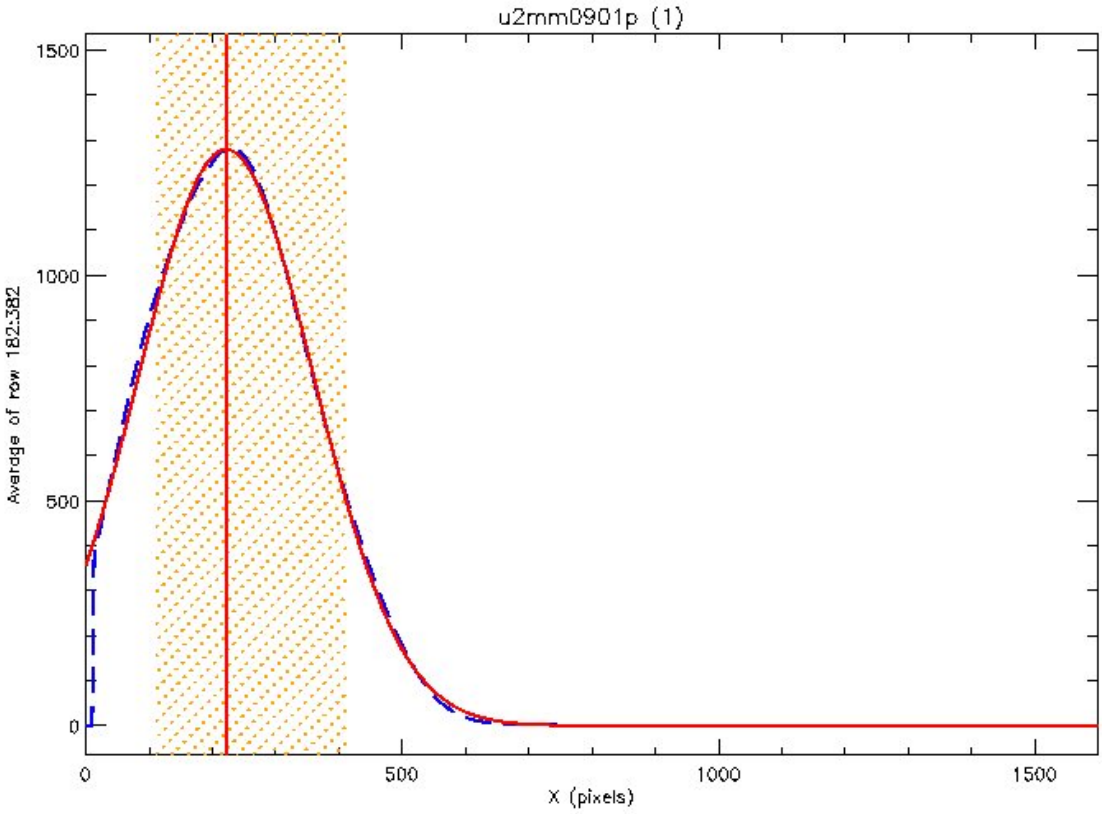

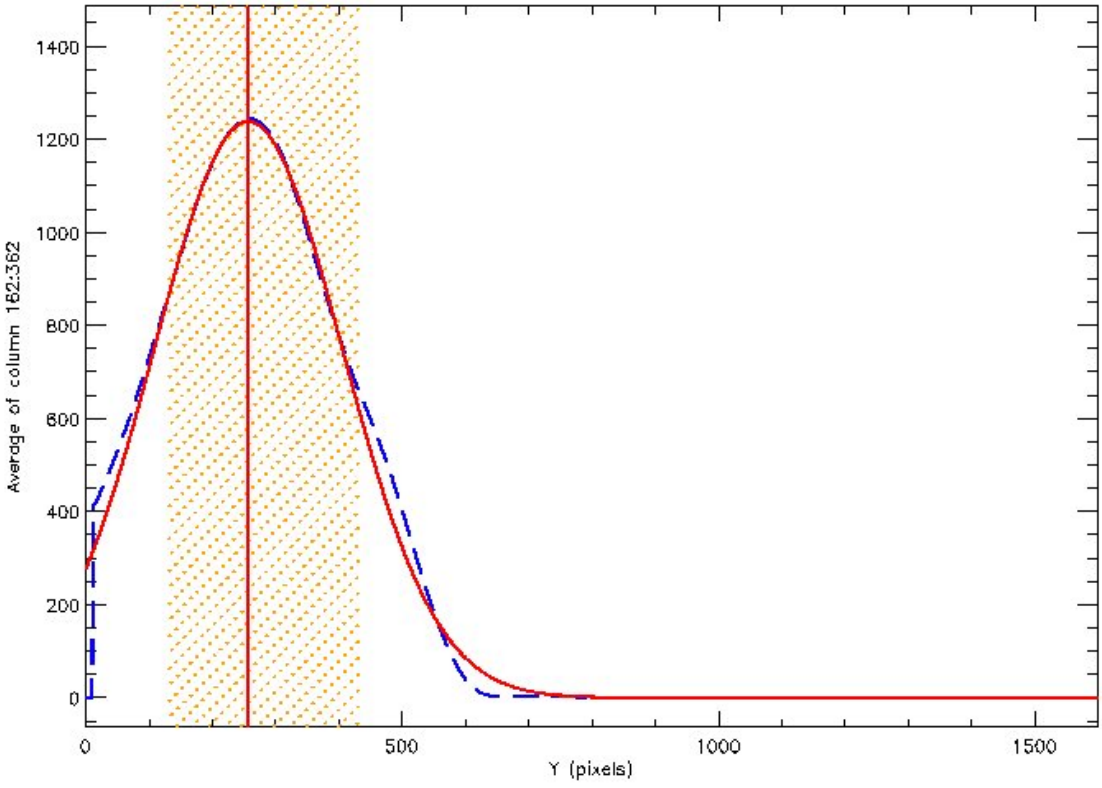

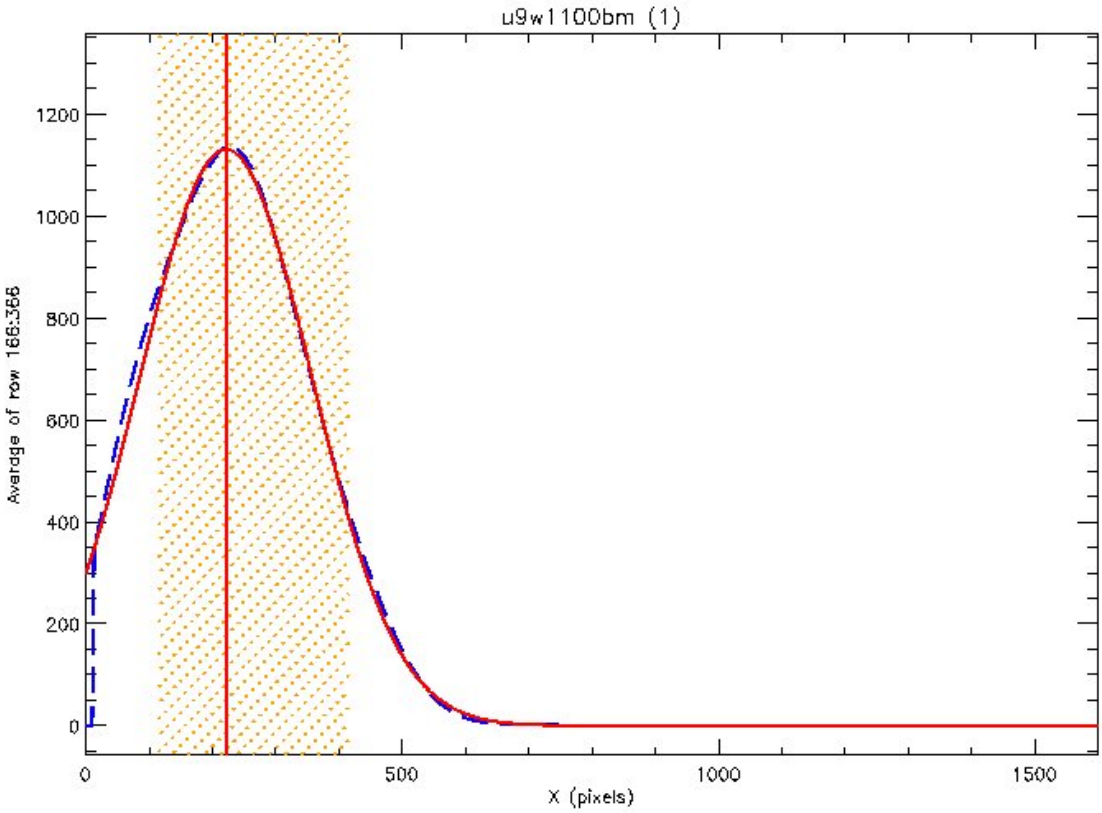
u9w1100bm (1)
Average of row 166:366
X (pixels)
0
200
400
600
800
1000
1200
0
500
1000
1500

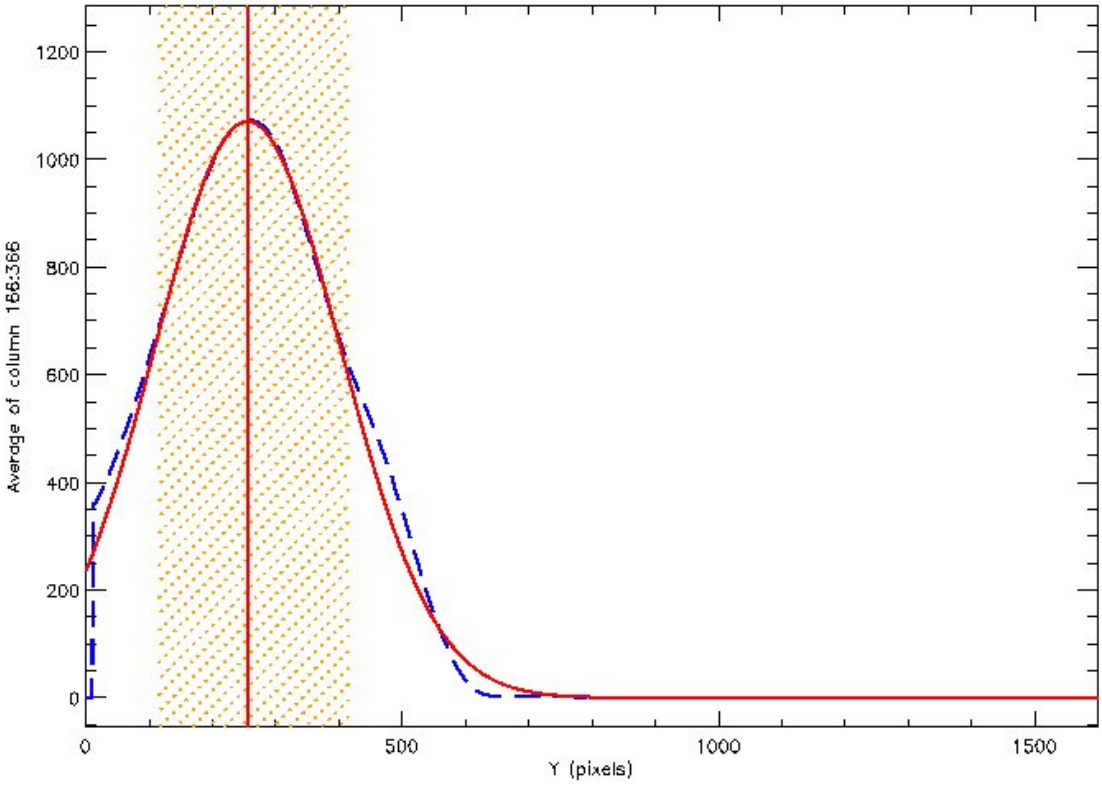
Average of column 166:366
Y (pixels)
0
200
400
600
800
1000
1200
0
500
1000
1500

XVI. FR680N + FQCH4N-C

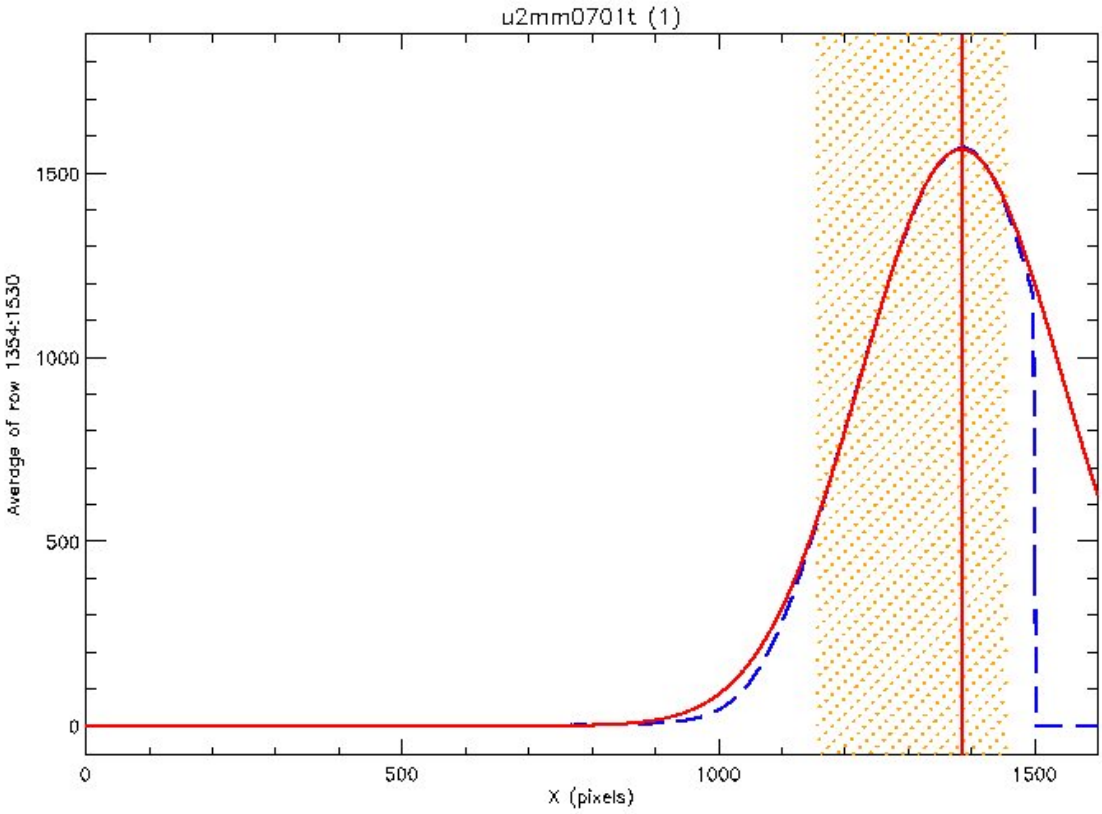

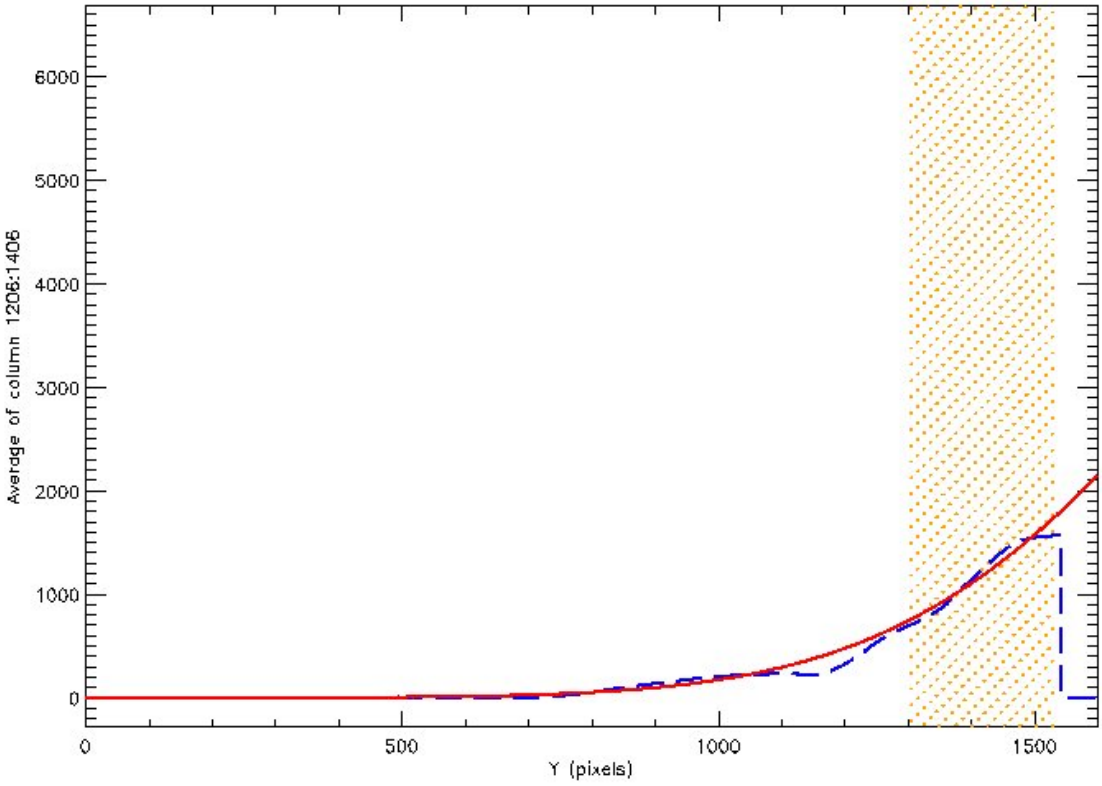

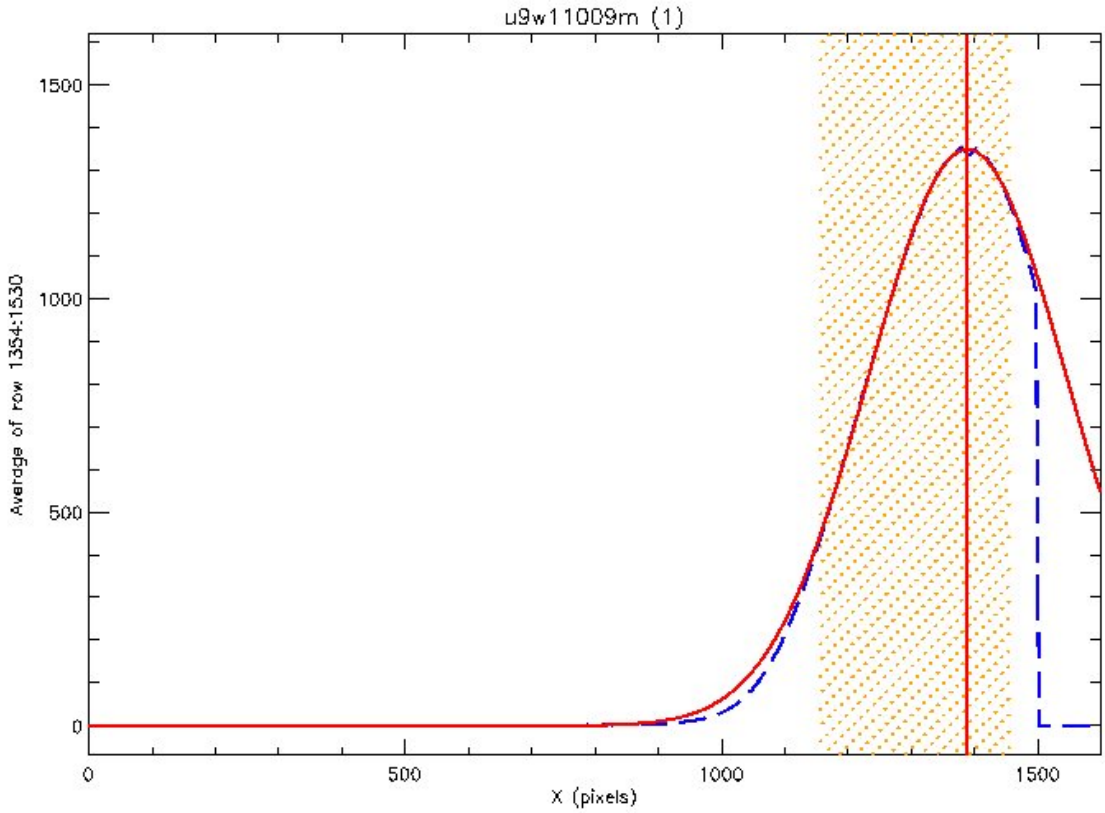
u9w11009m (1)
Average of row 1354:1530
X (pixels)
0
500
1000
1500

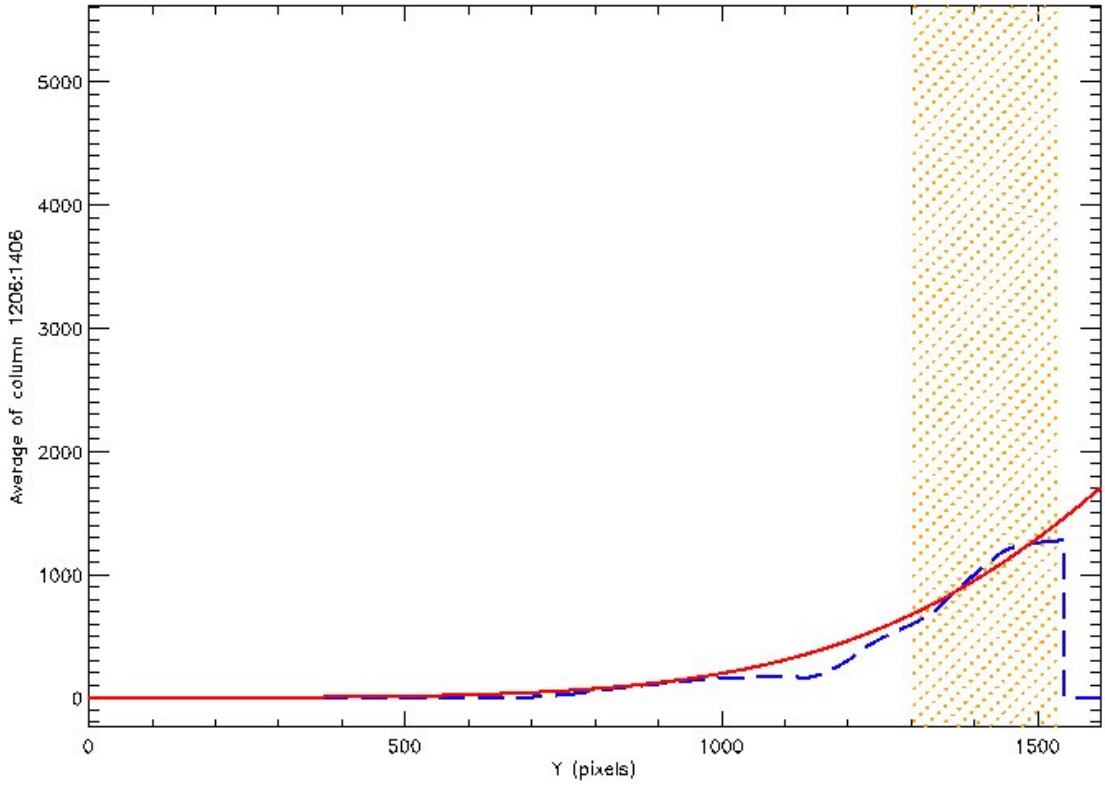
Average of column 1206:1406
Y (pixels)
0
1000
2000
3000
4000
5000
500
1000
1500

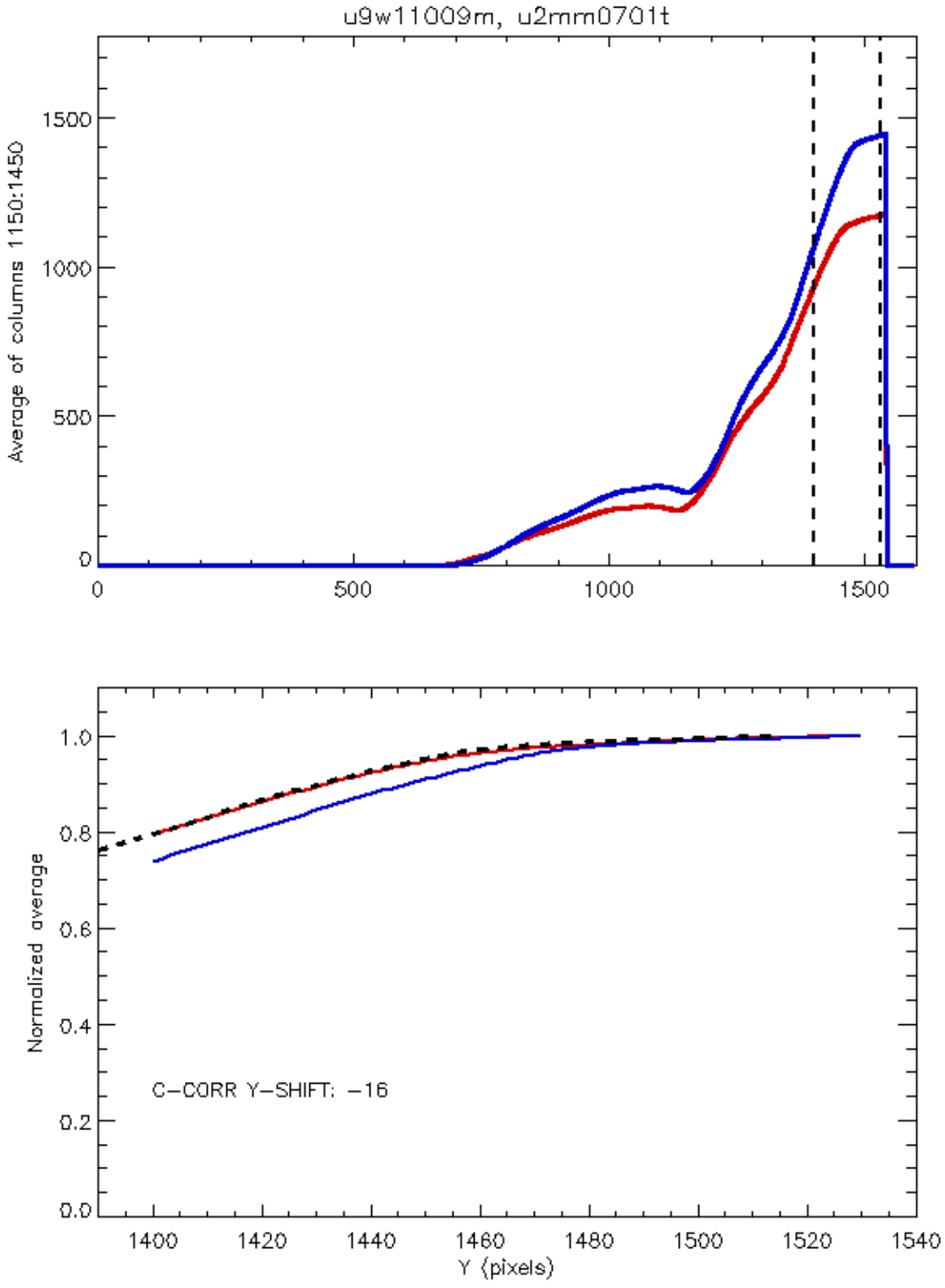
u9w11009m, u2mm0701t
Average of columns 1150:1450
1500
1000
500
0
0
500
1000
1500
Normalized average
1.0
0.8
0.6
0.4
0.2
0.0
C-CORR Y-SHIFT: -16
1400
1420
1440
1460
1480
1500
1520
1540
Y (pixels)

XVII. FR868N + F953N

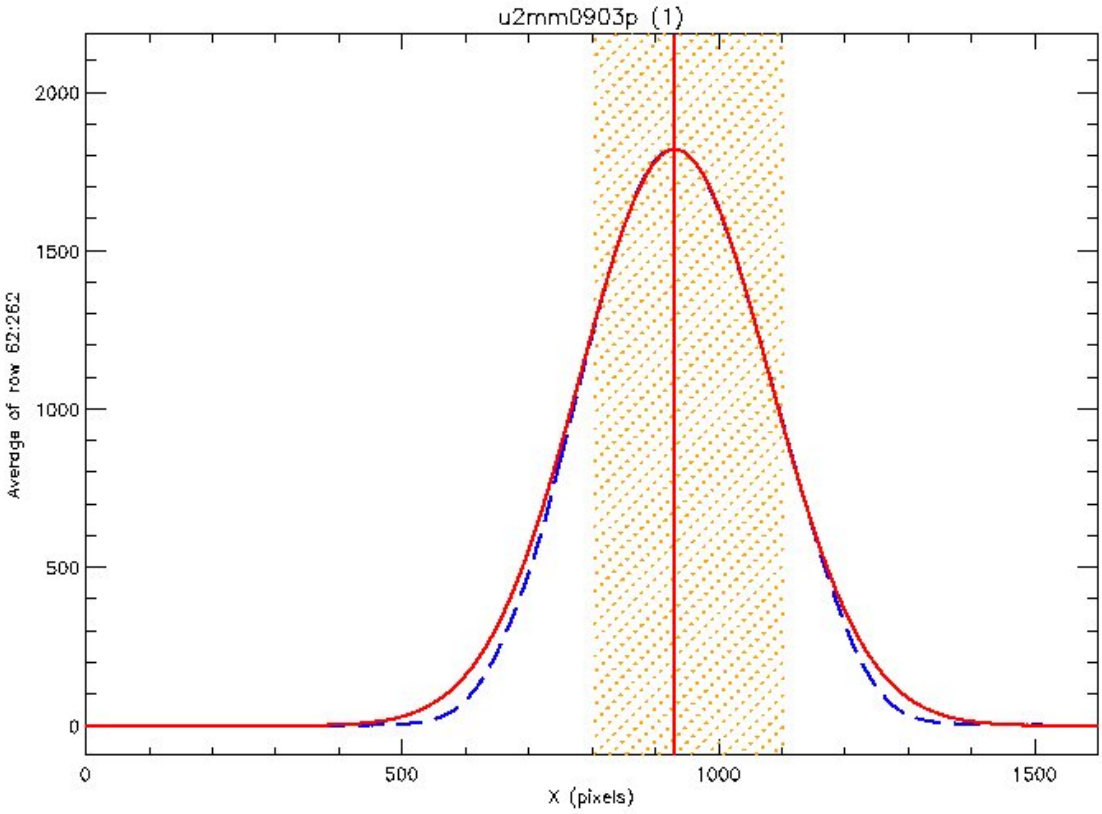

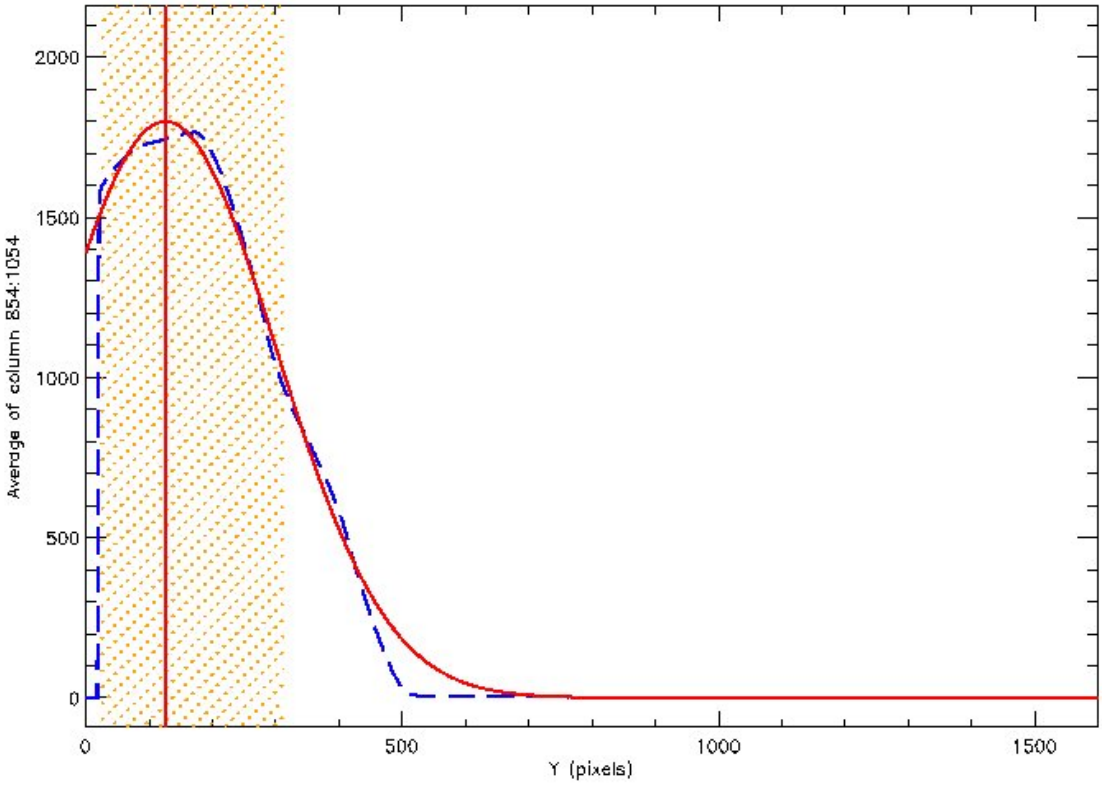

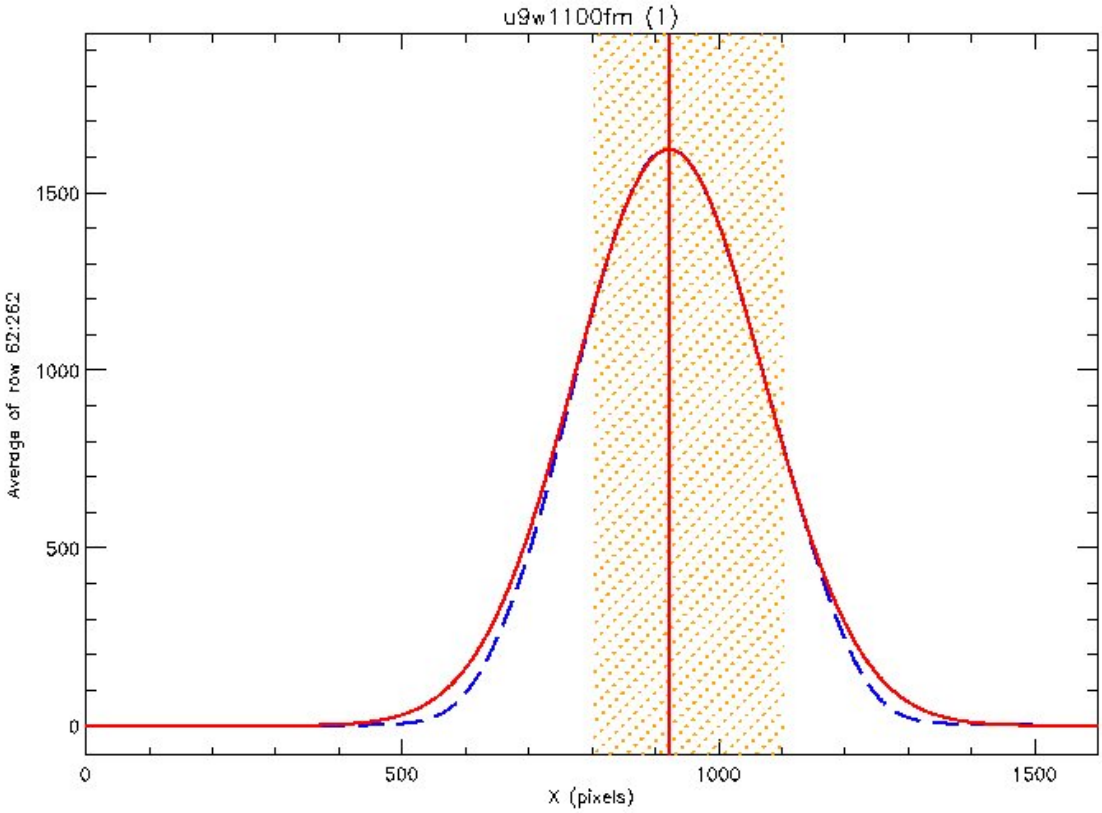
u9w1100fm (1)
Average of row 62:262
X (pixels)
0
500
1000
1500

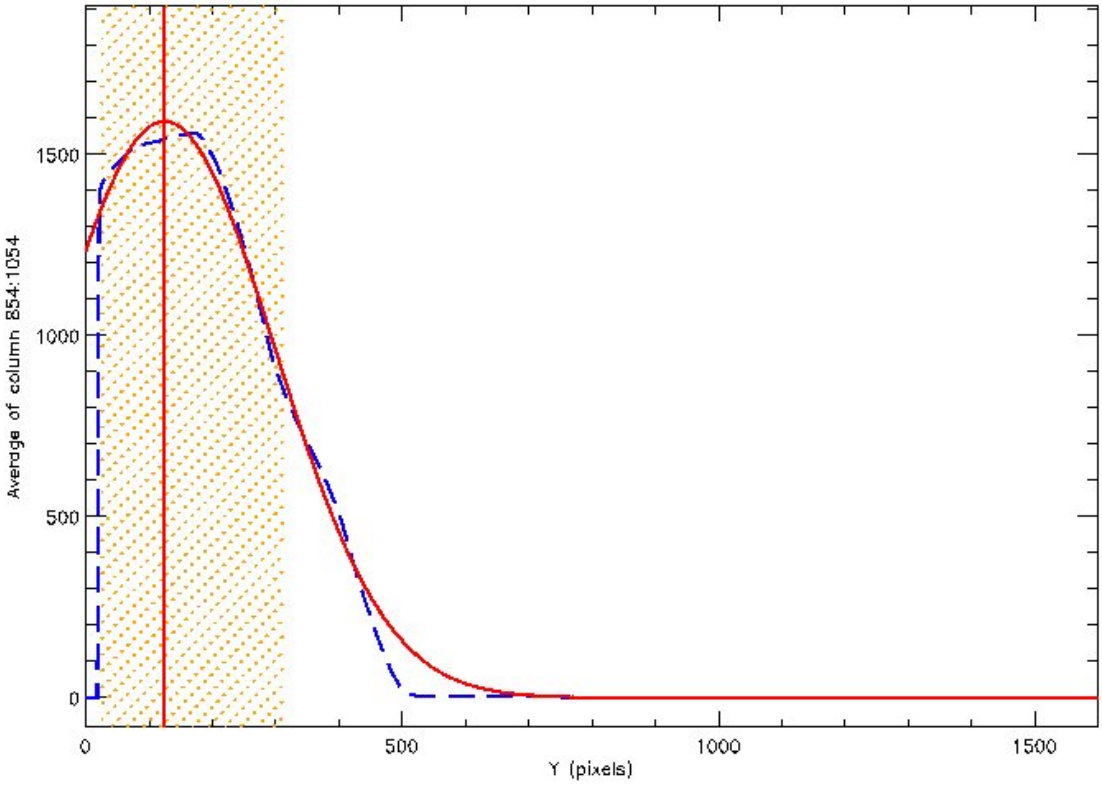
Average of column 854:1054
Y (pixels)
0
500
1000
1500